Rep. Prog. Phys. **63** (2000) 1575–1640. Printed in the UK PII: S0034-4885(00)94759-6

Experimental and phenomenological aspects of circular birefringence and related properties in transparent crystals*

Werner Kaminsky
Department of Chemistry, Box 351700, University of Washington, Seattle, WA 98195, USA

Received 6 October 1999, in final form 3 May 2000

Abstract

Here, we review the history, theory, measurement technique and experimental results on gyrotropic phenomena including optical rotation (optical activity), electrogyration, the Faraday effect and magneto-electrogyration in transparent crystals, including examples of structural phase transitions. Relations to the absolute structure are discussed and model calculations are performed on the basis of electronic polarizability and crystal structure.

* Part of this article was written during employment at the Institute for Crystallography, University of Cologne, Germany and the Clarendon Laboratory, University of Oxford, UK.

0034-4885/00/101575+66$90.00

Contents

1. Introduction

1.1. Aim of the review

Light propagation in a transparent medium is usually described by refraction and reflection. Introducing polarized light and optical anisotropy at the same time causes additional effects when the intensity output of an optical arrangement relative to the initial light wave is considered. The task, however, becomes even more difficult if not only effects such as linear birefringence ($n'' - n'$) (due to the direction dependence of refraction in crystals), but also optical effects of a chiral nature (gyro-optical effects or, for short, gyrotropy) are taken into account.

Linear birefringence is evident when for example two images of a single light source are seen through a calcite crystal ($CaCO_3$) (figure 1) which are found to be both linearly polarized. The electric light fields of the two images are perpendicular to each other. They vibrate in only one direction perpendicular to the propagation direction of the light wave and their velocities inside the crystals are c/n' and c/n'', respectively. If a plane wave enters a prism made from calcite, the difference of speed of the two modes is visible in a different amount of refraction of the *waves* from the initial direction of the wavevector (figure 2(*a*)). These two images are observed for any directions of the initial light wave except those parallel to the optic axis in calcite (figure 2(*b*)).

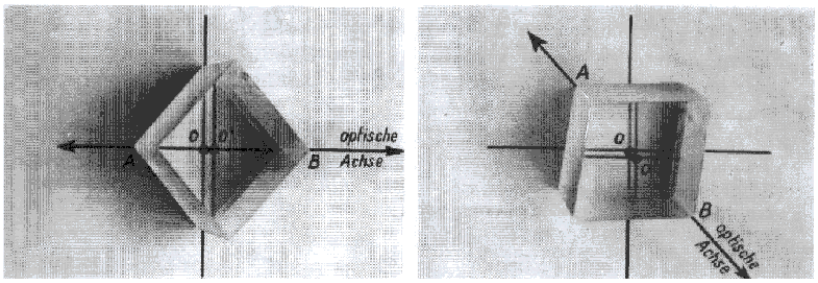

Figure 1. Linear birefringence causing the light *beam* to take two different paths through a calcite rhombohedron. The two modes with refractive indices n' and n'' are mutually perpendicularly polarized (source: Bergmann L and Schäfer C 1978 *Optik (Lehrbuch der Experimentalphysik, Band 3, Optik, 7. Auflage)* (Berlin: de Gruyter) p 487, figure 4, 37 Doppelbrechung des Lichtes durch ein Calcitrhomboeder.

If one allows the vibration direction (=polarization) to rotate around the propagation direction, the result is a circularly polarized wave. Given two opposite senses of optical rotation, there are circumstances in which one observes different velocities for the two circular polarizations c/n_R and c/n_L, where n_R and n_L are the refractive indices of the circularly polarized modes.

The circular birefringence ($n_L - n_R$), which is related to several chiro-optical effects, is typically about 10^3–10^5 times smaller than linear birefringence, ($n'' - n'$), but the state of light is affected much more than expected from that small numerical value. Moreover, if for example, integrated optical circuits are assumed to be as sensitive to polarization effects as an electronic circuit is to the resistance of a conducting component, it becomes obvious that even effects of the order of 10^{-6} of linear refraction cannot be neglected.

Although circular birefringence is just another effect among many other optical observations, it is special because of the close relation to the chiral nature of condensed matter. If there happens to be a difference between left and right circularly polarized light waves, the

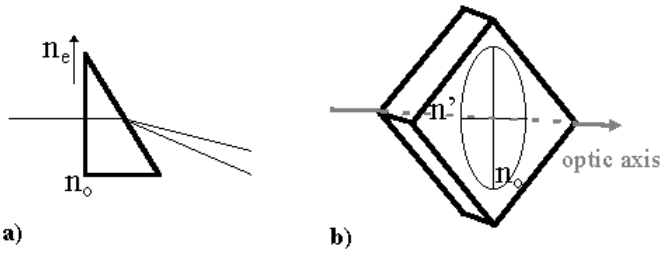

Figure 2. (*a*) Linear refraction of a non-polarized light *wave* by a calcite prism. Two polarized waves, which are polarized perpendicular to one other, are emerging from the prism. (*b*) The orientation of the refractive index $n_o > n_e$ in the case of an 'as-grown' rombohedral piece of calcite. n' is the projection of the extraordinary refractive index n_e. The principal vibration mode with refractive index n_e is called the optic axis; in the case of calcite it connects the two opposite corners of a rhombohedron (threefold axis in calcite).

matter itself must possess a handedness, which may be characterized as laevo (L) or dextro (D).

Different handednesses (figure 3) are frequently observed in nature and are of extreme importance. Almost 15% of the earth's crust (most of it is crystalline) is estimated to be chiral. Moreover, if we consider drugs such as L- and D-thalidomide we find the structures of the two versions of the drug (L and D) to be absolutely identical (all distances between the atoms and the moduli of the angles are equal), but when thalidomide was prescribed to pregnant women as a racemic mixture (L + D), deformed babies were born (figure 4), whereas a pure drug with only L-thalidomide caused no complications. We notice here the importance of chirality in nature.

Below we describe all chiral effects which contribute significantly to the interaction of light with crystals on the basis of empirical results and model calculations based on the x-ray structural parameters of the crystals. Because minute structural variations can cause large changes of the optical features, studies of structural phase transitions are included to serve as a further test of the model calculations.

The basic aim of the present text is to contribute to the fundamental understanding of the interaction of light with transparent crystals and their chiral features. A review of the available experimental data is given and we discuss which of the optical effects can be estimated from model calculations. A critical review of experimental techniques for determining chiral optical properties is presented since the success of a comparison of theory and experiment depends on the reliability of the experimental data.

1.2. State of polarization of the initial light wave

The properties which are the subject of this paper affect the way in which a light wave propagates through a crystal. The interaction with the medium is 'visible' in the resulting intensity and the state of polarization.

The report is restricted to that part of the light spectrum which is far from any absorption so that the average of all possible photon induced transitions contributes to the observed effects. The discussion is further restricted to what is seen in transmission. Effects which are related to absorption or to second-harmonic generation (SHG) are excluded here as well as optical properties of gases, fluids, ceramics, liquid solutions or liquid crystals.

In the following, the incident plane light wave is assumed to be linearly polarized and monochromatic. These three features of the wave (plane, linearly polarized, monochromatic)

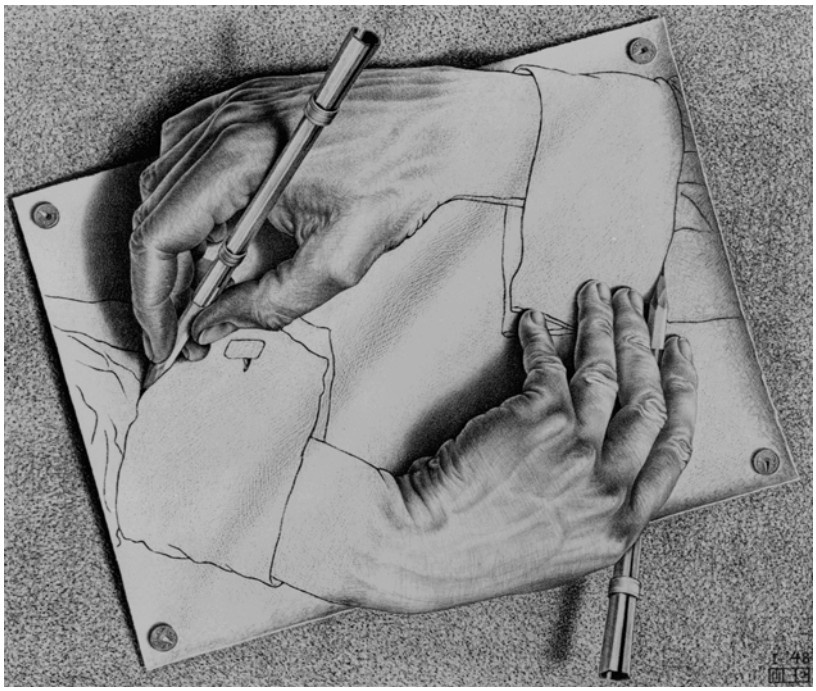

Figure 3. A drawing by Escher of two hands. The physiognomies of these hands are related to each other by point inversion (M C Escher's *Drawing Hands* © 1999 Cordon Art B V, Baarn, The Netherlands. All rights reserved).

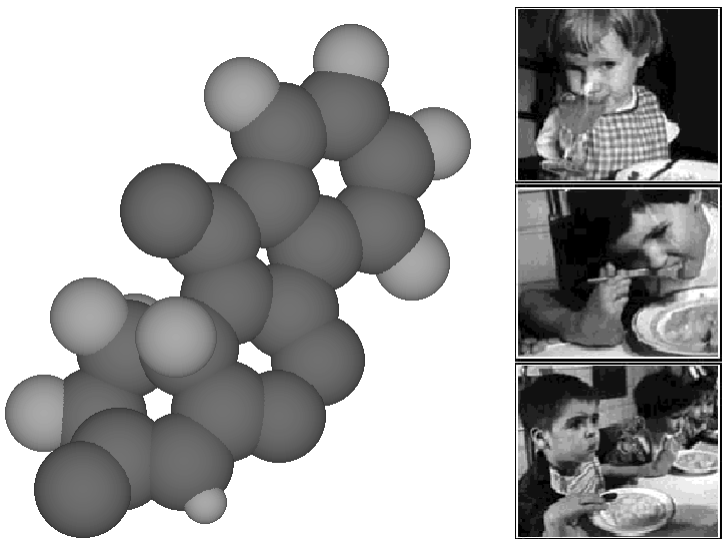

(*a*) (*b*)

Figure 4. (*a*) The D-thalidomide molecule and (*b*) its victims (source: *CNN-News*, 4 September 1997). The drug, banned in 1962, which was responsible for 12 000 babies born with all kinds of defects, has been reconsidered since 1997 for treatment of painful sores that afflict leprosy patients.

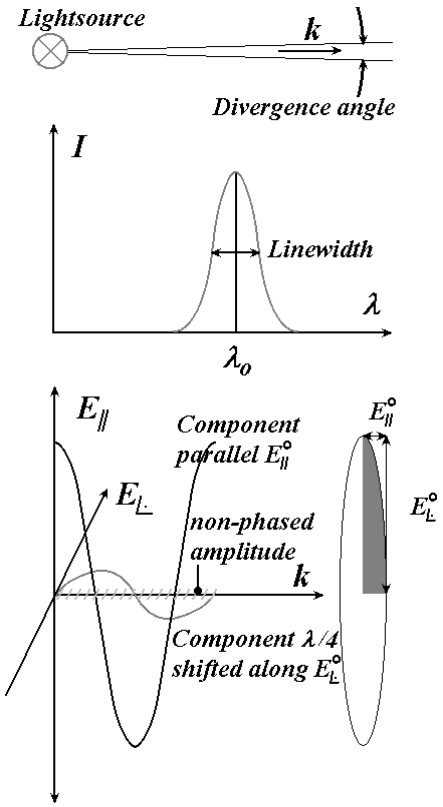

Figure 5. Realistic polarized light. Top: the divergence of the light wave, described by an angle. Middle: the linewidth, which is usually a continuum of wavelengths varying statistically around λ_0. Bottom: the ellipticity $E^{\circ}_{\parallel}/E^{\circ}_{\perp}$ of the light wave, which usually carries a non-polarized component.

have never been perfectly realized. The line width, however, is negligibly small if the measurements are carried out with laser light, but the linear polarization of the incident wave is typically not better than $1 : 10^{-5}$ (figure 5).

As a result, the incident light wave is more or less elliptically polarized; the polarization can be described by the superposition of a left- and a right-handed circularly polarized wave of different amplitudes. The difference in velocity of these two waves when travelling through the crystal is related to circular birefringence.

In the presence of linear birefringence the polarization of two circularly polarized waves changes and the situation is, in short, confusing. As part of this review, the theory which relates the measured polarization and intensity to the circular birefringence, which produces a gyrotropy under the obscuring effect of linear birefringence, is summarized. The resulting approximate expressions are suited for use in realistic experiment.

1.3. Gyrotropy

The optical phenomenon which can be related to circular birefringence is called gyrotropy. This can result from a number of effects with totally different physical origins. Table 1 summarizes which of these effects will be discussed here and gives a short description of the leading physical mechanisms. Some of the mechanisms have been a matter of controversy.

Circular birefringence $(n_{\mathrm{R}} - n_{\mathrm{L}})$, where n_{L} and n_{R} are the refractive indices for left and right circularly polarized light, respectively, can arise naturally in non-centrosymmetric

Table 1. The different effects which contribute to gyrotropy. An electron cloud shift arises when an external electric field is applied to the crystal structure. The amount of the shift between the electron cloud and an atom it surrounds is in proportion to its polarizability. The magnetic light field is related to the derivative of the electric light field with respect to time.

Name of the effect	Rank	Leading physical mechanism
Optical rotation	2 axial	Dipole–dipole interaction
Faraday effect	2 polar	Zeeman effect
Electrogyration	3 axial	Dipole–dipole interaction and electric polarization of atoms
Piezogyration	4 axial	Dipole–dipole interaction and induced structural changes
Electro-Faraday effect	3 polar	Zeeman effect and electric polarization of atoms
Magneto-activity	3 polar	Spatial dispersion of the magnetic light field and interaction with an external magnetic field
Magneto-electrogyration	4 polar	Electric polarization of atoms and spatial dispersion of the magnetic light field and interaction with an external magnetic field

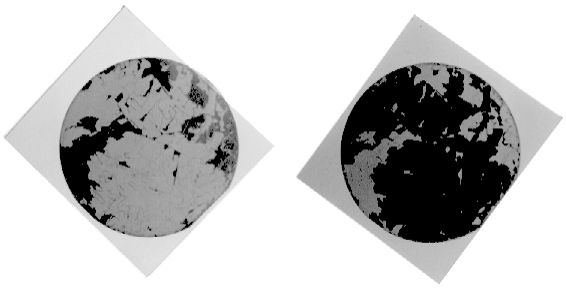

Figure 6. Intrinsic (spontaneous) Faraday rotation in an approximately 10 μm thick yttrium–iron garnet (YIG), diameter 70 mm, epitaxially grown on a single-crystal wafer made from yttrium–aluminium garnet (YAG). Analysers are at approximately + and -40° with respect to the polarizer. The ferromagnetic domains are easily switched with a magnetic field.

crystals and is usually called optical activity.

However, this historical term has been misused in recent years to describe SHG and related effects. Instead of optical activity, and to avoid further confusion, the effect is better named 'optical rotation', which is used in the following text.

$(n_R - n_L)$ can also result from a spontaneous magnetization of a ferromagnetic crystal and will be called the intrinsic Faraday effect in that case (figure 6). The intrinsic Faraday effect changes sign when the light path is reversed, whereas optical rotation, which in contrast to the Faraday rotation depends on the square of the wavevector, does not.

When an electric field is applied to a crystal it is possible to change the optical rotation or produce gyrotropy even in the case of a centrosymmetric crystal. An optical rotation produced via spontaneous polarization in a ferroelectric crystal is in principle indistinguishable from natural optical rotation except that the latter cannot be switched by an electric field†. The electric field induced optical rotation is called electrogyration. Similarly, an external magnetic field induces circular birefringence, which leads to the classical Faraday effect or produces magnetic field induced optical rotation (magneto-activity). When an external electric field and a magnetic field are applied to the crystal at the same time, either an electric field induced Faraday effect (electro-Faraday effect) or a magnetic field induced electrogyration (magneto-electrogyration) is observed. The greater the number of different external fields that are applied, the more tensor components are required to describe the effect.

Figure 7 shows the essential features of an experiment for measuring gyrotropy. Initial linearly polarized light is passed through the sample and the resulting rotation is measured

† The structure of a ferroelectric crystal depends on the sign of the external electric field, and as such can produce intrinsic optical rotation switched by an external field which still is not related via electrogyration to the spontaneous polarization.

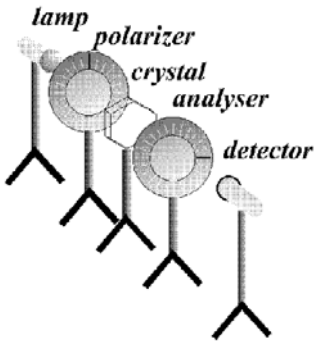

Figure 7. A simple polarimeter with a hexagonal shaped sample, which could be a piece of quartz cut on its optic axis (*c*-axis).

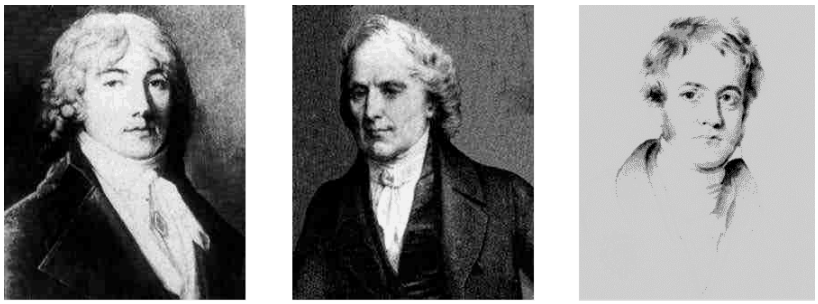

Figure 8. Jean-Baptiste Biot. Born 21 April 1774 in Paris, France. Died 3 February 1862 in Paris, France. Dominique Francois Jean Arago. Born 26 February 1786 in Estagel, Roussillon, France. Died 2 October 1853 in Paris, France. John Wilhelm Friedrich Herschel. Born 7 March 1792 in Slough, UK. Died 11 May 1871 in Hawhurst, UK (source: *The MacTutor History of Mathematics Archive*).

with another polarizer, called the analyser, which is rotated until the intensity of the light wave observed on looking through the analyser towards the light source is minimized. The deviation from the perpendicular configuration arises from the gyrotropy. In reality, polarizer and analyser do not polarize perfectly. The consequences of such imperfections are discussed below.

A clockwise rotation when viewed towards the light source is called 'positive' or 'dextrorotatory' (a 'negative' or anti-clockwise rotation arises in 'laevorotatory' substances)†.

However, in the Faraday effect, the definition of the sign was historically made independent of that of optical rotation. Here, it was defined to be positive if a clockwise rotation arises when looking along the direction of the magnetic field and the light path. With the exception of the Faraday effect, we will speak of a positive rotation if it is clockwise when looking towards the light source and when the inducing fields are parallel to the wavevector.

1.4. A brief history of gyrotropy

Optical rotation was formulated in 1812 by J B Biot (Biot 1812; figure 8) after an observation by F Arago (Arago 1811; figure 8) that polarized light from the sun, on passing through a quartz crystal, gives a solar image whose colour changes when an analyser crystal is rotated.

† This definition has developed through history and is unfortunately inconsistent with a mathematical definition of a right-handed screw along the wave propagation.

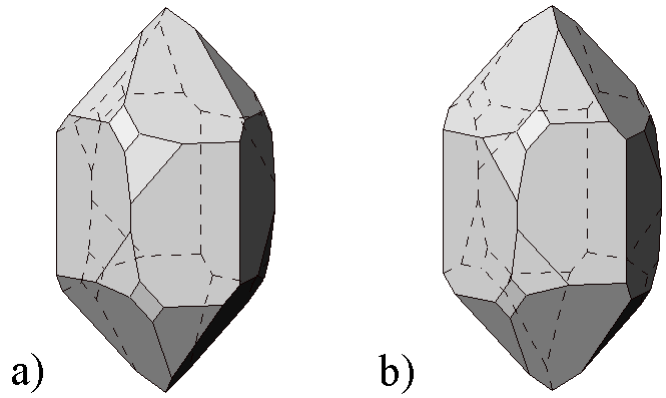

Figure 9. Idealized pictures of laevorotative left quartz (space group $P3_121$) on the left and dextrorotative right quartz ($P3_221$).

Figure 10. Augustin Jean Fresnel. Born 10 May 1788 in Broglie, France. Died 14 July 1827 in Ville-d'Avray, France. Louis Pasteur. Born 27 December 1822 in Dole, France. Died 28 August 1895 near Paris, France (source: *The MacTutor History of Mathematics Archive*).

Biot discovered also the optical rotation of liquids. This happened about 150 years after the discovery of linear birefringence (Bartholin 1669), which started the modern history of crystal optics with polarized light. Optical rotation was then measured over a wide spectral range in different isotropic media. John Herschel (figure 8) made the correlation of optical rotation with the habit of quartz (Herschel 1822; figure 9).

It was A Fresnel (Fresnel 1824; figure 10) who proposed the idea of circular birefringence ($n_L - n_R$), introducing the rotatory power ρ (given usually in degrees mm^{-1}), which is defined as $\rho = 180\frac{n_L - n_R}{\lambda}$, λ = wavelength in metres.

L Pasteur (figure 10) established a link between the handedness of crystals of sodium–ammonium tartrate and the sign of optical rotation of the tartrates in solution (see the examples of tartaric acid crystals in figure 11), which demonstrated the connection of molecular and crystalline chirality. After Pasteur proved the difference of optical rotation of the enantiomorphs of tartaric acid salts to the aged and very sceptical Biot, in Pasteur's own

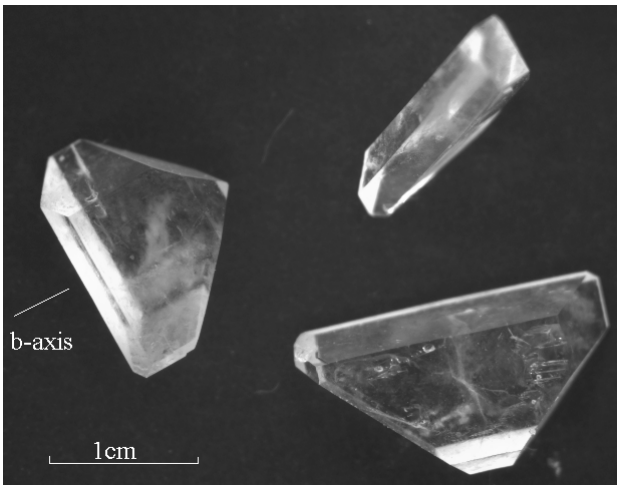

Figure 11. Crystals of tartaric acid showing monoclinic symmetry. The twofold axis is marked.

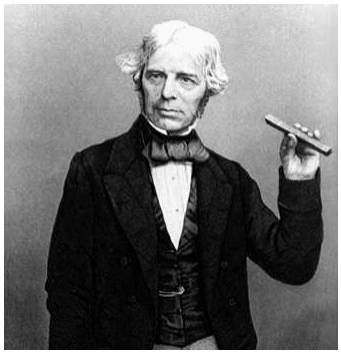

Figure 12. Michael Faraday. Born 22 September 1791 in Newington Butts near London, UK. Died 25 August 1867 in Hampton Court near Richmond, UK (source: *The Oxford Interactive Encyclopaedia* CD version).

apocryphal recollection of events, Biot's response was 'My dear child, I have loved science so much throughout my life that it makes my heart throb' (Pasteur 1897).

Just some years earlier, in 1845, M Faraday (1846; figure 12) found that magnetic fields induce gyrotropy in glass rods. Since then, most measurements have been carried out in directions where the material is optically isotropic, i.e. not birefringent, because the gyrotropy is obscured by the linear birefringence. This effect was demonstrated at the end of the 19th century on the Faraday effect of dilated glass rods (Wedding 1888, Wiener 1888).

Many attempts were made to describe the Faraday rotation empirically by adding up the specific molar ionic rotations (Schütz 1936). Figure 13 shows a 'periodic system' of specific molar Faraday effects from which the Faraday effect in an isotropic direction of a compound with any chemical composition can be calculated with satisfying accuracy.

The first reliable result of a gyrotropy measurement in a birefringent direction was obtained in quartz (Szivessy and Münster 1934). Further measurements of optical rotation in birefringent directions and the method in use are discussed below.

The first measurement of electrogyration in $Bi_{12}GeO_{20}$ was claimed by Lenzo *et al* (1966), where a change of optical rotation was induced by application of static electric fields. However, it has been shown that the electro-optic effect was responsible for almost all that had been measured (Miller 1973), thus electrogyration was observed most probably for the first time in

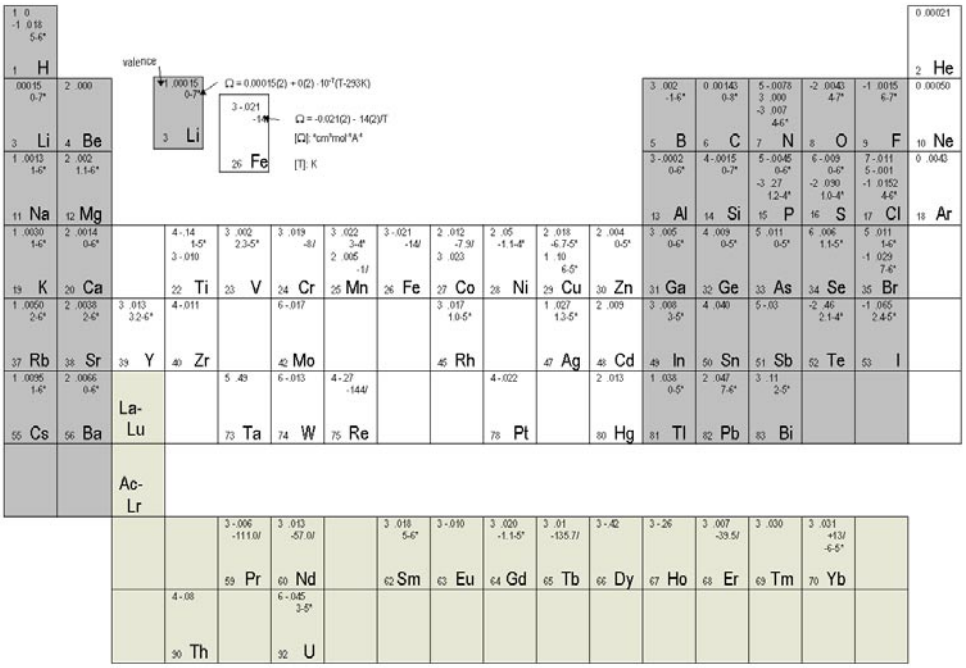

Figure 13. The periodic system of molar Faraday rotations to derive the Verdet constant of any (ionic) substance at 633 nm and at temperatures between 210 and 310 K. With the chemical formula represented by $n_i A_i$, A_i is an ion and n_i its occurrence in the substance, $V = n_i \Omega_i(T)\rho(T)M^{-1}$, Ω_i is the molar ionic Verdet constant of ion A_i, ρ = density of the substance (g cm^{-3}), and $M = n_i M_i$ the molar mass (g mol^{-1}), M_i = the atomic mass and T = temperature. The temperature coefficients can be used to estimate the thermal variation of the Faraday rotation φ. $\mathrm{d}\log\varphi/\mathrm{d}T = \mathrm{d}\log\Omega/\mathrm{d}T - 2\alpha$, where α is the thermal expansion coefficient.

low quartz by Miller (1973).

At about the same time, piezogyration was studied with success in $NaClO_3$ by Meyers and Vedam (1965, 1967) and later by Weber (1979).

Even more difficult, because of its smallness, is the measurement of magneto-electrogyration and related phenomena. The first report of Faraday rotation induced by an electric field via the magneto-electric effect in $Bi_{12}SiO_{20}$ was given by Odell and White (1970). A complete tensor determination of magneto-electrogyration was reported on cubic $Pb(NO_3)_2$ (Kaminsky *et al* 1992). Below we will discuss the symmetry and the physical mechanism of the effect. The electro-Faraday effect was found recently in $Cd_{0.49}Mn_{0.51}Te$ (Koyanagi *et al* 1989). A reliable measurement of magneto-activity has not been reported so far (Pisarev 1994).

1.5. Further reading

Some ideas of the following sections are the subject of books and other reviews on optical issues. The reader may refer to these for additional information (only books written in English or German are included). Technical aspects of ellipsometric measurements (Azzam and Bashara 1977) as well as a detailed treatment of optical rotation and the Faraday effect is covered by means of transition moments (Barron 1982, Caldwell and Eyring 1971, Charney 1979, Mason 1982, Piepho and Schatz 1983, Michl and Thulstrup 1986). Induced effects are discussed

elsewhere (Yamaoka and Charney 1972, Fredericq and Houssier 1973, Kielich 1976, Atkins and Miller 1968, Stedmann 1985, Haussühl 1983). A beautiful review of the history of optical activity is given by Applequist (1987). History and aspects of symmetry of optical rotation are discussed in detail by O'Loane (1980). A treatment of linear and circular birefringence by means of Poincare spheres is given in Ramachandran and Ramaseshan (1961).

2. Theory

2.1. The interaction of linear birefringence and gyration

A general direction in a non-cubic crystal exhibits linear birefringence (normally called simply 'birefringence'), which usually obscures the chiral effect. The involved relations need to be closely inspected. We therefore derive the equations connecting the intensity of light after having passed through crossed polarizers with a birefringent sample between them which exhibits gyrotropy up to quadratic order in the polarizer and analyser angles from first principles. We start by deriving the relevant expression with a perfect alignment of the crystal and perfect optical components. The effect of real experimental conditions (mainly due to parasitic ellipticities) is introduced later.

The constitutive equation, which forms the basis of the description in idealized form of the interaction of birefringence and, for example, optical rotation, results from a Taylor expansion of the dielectric displacement $\boldsymbol{D}$ (Born 1933), which in turn is related to the electric field $\boldsymbol{E}$ via the relative dielectric constant tensor ε and the gyrotropy (see also below, section 2.6), represented by a vector $\boldsymbol{g}$. Comparing this with the wave equation, an equation is formulated, which describes the propagation of a light wave in a gyrotropic medium (ε_0: permittivity of free space):

$$\varepsilon \cdot \boldsymbol{E} + \mathrm{i}\boldsymbol{g} \times \boldsymbol{E} = \frac{1}{\varepsilon_0}\boldsymbol{D} = n^2[\boldsymbol{E} - (\kappa \cdot \boldsymbol{E})\kappa] \tag{2.1.1}$$

where $\kappa = \boldsymbol{k}/|\boldsymbol{k}|$, is a unit vector along the wavevector $\boldsymbol{k}$ and n the refractive index governing the speed of propagation of the plane wave $\boldsymbol{D} = \boldsymbol{D}_0 \mathrm{e}^{\mathrm{i}(\boldsymbol{k}\cdot\boldsymbol{x}-\omega t)}$. ω is the angular frequency, $\boldsymbol{D}_0$ is the amplitude of the dielectric displacement associated with the light wave and $\boldsymbol{x}$ is a vector in real space.

In specifying a Cartesian reference system with its axes along the principal vibration modes of the indicatrix n_i and choosing† $\kappa \| n_1$, $\boldsymbol{D}_0 \| n_2$, the resulting equation is written as (see, e.g., Haussühl 1983):

$$(n^2 - n_2^2)(n^2 - n_3^2) = (\kappa \cdot \boldsymbol{g})^2. \tag{2.1.2}$$

There happen to be two modes $\boldsymbol{D}'$, $\boldsymbol{D}''$ (figure 14) which describe the wave propagation with refractive index n' and n'' and which are the solutions of this quadratic equation.

After passing through the crystal of thickness L and choosing the initial polarization parallel, say, $\boldsymbol{e}_2^{\mathrm{o}}$, $\boldsymbol{D}'$ and $\boldsymbol{D}''$ interfere to form a wave $\boldsymbol{D}(x|\boldsymbol{e}_1^{\mathrm{o}} > L)$, resulting in ($\boldsymbol{e}_i^{\mathrm{o}}$ are principal modes of the refractive indices, see Kaminsky and Haussühl 1993)

$$\begin{aligned} &\mathrm{Re}\,(D_2) \approx D_0 \cos(A), \qquad \mathrm{Re}\,(D_3) \approx 2uD_0 \sin\left(\frac{d}{2}\right)\cos(A-d), \\ &A = A_0 + \boldsymbol{k}\cdot\boldsymbol{x} - \omega t, \qquad d = 2L(k' - k'') \qquad u \approx \frac{g_1}{n_3^2 - n_2^2} < 1, \end{aligned} \tag{2.1.3}$$

where terms quadratic in u are neglected. The azimuth φ of the $\boldsymbol{D}$-mode is found by eliminating A in equations (2.1.3): $\tan(2\varphi) = -2D_2^{\mathrm{o}}D_3^{\mathrm{o}}\cos(d/2)/(D_2^{\mathrm{o}2} - D_3^{\mathrm{o}2})$, where $D_2^{\mathrm{o}} = D_0$ and $D_3^{\mathrm{o}} = 2uD_0 \sin(d/2)$.

† This means explicitly κ parallel to the vibration mode e_1^{o} of n_1.

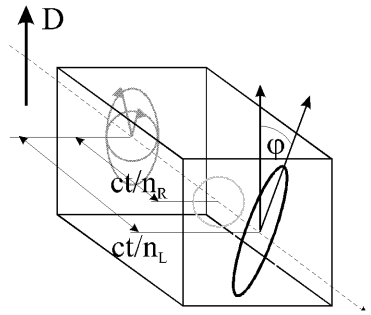

Figure 14. An initially linearly polarized wave $\boldsymbol{D}$ passes through the crystal in the form of two elliptically polarized waves of different amplitudes, ellipticities, speeds $ct/n_{\mathrm{R-L}}$ and rotation senses. The result is an azimuthal rotation φ which is much smaller than that which would be observed if the crystal where not birefringent.

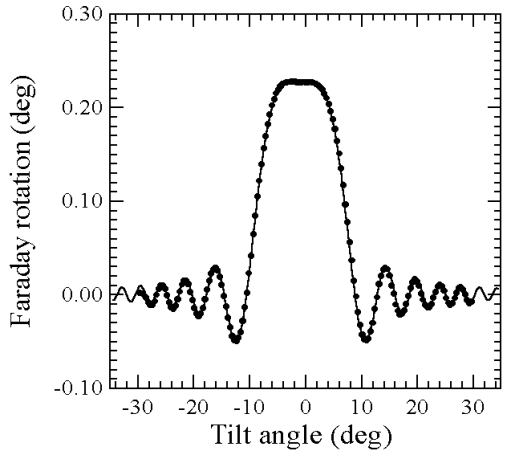

Figure 15. The variation of the magnetic field induced Faraday rotation of a (001) cut KH_2PO_4 sample. Experimental (filled circles) and the theoretical representation of the measurement, using equations (2.1.4).

For a small azimuth and neglecting again terms in u^2 it follows that $\varphi \approx u\sin(d)$. The ellipticity ε is found from $\varepsilon \approx \tan(\varepsilon) \approx \mathrm{Re}\,(D_2(A=\varphi))/\mathrm{Re}\,(D_3(A=\varphi+\pi/2))$.

With $\delta = kL(n_2 - n_3) \tilde{=} d, \varphi_0 = g_1 Lk/2n_2$. The final result for the 'idealized' experiment (see below, equations (2.1.6), for a real experiment) is, neglecting terms of magnitude u^2 (Kaminsky 1989),

$$\varphi = \varphi_0 \frac{\sin(\delta)}{\delta}, \qquad \varepsilon = \varphi_0 \frac{\sin^2(\delta/2)}{\delta/2}. \tag{2.1.4}$$

The expressions in equations (2.1.4) are easily generalized, assuming only that the birefringence is not too large (<0.2), replacing g_1 by the effective chiral component in the direction of the wavevector and replacing $(n_2 - n_3)$ by the birefringence of an arbitrary cross-section of the crystal normal to the wavevector. The equation is valid even for vanishing δ. The above equations were verified experimentally using an induced gyrotropy (Faraday effect) in a birefringent material (KH_2PO_4). (Figure 15 shows for example the dependence of azimuth rotation φ on phase δ.)

However, parasitic ellipticities of the polarizer and depolarizing effects of the sample cannot be neglected in the real experiment when gyrotropy is intrinsic. This means gyrotropy, like optical rotation, cannot be modulated, in contrast to the Faraday effect, which can be switched on and off with an external magnetic field to separate it from other contributions.

The intensity I behind the sequence light source, polarizer (parasitic ellipticity ε_{P}, rotated by Y), sample, analyser (ε_{A}, rotated by Ω) (figure 16) is in a first approximation related to the

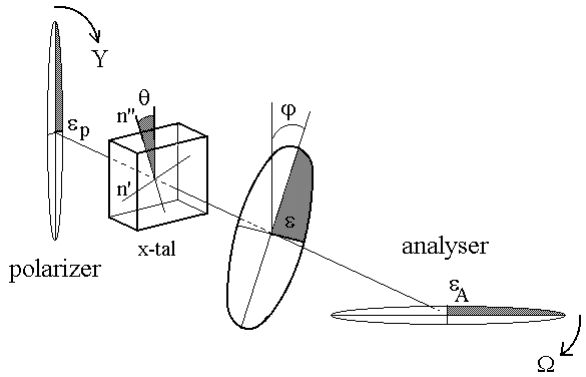

Figure 16. Principal components for measuring a gyrotropy (Kaminsky 1997). The polarizer is rotated by the angle Y. The vibration modes n' and n'' are inclined (relative to $Y = 0$) by θ. The azimuthal rotation of the light wave is denoted by φ and its ellipticity by ε. The analyser is rotated by Ω.

Table 2. The origin of different contributions to the azimuthal rotation φ and ellipticity ε of the light wave after passing through the sample. The incident linearly polarized wave is assumed to be polarized close to the slow axis of the sample.

Effect	Contribution to φ	Contribution to ε
Analyser (Ω, ε_A)	Ω	ε_A
Gyrotropy (φ_0)	$\varphi_0\delta^{-1}\sin\delta$	$2\varphi_0\delta^{-1}\sin^2(\delta/2)$
Extinction (θ)	$\theta(1-\cos\delta)$	$-\theta\sin\delta$
Polarizer (Y, ε_P)	$Y\cos\delta + \varepsilon_P\sin\delta$	$Y\sin\delta - \varepsilon_P\cos\delta$

azimuthal rotation φ and ellipticity ε of the light after the sample by

$$I \cong I_0[\varphi^2 + \varepsilon^2] \tag{2.1.5}$$

where I_0 is the initial intensity, and the polarizer and analyser are perpendicular: their angular position angles Y and $\Omega = 0$. Y and Ω are considered to be small (see figure 16 for a definition of Y and Ω).

The contributions to the azimuthal rotation φ and ellipticity ε of the elliptic polarized wave, resulting from different optical effects and the parasitic ellipticity of the polarizer, are summarized in table 2, where we assume that the extinction θ between the polarization of the refractive index, say, n'' and the initial polarization of the polarizer ($Y = 0$) is small as well.

$$\begin{aligned}\varphi &\approx \Omega + \varphi_0\frac{\sin\delta}{\delta} + Y\cos\delta + 2\theta\sin^2\frac{\delta}{2} + \varepsilon_P\sin\delta \\ \varepsilon &\approx \varepsilon_A + \frac{2\varphi_0}{\delta}\sin^2\frac{\delta}{2} + (Y-\theta)\sin\delta - \varepsilon_P\cos\delta.\end{aligned} \tag{2.1.6}$$

The resulting expression is written in the form of a bi-quadratic polynomial in Y and Ω. To make that equation realistic, we have to introduce an error Y_0 of the polarizer adjustment towards the assumed perfect vertical position and a similar error of the analyser, where $Y - \Omega = 2Y_0$ (with $\theta = \theta_0 - Y_0$).

Furthermore, we introduce the difference Λ between ε_P and ε_A: $\Lambda = \varepsilon_P - \varepsilon_A$. In Λ are also summarized all other parasitic effects: if the surface of the sample interacts with the incident light wave, this may increase the value of ε_P, and inhomogeneous samples increase

the value of ε_A. We find (neglecting products of the small parameters φ_0/δ, θ, ε_P, Λ and Y_0)

$$\begin{aligned}
\frac{I}{I_0} &= a_0 + a_1\Omega + a_2 Y + a_3\Omega Y + \Omega^2 + Y^2 \\
a_1 &= 2\left(\frac{\varphi_0}{\delta} + \varepsilon_P\right)\sin\delta + 2\theta(1-\cos\delta) - 2Y_0\cos\delta \\
a_2 &= 2\left(\frac{\varphi_0}{\delta} + \varepsilon_P - 2\Lambda\right)\sin\delta - 2\theta(1-\cos\delta) - 2Y_0\cos\delta \\
a_3 &= 2\cos\delta
\end{aligned} \tag{2.1.7}$$

where $\delta = 2\pi L(n'' - n')\lambda^{-1}$ is the phase factor, L is the length of the light path inside the sample and λ is the wavelength (see Kaminsky and Glazer 1996).

2.2. Gyrotropic measurement techniques in birefringent directions

The fraction I/I_0 depends on the externally accessible angles Y, Ω, θ, the retardation δ, the gyration φ_0 and ellipticities ε_P, ε_A. In a real experiment some or all of these properties are varied to separate out the different contributions to I/I_0. In most of the techniques in use, the azimuth φ of elliptic polarized light is found from a variation of Ω. From equation (2.1.5) it follows that such a modulation is equivalent to $\partial(I/I_0)/\partial\Omega = 0$. This derivative has indeed the result $\Omega = -\varphi$, so this approach can be used to find φ (Bruhat and Grivet 1935, Konstantinova *et al* 1969), where in φ are summarized the different contributions given in table 2.

If it is only of interest whether a material exhibits optical rotation, measurements on powdered samples embedded in refractive index-matching matrices can help to give an answer (Bartus and Vogel 1994, Bartus *et al* 1993, 1994a, b, Xi *et al* 1993, Berlin *et al* 1989). However, these experiments are not considered further because they provide no information about the anisotropy of the chiral effects.

Similarly, measurements with probably the most sensitive method, the Sagnac interferometer (see e.g. Dodge *et al* 1994) seem to be restricted to optically isotropic directions. This technique therefore is of less importance for the determination of gyro-optical tensors.

If the ellipticity of the analyser of an ordinary polarimeter with $Y = \Omega = 0$ is modulated by inserting a Pockels modulator between sample and analyser, and for $\varepsilon_A = \varepsilon_A^{o-}\cos\omega t$, ε_A^o small, we find from equation (2.1.5) and table 2

$$\begin{aligned}
I/I_0 &= \text{const} + 2\varepsilon_A^o\cos\omega t\,(\varphi_0\delta^{-1}(1-\cos\delta) - \theta\sin\delta - \varepsilon_P\cos\delta) - \tfrac{1}{2}(\varepsilon_A^o)^2\sin 2\omega t \\
&= \text{const} + I_\omega\cos\omega t + I_{2\omega}\sin 2\omega t.
\end{aligned} \tag{2.2.1}$$

From the averaged retardation δ of $\langle I_\omega\rangle_\delta$ and $\langle I_{2\omega}\rangle_\delta$ we find, independent of θ and ε_P,

$$|\varphi_0| = \varepsilon_A^o\delta\langle I_\omega\rangle_\delta/4\langle I_{2\omega}\rangle_\delta \tag{2.2.2}$$

but without the sign of φ_0 (Horinaka *et al* 1980). However, an offset in ε_A does contribute to $|\varphi_0|$.

Often, the condition $Y = \Omega = 0$ is required. When trying to set $\Omega = 0$, it has to be taken into account that this angle depends also on the parasitic ellipticities of the optical components (Kobayashi and Uesu 1983, 1985).

One problem which has not been treated explicitly is related to non-homogeneity of the sample. If the retardation varies, say, linearly from δ to $\delta + x$, $x \ll 1$, the average is

$$\langle\cos(\delta)\rangle_x = \frac{\int\cos(\delta)\,\mathrm{d}\delta}{\int\mathrm{d}\delta} \approx \cos(\delta)\frac{\sin(x)}{x}. \tag{2.2.3}$$

Similarly (see Kaminsky and Hartmann 1993; figure 17)

$$\left\langle\frac{\sin(\delta)}{\delta}\right\rangle_x \approx \frac{\sin(\delta)}{\delta}\frac{\sin(x)}{x}. \tag{2.2.4}$$

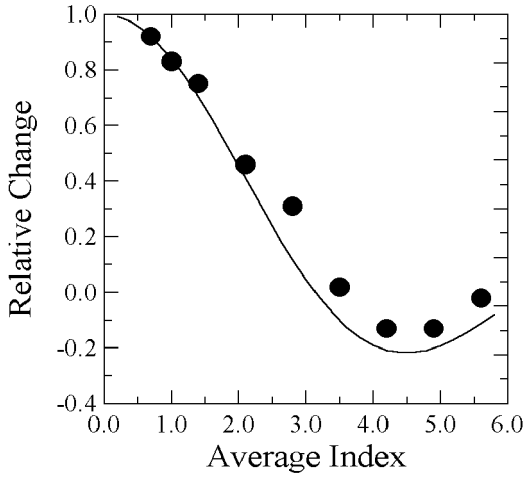

Figure 17. The additional modulation of a gyrative signal in a birefringent crystal that is inhomogeneous with respect to the retardation. Here, a TeO_2 crystal plate cut on (110) was slightly wedged. Increasing the illuminated region introduced a variation of retardation due to a linear variation in thickness. The gyrotropy was induced through the Faraday effect.

In case of an induced gyrotropy such as the Faraday effect, it is straightforward to separate out parasitic effects from a modulation of the gyrotropy itself (Kaminsky 1994). However, for the intrinsic Faraday effect, intrinsic electrogyration and optical rotation, further steps are required. So far, four different ways have been followed to reduce the obscuring effects of parasitic contributions:

(a) using optical components and samples of best possible quality and restricting measurements to large chiral effects at the same time (quartz for example);
(b) averaging two measurements with the sample at $\theta = 0$ and $\theta = 90^\circ$ (Moxon and Renshaw 1990);
(c) using additional compensator and polarization modulators to eliminate at least the parasitic contributions of the optical components (Becker *et al* 1990) and
(d) using a complete analytic expression of the equations relating I/I_0 and θ to δ. A variation of δ is introduced, for example, from a change of the sample orientation with respect to the direction of the wave vector when the sample is tilted. This allows a Fourier analysis of the different parts in equations (2.1.7) (Kaminsky and Glazer 1996).

For a small intrinsic gyrotropy, only (b) and (d) promised reliable results (where, of course, optical components and samples of good quality are still an advantage).

Equations (2.1.7) were approximated to quadratic order in the polarizing angles and for small azimuthal rotation and ellipticities. An exact solution with no restrictions was presented by Moxon and Renshaw (1990), who used the Jones matrix formalism. At the same time Becker *et al* (1990) derived similar expressions with an almost identical approach to the problem. Their final approximation up to quadratic order in the polarizing angles agrees with equations (2.1.7). On the same basis, Kremers and Meekes (1995a) derived approximate expressions up to fourth order in the polarizing angles.

Independently, and probably ignorant of the above results because of logistic problems, Konstantinova and co-workers found expressions equivalent to those of Kremers and Meekes (Konstantinova *et al* 1994, Fillipov *et al* 1994, Evdishenko *et al* 1991). In a recent paper, Konstantinova and Nabatov (1995) reported a technique more or less related to that of Szivessy and Münster (1934), where the optical parameters are derived from the rotation of the sample about the wavevector with arbitrary angles Y and Ω.

The different developments are summarized in table 3, where the expressions relating the

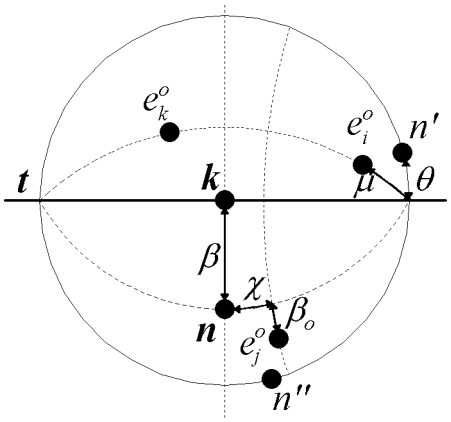

Figure 18. A stereographic projection showing the geometric relations of the indicatrix orientation and the laboratory reference system defined by the wavevector $\boldsymbol{k}$ and the tilt axis. $\boldsymbol{n}$ = plate-normal vector. e_i^o = principal axes of the indicatrix. β = tilt angle. n', n'' = vibration modes of the incident wave. θ = extinction angle. β_o, μ, χ = orientation of the indicatrix (Kaminsky 1994).

gyrotropy φ_0 to the measured values are easily derived from equations (2.1.5) and (2.1.7) and table 2.

The most recent experimental method (d), the 'tilter', is described below. The method is based on the idea proposed by Bruhat and Grivet (1935), and realized experimentally by Kobayashi and Uesu (1983), where I/I_0 is scanned against polarizer angle Y and analyser angle Ω, as well as Kurtzig's tilting of an $FeBO_3$ sample (Kurtzig *et al* 1969). In order to avoid retardation values δ where $\sin\delta$ and $\cos\delta$ reach unity or vanish, and to allow an analytic separation of optical rotation from parasitic effects, a plane-parallel shaped sample is tilted by an angle α with respect to the wavevector. The initial polarization is chosen parallel to the tilt axis. The variation of $\delta(\alpha)$ and $\theta(\alpha)$ is expressed analytically (β is measured 'between' n_j and n_i; see figure 18):

$$\begin{aligned} &\beta = \arcsin\left(\frac{\sin\alpha}{n_i}\right), \qquad \beta' = \beta - \beta_{\mathrm{o}}, \\ &\frac{1}{n'^2}(\beta) = \frac{\cos^2\beta'}{n_k^2} + \frac{\sin^2\beta'}{n_j^2}, \qquad n_i^2 = \frac{1}{a_{ii}^0} \end{aligned} \tag{2.2.5}$$

$$\tan 2\theta = 2\frac{(a_{kk} - a_{jj})\chi\sin\beta + (a_{kk} - a_{ii})\mu\cos\beta}{a_{kk} - a_{jj}\sin^2(\beta - \beta_{\mathrm{o}}) - a_{ii}\cos^2(\beta - \beta_{\mathrm{o}})}. \tag{2.2.6}$$

The polarization tensor $\{a_{ij}\}$ is defined by $\varepsilon_0 E_i = a_{ij} D_j$, where ε_0 is the permittivity of free space, $\boldsymbol{E}$ the electric field vector and $\boldsymbol{D}$ the dielectric displacement vector of the light wave. β and β_{o} are the tilt angles inside the sample and its offset with respect to the wavevector, respectively. μ and χ describe the orientation of the indicatrix with respect to the wavevector $\boldsymbol{k}$ and $\boldsymbol{k} \times \boldsymbol{t}$, respectively. The direction of vector $\boldsymbol{t}$ is along the tilt axis (figures 19(*a*) and (*b*)).

The intensity as a function of Y and Ω follows equations (2.1.7). A numerical method was developed to find (a) φ_0, μ, χ, (b) refined values of $n_i - n_k$, $n_j - n_k$, β_{o} and (c) ΔY, the effective deviation from $Y = 0 = \Omega$ as a result of parasitic ellipticities and the primary set-up of the polarizer (figure 20) (Kaminsky 1997, Mucha *et al* 1997).

The advantage of the tilter technique (d) over method (b) is its speed, resulting from a much higher initial intensity I_0 when using a laser. In (b) a monochromator is used in combination with a white-light source (Moxon *et al* 1991). The parasitic ellipticities are separated out in repeating the measurement with the sample rotated by 90°, which transforms δ into $-\delta$. The average scan calculated from the first and the repeated wavelength scan is independent of the parasitic contributions. However, the ΔY error is not completely eliminated with method (b) when the primary adjustment of the polarizer is not perfect.

Table 3. Historical developments in measuring gyrotropy. The results are obtained from equations (2.1.5) and (2.1.7), and table 2. For Horinaka *et al* (1980) see the text, section 2.1. In cases where the constraint $Y = \theta$ or $\Omega = 0$ is considered, an additional term arises which depends on ε_A and ε_P due to the parasitic ellipticities of the polarizer. The equations are approximated for small φ_0/δ and ε_A°. $\partial(I)/\partial\Omega = 0$ indicates the use of a lock-in amplifier to find the azimuthal rotation of the light after passing through the sample. Becker *et al* (1990) detect with a lock-in amplifier, in dependence of the problem, on ω_1, ω_2, ω_3, $\omega_1 - \omega_2$, $\omega_1 - \omega_3$, $\omega_2 - \omega_3$.

Authors	Property	Constraints/modulation	Equation
Szivessy and Minister (1934)	φ	$Y = \theta = \varphi = 0$	$\varphi_0 = \delta(\theta[\cos\delta - 1]\sin^{-1}\delta - \varepsilon_P)$
Bruhat and Grivet (1935)	φ	$Y = \theta = \varphi = 0/\delta(\lambda)$	$\varphi_0 = \delta(\theta[\cos\delta - 1]\sin^{-1}\delta - \varepsilon_P)$
Konstantinova *et al* (1969)	φ, $\partial(I)/\partial\Omega = 0$	$Y = \theta = 0/\delta(\lambda)$, $\Omega(\omega)$	$\varphi_0 = \delta(\varphi\sin^{-1}\delta - \varepsilon_P)$
Kurtzig *et al* (1969)	φ	$Y = \Omega = \theta = 0/g(H,\alpha)$, $\delta(\alpha)$	$\varphi_0(H) = \delta(\varphi(H)\sin^{-1}\delta)$
Anderson and Phil Won Yu Park (1974)	I/I_0	$Y = \Omega = \theta = 0/\delta(\lambda)$	$\lvert\varphi_0\rvert = (I/I_0)^{-1/2}\delta/\sin\delta/2 + \mathrm{O}(\varepsilon_A, \varepsilon_P)$
Horinaka *et al* (1980)	$\langle I_\omega\rangle_\delta/\langle I_{2\omega}\rangle_\delta$	$Y = \Omega = \theta = 0/\varepsilon_A^\circ\cos\omega t$, $\delta(\lambda)$	$\lvert\varphi_0\rvert = \varepsilon_A^\circ\delta\langle I_\omega\rangle_\delta/4\langle I_{2\omega}\rangle\delta + \mathrm{O}(\varepsilon_A)$
Kobayashi and Uesu (1983)	I/I_0	$\Omega = 0/Y, \theta$	Equations (2.1.7)
Moxon and Renshaw (1990)	I/I_0	$\Omega = 0/Y, \theta, \delta(\lambda)$	Equations (2.1.7)
Becker *et al* (1990)	$I/I_0, \varphi, \varepsilon$	$\varepsilon_P = 0/Y(\omega_1)\varepsilon_A(\omega_2)\Omega(\omega_3)$	Equations (2.1.7)
Kaminsky (1994)	φ, $\partial(I)/\partial\Omega = 0$	$Y = 0/g(E)\delta(\alpha)\theta(E,\alpha)\Omega(\omega)$	Table 2, equations (2.2.5), (2.2.6)
Kaminsky and Glazer (1996)	I/I_0	No constr./Y, Ω, $\theta(\alpha)$, $\delta(\alpha)$	Equations (2.1.7), (2.2.5) and (2.2.6)

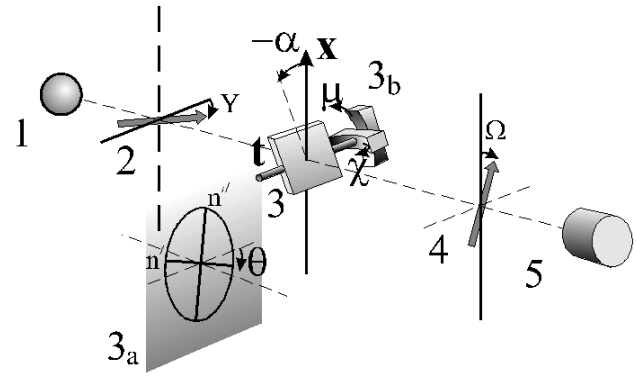

(*a*)

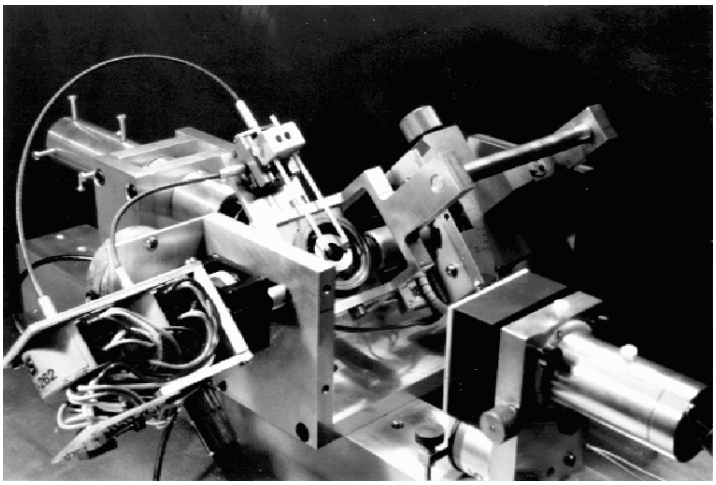

(*b*)

Figure 19. (*a*) The working principle of the tilter. 1, light source; 2, polarizer; 3, sample, where $\boldsymbol{t}$ is the direction of the tilt axis, $\boldsymbol{x}$ the direction normal to $\boldsymbol{t}$ and the direction of the light wave and finally μ, χ describe the orientation of the sample; α is the tilt angle; 4, analyser; 5, detector. 3_a shows the vibration modes of n' and n''. (*b*) A photograph of the first tilting polarimeter (size $50 \times 50 \times 15$ cm^3) to measure intrinsic optical rotation.

2.3. Theory of optical rotation

Circular birefringence effects are discussed in the following in the long-wavelength approximation, i.e. for a light wave far outside absorption.

As there are several explanations describing the origin of optical rotation, the question arises as to their differences. In the first interpretation, optical rotation is explained by the generation of a circularly polarized reflected wave in a pile of birefringent plates, the thickness of which then is successively lowered ('Reuschsche Glimmersäule'). A theoretical description of the small reflections arising from the discontinuities between the plates, which are arranged in a helix, i.e. each plate is rotated slightly with respect to the previous one, results in (see

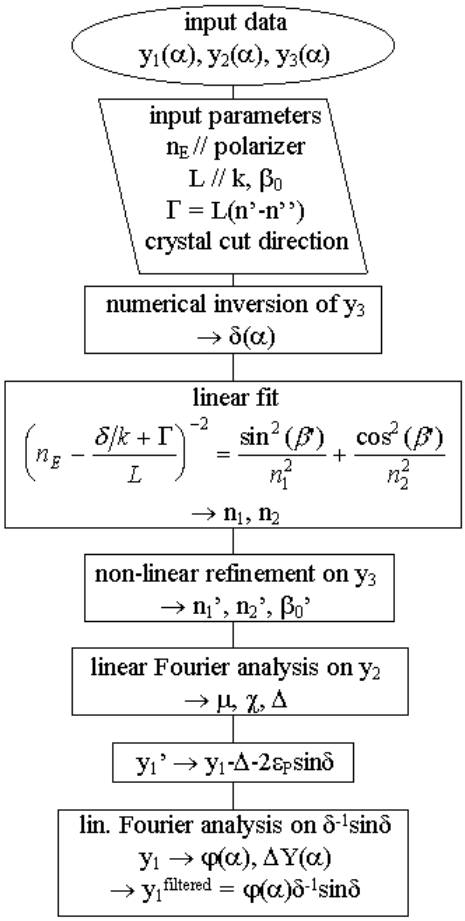

Figure 20. A flow chart of a data analysing program used for tilt scans measured with the tilter method. The program needs as its input the retardation $\Gamma = L(n' - n'')$ of the crystal section where L = thickness of the sample and n' and n'' are refractive indices of the section. Further, the basic orientation of the section has to be specified (acute bisectrix, obtuse bisectrix, optic axis plane (flash figure), the tilt offset β_o), and the refractive index $n(E)$ is basically equal to either n' or n'' parallel to the polarization of the incident wave. The input data are the raw parameters as in equation (2.2.4) with data pairs $y_1(\alpha)$ representing the contribution assigned with the tilter procedure to $\sin\delta$, $y_2(\alpha)$ assigned to $(1-\cos\delta)$ and parasitic effects and $y_3(\alpha)$ assigned to $\cos\delta$. This results from a fit to the intensity surface, equations (2.1.7) and tilting of the sample, see equation (2.2.3). The program first finds from $y_3(\alpha)$ the start values n_1, n_2 for the refractive indices along the principal directions of the indicatrix relative to that of $n(E)$ by a numerical procedure which enables an analytic expression $\delta(\beta)$, where β is the tilt angle inside the sample. Further refinements of these values (n_1', n_2', β_o'; n_1'', n_2'', β_o'') and exclusion of the parasitic effects leaves as output the refined birefringence, the orientation of the indicatrix (β_o'', μ, χ) and the optical activity $\varphi(\beta)$, as well as the filtered function $\varphi(\beta)\sin[\delta(\beta)]/\delta(\beta)$ by subtracting from $y_1(\beta)$ the excluded parasitic effects.

Bergmann and Schäfer 1978)

$$\rho = \frac{180}{p}\frac{r^2}{\lambda'^2(1-\lambda'^2)}, \qquad \lambda' = \frac{\lambda}{pn}, \qquad p = \text{ pitch of helix},$$
$$r = \frac{n_1 - n_2}{n_1 + n_2}, \tag{2.3.1}$$
$$n_{1/2} = \text{refractive indices of each plate.}$$

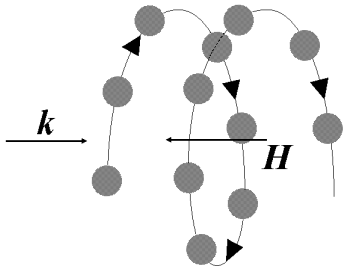

Figure 21. A light with wavevector $\boldsymbol{k}$ passes through a helix. Atoms are *coupled* in such a way that an oscillating current moves along the helix chain, which produces an oscillating magnetic field $\boldsymbol{H}$.

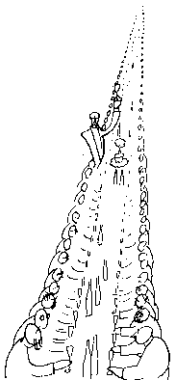

Figure 22. This drawing by Olaf Gulbransson shows nicely the interaction between a single individual with all the others in a periodic structure. (Courtesy of Albert Langen Georg Müller Verlag, München. From Gulbransson D B 1977*Das Olaf Gulbransson Buch*.)

This explanation could be considered to be related to the effect of texture of an anisotropic material rather than describing intrinsic optical rotation.

Optical rotation is also connected to the electric dipole $\boldsymbol{R}$ and magnetic dipole $\boldsymbol{M}$ as well as electric quadrupole moments $\boldsymbol{Q}$ (Rosenfeld 1928, Condon 1937) of a single molecule (see figure 21), where the effect of an incoming field generates an oscillating current in the chiral molecule along the helix. It should be pointed out that this current is possible only if the atoms on the helix interact.

The effect of a periodic infinite structure is that an atom has to be related to the effect of all other atoms within the structure due to the long-range nature of electrodynamics interactions (see below and figure 22).

For the sake of simplification, depolarization effects (to be taken into account in dense media) are neglected when describing the electrical and magnetic moments. The following is an expression of the complex refractive index n (Michl and Thulstrup 1986):

$$n = 1 + \frac{2N\pi^2}{hvk^3c^3}\left|\langle f|\frac{e}{m}\mathrm{e}^{\mathrm{i}\boldsymbol{k}\cdot\boldsymbol{r}}\boldsymbol{e}\cdot\boldsymbol{p}|i\rangle\right|^2 (S' + \mathrm{i}S). \tag{2.3.2}$$

Here, N is the number of particles in volume v, h is Planck's constant, k is the wavenumber ($k = 1/\lambda$), c is the vacuum velocity of light, e AND m are the charge and mass of the electron, $\boldsymbol{e}$ is the polarization of the wave at space point $\boldsymbol{r}$, $|i\rangle$ and $\langle f|$ are initial- and final-state wavefunctions, S' is the dispersion line-shape function and S describes spectral dependence on dissipation.

Next, the exponential needs to be expanded in a Taylor series:

$$\mathrm{e}^{\mathrm{i}\boldsymbol{k}\cdot\boldsymbol{r}} = 1 + \mathrm{i}\boldsymbol{k}\cdot\boldsymbol{r} - 0.5(\boldsymbol{k}\cdot\boldsymbol{r})^2 + \cdots$$

and the polarization has to express left and right circular polarization:

$$\boldsymbol{e} \to \boldsymbol{e}_L = (\boldsymbol{x}_1 + \mathrm{i}\boldsymbol{x}_2)/\sqrt{2}, \qquad \boldsymbol{e} \to \boldsymbol{e}_R = (\boldsymbol{x}_1 - \mathrm{i}\boldsymbol{x}_2)/\sqrt{2},$$

respectively, $\boldsymbol{k} = k\boldsymbol{x}_3$, where $\boldsymbol{x}_i$ are the unit vectors of a Cartesian reference system. From the difference of circular birefringence $n_\mathrm{L} - n_\mathrm{R}$ as a result of insertion of the circular polarization, the optical rotation ($^\circ$ m^{-1}) is calculated (Rosenfeld equation):

$$\delta = 180\frac{2kN\pi}{nhvc}\left\{\mathrm{Im}\,[R_j^{fi}M_j^{if}]_{j=1,2} + \frac{k}{2}[R_2^{if}Q_{13}^{fi} - R_1^{if}Q_{23}^{fi}]\right\}(S' + \mathrm{i}S) \tag{2.3.3}$$

where $R_j^{fi} = \langle f|er_j/m|i\rangle$ (electric dipole moment), $M_j^{if} = \langle i|e(\boldsymbol{r}x\boldsymbol{p})_j/2mc|f\rangle$(magnetic dipole moment) and $Q_{jk}^{fi} = \langle f|er_jr_k|i\rangle$ (electric quadrupole moment).

This model in principle describes optical rotation of organic molecules in solution (Michl and Thulstrup 1986). Since all possible transitions contribute, the optical rotation is to be calculated from the sum over all excited states f, which in general does not converge (Eyring, Walter and Kimball 1944). Amos (1982) applied a static field approximation to the Rosenfeld equation, and a practical solution is found when simplifying further, introducing linear response functions. When neglecting the quadrupole terms, the sum over Im $[R^{fi}M^{if}]S'$ is replaced by the sum over all states k in $\langle n|\boldsymbol{R}|k\rangle\langle k|\boldsymbol{M}|n\rangle/(\omega - \omega_k + \omega_n) - \langle i|\boldsymbol{M}|k\rangle\langle k|\boldsymbol{R}|i\rangle/(\omega + \omega_k - \omega_n)$. Here, n and k denote ground and excited states, i.e. no excited state wavefunctions have to be computed. Within this approximation, $\boldsymbol{R}$ and $\boldsymbol{M}$ are interpreted as interaction operators (Jørgensen *et al* 1988, Helgaker *et al* 1994). Further details are given by Kondru *et al* (1998, 1999), who applied the theory successfully for assigning stereochemistry using optical rotation.

The following will attempt to show the close connection between the Rosenfeld equation and other models, and especially the dipole–dipole interaction theory. Condon, Altar and Eyring (1937) introduced an anharmonic oscillator potential which takes account of the bond in which a valence electron moves (A: anharmonic 'amplitude'):

$$V = \tfrac{1}{2}m\omega_i^2x_i^2 + Ax_1x_2x_3. \tag{2.3.4}$$

The bond is oriented along x_1, x_2, x_3, and only bonds with orthorhombic symmetry are described by this potential. The matrix elements of the Rosenfeld equation are calculated from this, using first-order perturbation theory and neglecting quadrupole terms. The model connects the matrix elements to an anharmonic potential but does not specify what the physical origin of this potential is related to. The constant A is taken from experiment and, because the model describes the nonlinear effect of frequency doubling (SHG) as well, it is possible to compare an experiment with a calculation of optical rotation, using an A-value for such a calculation which stems from the independent measurement of the SHG coefficients (Jeggo 1972).

Optical rotation of transparent crystals was calculated from self-energy correction to the local density approximation theory without success because of a strong deviation from the experimental results despite the fact that the same theory describes well the linear and second-harmonic susceptibilities (see the review by Levine (1994)). It was shown recently that 'scalar local fields' resulting from an interaction between the atoms within a structure have to be introduced, which changed the calculations by a factor of seven in quartz, for example (Jonsson *et al* 1996), and the final result of these nearly first-principles calculations is within 30% of the experimental result in quartz.

Another example employing the local density approximation theory was published recently (Yabana and Bertsch 1999). Here, time-dependent local density approximations are used to produce spectra of optical rotation and circular dichroism in R-methyloxirane and the double-helical fullerene C_{76}. The theory outlined in this paper automatically satisfies sum rules and the Kramers–Kronig relation between circular dichroism and the rotatory power. The chiroptical properties are described qualitatively as considerable deviations (a factor of two to four) are found in the dichroism of the lowest states and in C_{76} the spectra are all shifted along the wave energy.

Figure 23. Max Born. Born in Breslau, Germany, 11 December 1882. Died Göttingen, Germany, 6 January 1970. Nobel price 1954 (source: *The MacTutor History of Mathematics Archive*).

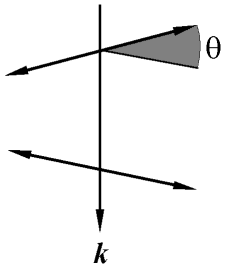

Figure 24. Two coupled oscillators, tilted towards each other by an angle θ (Chandrasekhar 1961).

There had been earlier attempts to work out how optical rotation is related to the interaction phenomena between atoms. Born (1915) (figure 23) writes for example 'Wenn ein Partikel mit den übrigen nicht mechanisch gekoppelt ist, so trägt es nichts zur optischen Aktivität bei' ('if a particle is not mechanically coupled to the others it does not contribute to optical rotation'). Chandrasekhar (1961) took advantage of the theory by Born and introduced a coupled oscillator model to derive the dispersion of optical rotation. Two oscillating electrical dipoles qr_1 and qr_2, separated by a distance d, are tilted with respect to one another about d by the angle θ (figure 24).

The anharmonic dipole–dipole interaction contribution to the potential energy is $q^2 r_1 r_2 \cos\theta/d^3$. It is different from Condon's potential but depends also on a product of all three coordinates of the reference system. It is to be expected that, using first-order perturbation theory, again an expression for the matrix elements is obtained which leads to optical rotation as is described by the Rosenfeld equation. The dispersion derived by this model† describes well the observed wavelength dependence for example in quartz along the optical axis:

$$\rho = \frac{Ne^4\lambda_o f^2 \sin\theta\cos\theta}{2\pi m^2 d^2 c^4}\frac{\lambda^2}{(\lambda^2-\lambda_o^2)^2}. \tag{2.3.5}$$

Further work by Ramachandran and Ramaseshan (1961) based on the anisotropic polarizability theory resulted in the following expression for optical rotation:

$$\rho = \frac{3pl^2\pi^2(n^2-1)(\alpha_r^2-\alpha_t^2)}{4\lambda^2[\pi R^5(\alpha_r-\alpha_t)+(3l^2-R^2)\alpha_r\alpha_t]} \tag{2.3.6}$$

where l is the distance from an atom to the helix axis, R the distance between neighbouring atoms, p the helix repeat distance, λ the wavelength of light, n the (ordinary) refractive index

† Although there is an error in the equations leading to (2.3.5), this expression is a good appproximation at least.

Figure 25. Paul Peter Ewald, 1888–1985 (courtesy of the *AIP Emilio Segri Visual Archives*).

and α_r and α_t are the polarizability components directed parallel and perpendicular to the distance l, respectively.

The above treatment does not take account of the special case of a crystal lattice and its periodicity. However, the Hertz-vector potential and formalism (Born and Goeppert-Mayer 1933, Beurskens-Kerssen *et al* 1963, Van Laar *et al* 1968) does take account of all interactions between the atoms inside a crystal acting on an atom at position s in the unit cell l:

$$\boldsymbol{Z}_{s'}^{l'}(\boldsymbol{r}_s^l) = \exp(-\mathrm{i}\omega t)\sum_{s'}\boldsymbol{p}_{s'}\exp(\mathrm{i}\boldsymbol{k}\cdot\boldsymbol{r}_s^l)\left\{\sum_{l'}{}' \frac{\exp[\mathrm{i}k_o|\boldsymbol{r}_s^l-\boldsymbol{r}_{s'}^{l'}|-\mathrm{i}k(\boldsymbol{r}_s^l-\boldsymbol{r}_{s'}^{l'})]}{4\pi\varepsilon_0|\boldsymbol{r}_s^l-\boldsymbol{r}_{s'}^{l'}|}\right\}. \tag{2.3.7}$$

$\boldsymbol{p}_{s'}$ is the polarization of atom s', $\boldsymbol{r}_s^l = (r_i\boldsymbol{x}_i)_s^l$ is the local vector of the atom s on which all fields act and $\boldsymbol{r}_{s'}^{l'}$ points to all other atoms.

The term in curly brackets is independent of the choice of unit cell index l' and has the periodicity of the lattice. The sum† which represents a series of only conditional convergence is decomposed into a Fourier series, and the Ewald theorem (Ewald 1921; figure 25) is used to produce convergence by splitting the Fourier series into a part in real space and a part in reciprocal space, each absolutely convergent.

The electric field $\boldsymbol{E}(\boldsymbol{r}_s^l)$ at atom $\boldsymbol{r}_s^l$, which originates from the dipole waves emanating from all the other atoms (point dipoles) in the structure, is given as

$$\begin{aligned}\boldsymbol{E}(\boldsymbol{r}_s^l) &= \operatorname{grad}\operatorname{div}\boldsymbol{Z}_{s'}^{l'} - \frac{\partial^2\boldsymbol{Z}_{s'}^{l'}}{c^2\partial t^2} = \alpha_s^{-1}\boldsymbol{p}_s^l = \sum_{s'}A_{ss'}\boldsymbol{p}_{s'}^l \\ &= \sum_{s'}\left(Q_{ss'} + \frac{\delta_{ij}-n^2k_ik_jk^{-2}}{v\varepsilon_0(n^2-1)}\right)\boldsymbol{p}_{s'}^l\end{aligned} \tag{2.3.8}$$

where α_s is the polarizability volume of atom‡ s and where $A_{ss'}$ is the complex tensor independent of cell choice l from which optical rotation is derived (Reijnhart 1970, Devarajan and Glazer 1986) as

$$\begin{aligned}&\rho(\boldsymbol{k}) = \sum_{ijk}\frac{-e_{ijk}k_i}{2nv}\operatorname{Im}\sum_{ss'}(\alpha_s^{-1}\delta_{ss'}-Q_{ss'})_{jk}^{-1}, \\ &e_{ijk} = \text{Levi-Cività symbol.}\end{aligned} \tag{2.3.9}$$

† The Ewald sum is not just summing up the polarizabilities of the atoms in a unit cell. It is instead a sum of all interacting fields and possesses as such a completely different symmetry.

‡ Summations are written out explicitly in equations (2.3.8) and (2.3.9).

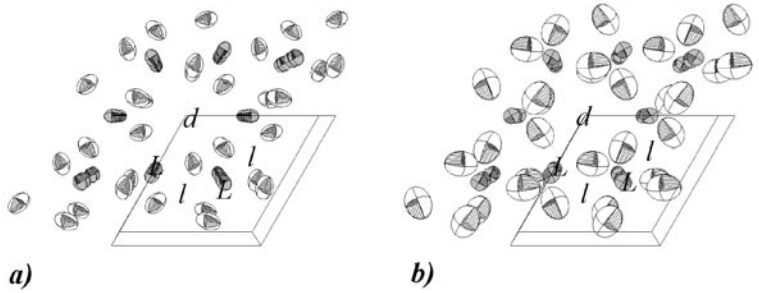

Figure 26. The structure of laevorotative α-quartz (SG $P3_121$). (*a*) Thermal ellipsoids, shown at their 99% probability value. (*b*) Anisotropic polarizabilities calculated with the dipole–dipole model. The letters L, l, d are positioned in the centre of a helix. L: laevorotative helix with tangential thermal ellipsoids. l, d: laevorotative or dextrorotative helices with radial thermal ellipsoids.

The symmetrical real part of $(\alpha_s^{-1}\delta_{ss'} - Q_{ss'})^{-1}_{jk} = C_{ss'}$ is taken to calculate the refractive indices and an 'effective' anisotropic polarizability according to

$$\varepsilon_{ij} = \delta_{ij} + \frac{1}{v}\sum_{ss'}(C_{ss'})_{ij}; \qquad \alpha_s^{\text{eff}} = \text{Re}\,\Sigma_{s'}C_{ss'}. \tag{2.3.10}$$

The effective polarizabilities α_s^{eff}, however, are not to be mistaken for the atomic polarizability. Instead, they result from a superposition of isotropic polarizability volumes α_s and the effects of the dipole–dipole interaction. Along short atomic distances, this interaction is expected to be larger than elsewhere in contrast to the thermal motion of the atoms, which is restricted in these directions. Thus, an inverse correlation is observed between the thermal ellipsoids of a structure and the shape of the effective polarizabilities.

In analysing expression (2.3.6) optical rotation φ can be discussed qualitatively from a known structure and the anisotropic polarizabilities (Glazer and Stadnicka 1986):

$$\varphi \propto \frac{l^2 tnN}{u}(\alpha_r^2 - \alpha_t^2). \tag{2.3.11}$$

This relation enables one to determine the sign of optical rotation by inspection of the helical arrangements of atoms in a structure according to the following principles.

(1) All $\boldsymbol{N}$ helixes found in the structure contribute to optical activity independently.
(2) The highly polarized atoms will give the main contribution.
(3) The directions of shortest distances between polarized atoms will correspond to the direction of highest polarizability.
(4) Incident light will be rotated in an opposite sense to that of the helix if the component of the anisotropic electronic polarizabilities in the direction of the helix axis is largest (radial polarizabilities, $\boldsymbol{\alpha_r > \alpha_t}$).
(5) The effect increases with the distance $\boldsymbol{l}$ of the atoms towards the screw axis and number of turns $\boldsymbol{t}$ per screw and decreases with the pitch $\boldsymbol{u}$ of the screw (but increases if the unit cell is larger).
(6) The effect is largest for $\boldsymbol{n} = 4$ atoms per screw unit.

As an example, let us consider laevorotative α-quartz, SiO_2. Figure 26 shows the structure, space group $P3_121$ (Le Page and Donnay 1976). The four laevorotative and one dextrorotative helices found in the structure along the *c*-axis favour a laevorotative optical rotation along the *c*-axis.

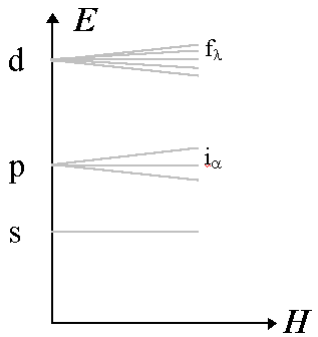

Figure 27. Zeeman splitting of energy, E of s, p and d orbitals in a magnetic field, H.

2.4. The Faraday effect

The Faraday effect can be described as (Bequerel and de Haas 1928, Schütz 1936, Smith 1976)

$$\rho = \frac{\partial n}{\partial E}\Delta E + \frac{\partial n}{\partial R}\Delta R + \frac{\partial n}{\partial N}\Delta N \tag{2.4.1}$$

where E is the energy of a transition, n the refractive index of the material, R the dipole moment and N the number of states of an energy level in a paramagnetic ion. However, these three terms do not follow from optical rotation. Zeeman splitting (figure 27) of a single transition $i \rightarrow f$ into d energy levels $i \rightarrow i_\alpha$ and the splitting of final states $f \rightarrow f_\lambda$ changes the interpretation significantly and the calculations start directly from inserting the circular polarization into the refractive index in equations (2.3.1). $\Delta R\partial n/\partial R$ is that part of the Faraday rotation which depends on the dipole transition moments $\boldsymbol{R}(\boldsymbol{B})$ changed by a magnetic induction $\boldsymbol{B}$. The effects on the dipole transition moment, number of states N and energy levels E are calculated from first-order perturbation theory (Stephens 1965, 1974); ($[\rho] = {}^\circ\ \mathrm{m}^{-1}$). B_j is the component of the magnetic induction along the magnetic dipole moment M_j:

$$\begin{aligned}\rho = 180\frac{2Nk\pi}{nhcv}B_j\Bigg[&\frac{1}{d}\frac{\partial(S'+\mathrm{i}S)}{\partial E}\mathrm{Im}\,(R^{f_\lambda i_\alpha}\times R^{i_\alpha f_\lambda})_j(M_j^{f_\lambda f_\lambda}-M_j^{i_\alpha i_\alpha})\\ &+2\Bigg((R^{if}\times R^{i\alpha})_j\frac{M_j^{i_\alpha}}{E_\alpha-E_i}+(R^{fi}\times R^{i\lambda})_j\frac{M_j^{f_\lambda}}{E_\lambda-E_f}\Bigg)(S'+\mathrm{i}S)\\ &+\frac{1}{d}(R^{f_\lambda i_\alpha}\times R^{i_\alpha f_\lambda})_j\frac{M_j^{i_\alpha i_\alpha}}{KT}(S'+\mathrm{i}S)\Bigg]\end{aligned} \tag{2.4.2}$$

(K Boltzmann constant, T temperature). Within this expression the sum of all possible allowed transitions has to be taken to find the magnetic field induced rotation outside an absorption peak. It is obvious from equation (2.4.2) that any Faraday rotation vanishes if the wavevector and the magnetic induction are perpendicular to each other, because then the effective component of the magnetic moment is a linear combination of the effective electric dipoles†.

Since $\boldsymbol{B} = \boldsymbol{H} + \boldsymbol{M}$, the Faraday tensor depends on the direction of the applied field, the angle between the wavevector and the applied magnetic field $\boldsymbol{H}$ and any macroscopic magnetization $\boldsymbol{M}$:

$$\delta(\boldsymbol{k}, \boldsymbol{H}) = \frac{1}{kH^2}H_i H_j V_{ij}(\boldsymbol{k}\cdot(\boldsymbol{H}+\boldsymbol{M})), \tag{2.4.3}$$

† The dielectric dipole moments $\boldsymbol{R}^{if} = \langle f|e\boldsymbol{r}/m|i\rangle$ are in proportion to the vectors $\boldsymbol{r}$, which are the displacements of charges perpendicular to $\boldsymbol{k}$ of the transitions (i–f and f–i); any electronic magnetic moment $\boldsymbol{M}$ is parallel to the magnetic induction $\boldsymbol{B}$; $\rho \propto (\boldsymbol{R}^{if}\times\boldsymbol{R}^{fi})\cdot\boldsymbol{M} \propto \boldsymbol{k}\cdot\boldsymbol{B}$.

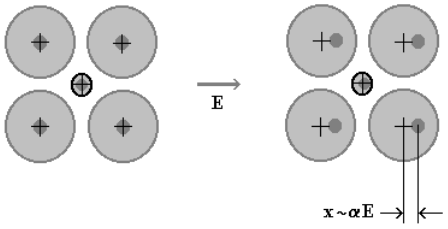

Figure 28. The nuclei inside the atoms are assumed to be slightly dislocated along the direction of an external static electric field. Because this effect depends on the polarizability of the atoms, the positions of which are mainly fixed via the interactions between the electron shells, the symmetry of the structure is changed.

where V_{ij} is the Verdet constant. Equation (2.4.3) implies that a transversal Faraday rotation in a monoclinic or triclinic crystal is possible when the effective magnetic induction $\boldsymbol{B}$ is not perpendicular to the wavevector.

Although the induced changes of the electric dipole moments are small, a change of the dipole–dipole interaction may contribute to the rotation in a crystal (magneto-activity).

According to observation the Faraday effect is rather insensitive to the structure and, in the case of a phase transition, is affected mainly through an additional birefringence or changes of the sample's density (Kaminsky and Bismayer 1993, Kaminsky and Haussühl 1993, Haussühl and Effgen 1988).

Some kind of spontaneous Faraday effect may exist in antiferromagnetic crystals. A careful and thorough study of high-order contributions by electric octupole and magnetic quadrupole moments lead to a characteristic geometry of this effect in cubic antiferromagnets (Graham and Raab 1991).

Another theoretical approach to explain the Faraday rotation of semiconductors was derived by Boswarva *et al* (1962), which takes account of the details of semiconducting bonds. However, the result does not describe well the Faraday effect of transparent organic or inorganic crystals.

2.5. Electrogyration

The effect of a static electric field on the structure is, first, to polarize the atoms, which in a crude approximation can be seen as a shift x of the nuclei along the field relative to the electron clouds which surround the atom's nuclei. Second, the field affects the wavefunctions governing the electronic transitions (see below), which, in classical terms, leads to a change of the polarizability volume due to the electric field and results in Miller (1973)

$$\rho(E) = \frac{\partial \rho}{\partial x}\frac{\partial x}{\partial E} + \frac{\partial \rho}{\partial \alpha}\frac{\partial \alpha}{\partial E}. \tag{2.5.1}$$

The shift of the cloud of the kth atom is† (figure 28)

$$x_i(k) = \frac{4\pi\varepsilon_0}{e}\alpha_{ij}(k)E_j^{\mathrm{loc}}, \tag{2.5.2}$$

where α_{ij} is the polarizability volume tensor, e the electron charge and E_j^{loc} the electric field at the atom.

A simple method of calculating electrogyration uses the dipole–dipole interaction model of Devarajan and Glazer (1986) as a starting point, which calculates the optical rotation and the refractive indices via the optical dielectric tensor $\varepsilon_{ij}^{\mathrm{o}}$ (see above). n = average refractive index, polarizability tensor $\{a_{ij}\}$ is the inverse of $\{\varepsilon_{ij}^{\mathrm{o}}\}$, λ = wavelength, ρ_{ij} ($^\circ\,\mathrm{m}^{-1}$) is rotatory power

† In a static field, the polarization results from a shift of the nucleus in the direction of the electric field vector because the electron clouds (in the hard-sphere approximation) cannot move in a crystal. At optical frequencies these clouds vibrate about the position of the nuclei, the position of which is used for the calculations.

and ε' the effective (low-frequency) dielectric constant along the external electric field $\boldsymbol{E}$. Assuming a spherical depolarization field (Lorentz depolarization), it follows that

$$\begin{aligned} \rho_{ij}(E_k) - \rho_{ij}(0) &= \frac{180}{n\lambda} E_k g_{ijk}, \\ a_{ij}(E_k) - a_{ij}(0) &= E_k r_{ijk}, \\ E_j^{\mathrm{loc}} &= \frac{\varepsilon' + 2}{3} E_j, \end{aligned} \tag{2.5.3}$$

where g_{ijk} are the tensor components of the electrogyration and r_{ijk} those of the linear electro-optic effect at constant strain (Kaminsky and Glazer 1997, 1998).

Using this model (dipole–dipole interaction and electron-cloud shifting: DES model, with minor modifications) the d-coefficients of SHG are calculated with some success (Kaminsky and Glazer 1997). However, in neglecting the change of the polarizability, the model is limited to structures consisting of atoms with a relatively small polarizability.

In general, the shift or splitting of energy levels due to an electric field (linear Stark effect) is small or forbidden by parity rules. The wave functions, however, are affected by the field (Hameka 1970):

$$\begin{aligned} |i\rangle(E) &= |i\rangle - E_k \sum_\alpha \frac{\langle \alpha | e r_k | i \rangle}{E_i - E_\alpha} |\alpha\rangle, \\ \langle f|(E) &= \langle f| - E_k \sum_\alpha \frac{\langle f | e r_k | \alpha \rangle}{E_f - E_\alpha} \langle \alpha|, \end{aligned} \tag{2.5.4}$$

$|\alpha\rangle$ are all states belonging to energy niveaus different to the ground state $|i\rangle$ with energy E_i and final state $\langle f|$ with energy E_f; er_k is the electric dipole of the atom. Following the Rosenfeld equations (2.3.1), we find (neglecting quadrupole terms) with wavevector $\boldsymbol{k} = (0, 0, k)$

$$\rho(E_k) = 180 \frac{2Nk\pi}{nhvc} E_k (S' + \mathrm{i}S) \mathrm{Im} \left[\sum_\alpha \left(R_j^{i\alpha} \frac{R_k^{\alpha f}}{E_\alpha - E_f} + R_j^{\alpha f} \frac{R_k^{i\alpha}}{E_\alpha - E_i} \right) M_j^{fi} \right]_{j=1,2}. \tag{2.5.5}$$

The correction to (2.3.2) related to perturbed wavefunctions seems to be approximately in proportion to the square of the electric dipole transition moments to which the polarizability volume is correlated. The states α, i, and f need to be non-degenerate to allow for electrogyration which may result from internal crystal fields.

Stasyuk and Kotsur (1985a, b) argue that one can treat electrogyration in a similar way in the degenerate case, introducing 'proper' wavefunctions describing the 'zero-order' approximation of electrogyration.

Further, a result of Miller (1973) can be used to derive an expression relating the magnitude of the two different contributions to electrogyration:

$$\frac{\partial \rho}{\partial x} \frac{\partial x}{\partial E} : \frac{\partial \rho}{\partial \alpha} \frac{\partial \alpha}{\partial E} \cong \pm \frac{4\pi a_1^3}{(n^2 - 1) a_0^3} \tag{2.5.6}$$

which depends on the difference of stiffness constants describing the difference in the mobility of the atoms (a_1) inside the structure with lattice constant a_0 and the magnitude of the polarizability, which is crudely in proportion to $(n^2 - 1)a_0^3/4\pi$, confirming that the effect of the electric field on the polarizability is to be considered only in strongly polarized atoms.

The second conclusion is that the simple electron cloud shifting model is not able to calculate electrogyration or any other electric field induced effect in monatomic crystals such as Te or those which consist of very similar atoms. The applicability of the model to other structures is demonstrated below when its results are compared with experimental values.

In addition, Miller (1973) proposed the idea that nonlinear third-rank optical properties t_{ijk} are described by a constant $= t_{ijk}(n^2-1)^{-2}(\varepsilon-1)^{-1}$, which was found to be consistent with experiment in case of the SHG and the electro-optic effect (Miller 1964). However, Weber and Haussühl (1976) showed that this rule is not applicable to electrogyration.

2.6. Combined effects

A Taylor expansion of the constitutive equation gives insight into some relations concerning high-order effects (see also Kharchenko (1994), Graham and Raab (1992)):

$$\begin{aligned}\frac{1}{\varepsilon_0}D_i = \varepsilon_{ij}E_j + z_{ijk}\frac{\partial E_j}{\omega\partial t}H_k + z^{\mathrm{eFr}}_{ijkl}\frac{\partial E_j}{\omega\partial t}H_kE_l \\ + g^{\mathrm{oa}}_{ijk}\frac{\partial E_j}{\partial x_k} + g^{\mathrm{egy}}_{ijkl}\frac{\partial E_j}{\partial x_k}E_l + g^{\mathrm{moa}}_{ijkl}\frac{\partial^2 E_j}{\omega\partial x_k\partial t}H_l \\ + g^{\mathrm{meg}}_{ijklm}\frac{\partial^2 E_j}{\omega\partial x_k\partial t}E_lH_m + g^{\mathrm{p}}_{ijklm}\frac{\partial E_j}{\partial x_k}\sigma_{lm}\end{aligned} \tag{2.6.1}$$

where we find the Faraday tensor z_{ijk}, electro-Faraday rotation z^{eFr}_{ijkl}, optical rotation g^{oa}_{ijk}, electrogyration g^{egy}_{ijkl}, magneto-activity g^{moa}_{ijkl}, magneto-electrogyration g^{meg}_{ijklm} and piezogyration g^{p}_{ijklm}. ω is the angular frequency of a plane light wave $\boldsymbol{E} = \boldsymbol{E}_0\mathrm{e}^{\mathrm{i}(\boldsymbol{kx}-\omega t)}$. These expressions are allowed in dia- or paramagnetic materials satisfying time inversion symmetry. If this plane wave is inserted for E_j, it follows that

$$\frac{\partial E_j}{\partial x_k} = \mathrm{i}k_kE_j = k_k\frac{\partial E_j}{\omega\partial t} \tag{2.6.2}$$

and reversal of time t results in $H(t) = -H(-t)$, $E_j(t) = E_j(-t)$, $k_k(t) = -k_k(-t)$. If only a non-dissipative contribution of the different effects is allowed we have $g_{ijklm\ldots} = e_{ijp}k\Gamma_{pklm\ldots}$, and $z_{ijk\ldots} = e_{ijp}Z_{pk\ldots}$. $e_{ijp} = -e_{ipj}$: Levi-Cività symbol, $\kappa = \boldsymbol{k}/k$. With these definitions the equation becomes

$$\begin{aligned}\frac{1}{\varepsilon_0}D_i = \varepsilon_{ij}E_j + e_{ipj}\frac{\partial E_j}{\omega\partial t}[Z_{pk}H_k + Z^{\mathrm{eFr}}_{pkl}H_kE_l + \kappa_k(\Gamma^{\mathrm{oa}}_{pk} + \Gamma^{\mathrm{egy}}_{pkl}E_l + \mathrm{i}\Gamma^{\mathrm{moa}}_{pkl}H_l \\ + \mathrm{i}\Gamma^{\mathrm{meg}}_{pklm}E_lH_m + \Gamma^{\mathrm{p}}_{pklm}\sigma_{lm})] = \varepsilon_{ij}E_j - \mathrm{i}(\boldsymbol{g}\times\boldsymbol{E})_i.\end{aligned} \tag{2.6.3}$$

The fact that the coefficients for magneto-activity and magneto-electrogyration are imaginary shows that this formalism may be insufficient to treat them as a gyrotropy. More details are given in section 3.2.3.

Equation (2.6.3) is connected with the wave equation. In using equation (2.1.2) and assuming cubic symmetry ($\varepsilon_{ij} = \varepsilon = n_2$) it follows that

$$\begin{aligned}(n^2_{\mathrm{L/R}} - n^2_{\mathrm{o}})^2 = (\kappa_ig_i)^2 \\ \varphi = \frac{180L}{\lambda}(n_{\mathrm{L}} - n_{\mathrm{R}}) = \frac{180}{n\lambda}L\kappa_ig_i.\end{aligned} \tag{2.6.4}$$

A rotation of the sample by 180° perpendicular to the wavevector changes the sign of the electric field and of the observed electrogyration $\Gamma^{\mathrm{egy}}_{pkl}E_l$. In an isotropic medium such rotation is not distinguished in $\Gamma_{pkl} \equiv \Gamma$ and electrogyration cannot exist in gases or fluids. The same argument holds for the magneto-electrogyration. Further crystal symmetry related restrictions are derived in analysing the transformation of tensors†:

$$t_{ij,\ldots,k} = u_{i\alpha}u_{j\beta}\cdot\ldots\cdot u_{k\chi}t_{\alpha\beta\chi} \tag{2.6.5}$$

† Again, we use the Einstein convention for sums which have to be carried out over each pair of identical indices.

where u_{ij} represents one of the point symmetry operations of a point group. If we ask for invariance of a tensor component $t_{ij,\ldots,k}$ it has to be equal to $t_{\alpha\beta\chi}$. This often leads to the relation $t_{ij,\ldots,k} = -t_{ij,\ldots,k}$ and this component is forbidden by symmetry (see further Haussühl (1983) or Nye (1957)).

An external stress or electric field deforms the crystal, causing additional birefringence via the electro- and piezo-optic effect ($\Delta a_{ij} = r_{ijk}E_k + q_{ijkl}\sigma_{kl}$). This results in optical effects which are difficult to separate from intrinsic gyrations and exceed them often by several hundred-fold!

In most common electro-optic experiments the crystals under investigation are mechanically unconstrained. The stress in these experiments is constant and tensors derived under such conditions have to be marked as 'unclamped'. The quasi-static electric field causes an additional strain via the inverse piezo-electric effect ($\varepsilon_{ij} = d_{kij}E_k$). This in turn changes the gyration by an effect called elastogyration g^{elagy}_{ijkl}. Similar, the elastic compliance S_{ijkl} changes the crystal dimensions ($\varepsilon_{ij} = S_{ijkl}\sigma_{kl}$) and causes elastic-compliance gyration ($g^{\text{elcomp}}_{ijkrs}$).

$$\begin{aligned}\frac{1}{\varepsilon_0}D_i &= \cdots + g^{\text{egy}}_{ijklm}\frac{\partial E_j}{\partial x_k}(c_{lmpq}[d_{rpq}E_r + S_{pqrs}\sigma_{rs}]) \\ &= \cdots + (g^{\text{elagy}}_{ijkr}E_r + g^{\text{elcomp}}_{ijkrs}\sigma_{rs})\frac{\partial E_j}{\partial x_k}. \qquad (2.6.6)\end{aligned}$$

c_{lmpq} are the stiffness constants of the crystal. If the electric polarization caused by an external force in a piezo-electric crystal is not short-circuited, a contribution to the piezo-gyration arises as secondary electrogyration. This effect may be small if the susceptibility of the crystal is not large. Weber (1979) showed that the secondary effects in $NaClO_3$ are almost as small as the error limits of the experimental tensor coefficients.

Semiconductors under stress have been studied in detail elsewhere (see the reviews by Koopmans *et al* (1996, 1998)). The gyrotropy is related to interband coupling in the electronic band structure of these materials. Likewise for the treatment of the Faraday effect by Boswarva *et al* (1962) the reader is referred for details to the articles of above authors.

3. Experiment

3.1. Intrinsic effects

3.1.1. Natural optical rotation at room temperature. Here we give a summary of optical rotation measurements in optical isotropic directions, where for most of the examples the absolute structure assignment is known (table 4). The detection of complete tensors in non-cubic crystals requires measurements in birefringent crystal sections. Methods applicable to those cases are outlined in section 2.2. Measurements have been excluded where a correction for parasitic ellipticities has not reliably been made (when measured with method (a) in section 2.2 and $g/\Delta n$ is equal to or smaller than $g_{11}/\Delta n$ in quartz) and where a connection to the absolute structure has *not* been established. The result of this review is listed in table 5.

As an example of a tensor determination with the 'tilter', the spectra of $\varphi_0(\delta)\sin(\delta)/\delta$ against tilt angle α for different crystal sections in tartaric acid, $C_4H_6O_6$, are shown in figure 29. The over-determined system of equations and additional information is found in table 6 (Mucha *et al* 1997). Another case is orthorhombic mannitol, $C_6H_{14}O_6$, where similar large tensor components are observed (Kaminsky and Glazer 1997).

A speciality of the tilter method is the determination of tensor components in a direction perpendicular to the normal vector of the crystal plate. As shown in KH_2PO_4 the component ρ_{11}, and in $RbOTiAsO_3$, K_2ZnCl_4 the component ρ_{12} is found with the same or even a better

Table 4. Optical rotation along isotropic directions and absolute configuration in crystals. $\rho = k_o^\rho + \sum_i \frac{k_i^\rho \lambda^2}{(\lambda^2-\lambda_i^2)^2}$; $\rho = \frac{k_D^\rho}{(\lambda^2-\lambda_D^2)}$; $n^2 = 1+k_o+\sum \frac{k_i\lambda^2}{\lambda^2-\lambda_i^2}$; [λ]: μm. The rotatory powers may be compared with those of $AgGaS_2$ ($\rho_{11} = \pm 950.0^\circ$ mm^{-1} at 485 nm, Hobden 1968), poly-L-lactic acid ($\rho = 9200^\circ$ mm^{-1} at 514.5 nm, Kobayashi *et al* 1995a). The thermal coefficients for quartz are $\partial\rho/\rho\partial T = 1.06$ (170 K); 1.60 (370 K); 1.96 (570 K).

Substance	SG	ρ (633 nm)	i	K_i^ρ	K_i	λ_i (μm)	Reference
α-$AlPO_4$	$P3_221$	−14.6					Schwarzenbach (1966)
$(C_6H_5)_2(CO)_2$	$P3_22$	−23	0		n_o : 1.08	—	Chandrasekhar (1961)
(Benzil)			1		0.535	0.240	
			2		0.0150	0.398	
			0	—	n_e : 1.35	—	
			1	6.27	0.370	0.240	
			2		0.0138	0.395	
α-$GaPO_4$	$P3_221$	−16					Glazer and Stadnicka (1986)
α-HgS	$P3_121$	320	1	19.13		0.243	
α-LiO_3	$P6_3^a$	−86.7	D	−28.8		0.238	Stadnicka *et al* (1985)
α-SiO_2	$P3_221$	19.1	0	—	—	—	Chandrasekhar (1961)
			1		n_o : 1.35	0.092 63	
			1	7.19	n_e : 1.378	0.092 63	
$Bi_{12}GeO_{20}$	$I23^a$	−19.5					Abrahams *et al* (1977)
$Bi_{12}SiO_{20}$	$I23^a$	−20.5					Abrahams *et al* (1977)
$Bi_{12}TiO_{20}$	$I23$	> -6					Swindells and Gonzales (1988)
$Ca_2Pb[C_2H_5COO]_6$	$P4_1$	−10					Singh (1984)
$Ca_2Sr[C_2H_5COO]_6$	$P4_12_12$	−6.2					Glazer *et al* (1981)
							Itoh *et al* (1981)
$Cd_2(NH_4)_2(SO_4)_3$	$P2_13$	0.28	1	0.115		0.158 3	Ivanov and Koniak (1975)
$Cs_2[(2R, 3R)\text{-}C_4H_4O_6]$	$P3_221$	−9.67(9)	1	−3.640		0.150	Stadnicka and Brozek (1991)
$K_2S_2O_6$	$P32_1^a$	−6.57					Gomes *et al* (1996)
$NaBrO_3$	$P2_13^a$	−1.65					Chandrasekhar (1961)
$NaClO_3$	$P2_13^a$	2.44	0	0.123	$-0.0086\lambda^2$	—	Chandrasekhar (1961)
			1	−1.238	1.1825	0.090	
			2	0.1374	0.0799	0.185	
$Rb_2[(2R, 3R)\text{-}C_4H_4O_6]$	$P3_221$	−8.65(8)	D	−3.201		0.185	Stadnicka and Brozek (1991)
$Rb_4LiH_3(SO_4)_4$	$P4_1$	−0.28					Zuniga *et al* (1990)
Te	$P3_12$	−740					Brown and Forsyth (1996)

[a] See structural coordinates (appendix, table A.2).

precision as if a cut along the direction with maximum effect had been examined (Kaminsky and Glazer 1996; figure 30; Kim *et al* 2000; figure 31). Figure 32 presents the result of a tilt scan in another uniaxial material: $LaBGeO_5$. The reinvestigation of the absolute structural configuration revealed the space group $P3_2$ (Kaminsky, Corker and Glazer 2000). The sign and magnitude are in accord with a calculation using the dipole–dipole model.

3.1.2. Natural optical rotation and phase transitions

3.1.2.1. Earlier results. The temperature dependence of optical rotation has not very often been determined. Studies in ferroelectric crystals such as KDP and related crystals (Vlokh, Klepatch and Shopa 1986a,b) claim that the observed gyration is often accompanied by intrinsic electrogyration. The symmetry allows only for quadratic electrogyration to contribute to the optical rotation along the $\boldsymbol{a}$- and $\boldsymbol{b}$-axes in the ferroelectric phase (the linear electrogyration does exist, but does not contribute in the case of wavevector and electric field along the $\boldsymbol{a}$-

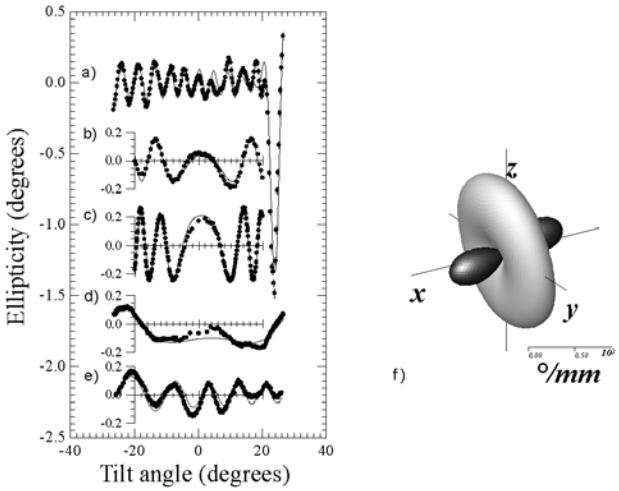

Figure 29. Tilt scans in tartaric acid samples at a wavelength of 680 nm. (*a*) 45° cut to approximately [100] and [010] (close to one of the optical axes), tilt axis $\|n_\beta \approx [001]$, thickness $L = 0.130(5)$ mm; the optical rotation changes its sign close to the optical axis. (*b*) Cut 'on' $n_\alpha = [010]$ (obtuse bisectrix), tilt axis $\|n_\gamma \approx [100]$, $L = 0.250(5)$ mm. (*c*) Cut 'on' n_γ (acute bisectrix), tilt axis $\|n_\beta \approx [001]$ (optic axis plane, flash figure), $L = 0.360(5)$. (*d*) Cut 'on' n_β, tilt axis $\|n_\gamma$, $L = 0.290(5)$ mm. (*e*) 45° cut to $[0\bar{1}0]$ and [001], tilt axis $\|[010](n\alpha)$, $L = 0.200(5)$ mm; in the diagonal cut to [010] and [001] the optical rotation was found to change sign similar to the tilt scan about the optic axes. (*f*) The representation surface of optical rotation with respect to the physical reference system (see further Mucha *et al* 1997).

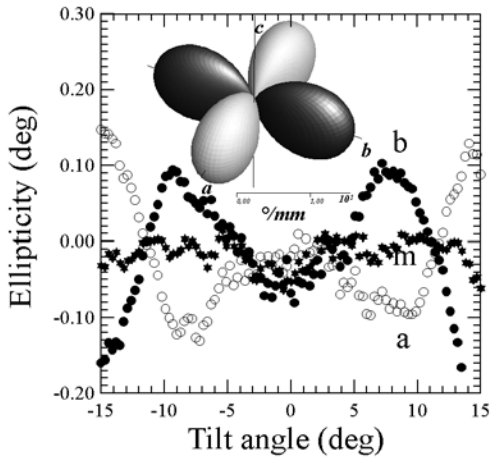

Figure 30. Tilt scans in KDP (Kaminsky and Glazer 1996), cut on (001) with a tilt towards the crystallographic axis $\boldsymbol{a}$. *b*, tilt towards $\boldsymbol{b}$; *m*, tilt towards the meridian between $\boldsymbol{a}$ and $\boldsymbol{b}$. The inset shows the representation surface of optical activity in KDP (the sample needs special preparation to avoid a surface related phenomenon).

or the $\boldsymbol{b}$-axis). However, the gyration is derived from the azimuthal rotation measurements (Konstantinova *et al* (1969), see section 2.3) and parasitic contributions are not properly separated out. Nevertheless, the number of optical components has been kept small to simplify the problem. In KH_2PO_4, $KH_{2-x}D_xPO_4$, $x = 89\%$ and CsH_2AsO_4 peaks of the only gyration component $\rho_{11} = -\rho_{22}$ were found at the Curie points. In RbH_2PO_4 the gyration just dropped off from the high-temperature value. The measurements were repeated later on, using the HAUP technology, by Kobayashi *et al* (1987) and the existence of a quadratic electrogyration in KDP was confirmed. In the ferroelectric phase below 123 K a linear component was found.

Table 5. Complete tensors of optical rotation in crystals at room temperature. References 1, this paper; 2, Stadnicka *et al* (1992); 3, Ortega *et al* (1993); 4, Kaminsky and Hartmann (1993); 6, Kaminsky and Glazer (1997); 7, Kremers and Meekes (1995); 8, Moxon *et al* (1991); 9, Stadnicka *et al* (1987); 11, Lingard (1994); 12, Gomez *et al* (1994); 14, Arzt and Glazer (1994); 15, Thomas *et al* (1991); 16, Chandrasekhar (1960); 17, Mucha *et al* (1997); 18, Asahi *et al* (1992); 19, Arzt (1995); 20, Iwasaki *et al* (1972); 21, Vlokh *et al* (1992); 22, Kaminsky *et al* 1999; 23, Kaminsky (1996); 24, Matsuda *et al* (1990); 25, Glazer *et al* (1981); 26, Saito *et al* (1992); 27, Saito *et al* (1994); 28, Vlokh *et al* (1986); 29, Kaminsky *et al* (2000); 30, Tebutt (1991); 31, Kim *et al* (2000).

Formula	SG	λ (nm)	ρ_{11}	ρ_{22}	ρ_{33}	ρ_{12}	ρ_{23}	ρ_{13}	Reference
$(NH_3(CH_3))_5(Bi_2Br_{11})$	$Pca2_1$	587	—	—	—	−3(1)	—	—	11
$AlPO_4$	$P3_22$	632.8	12(1)	$=\rho_{11}$	−14.6(1)	—	—	—	19
$BaMnF_4$	$A2_1am$	632.8	—	—	—	—	−16(3)[b]	—	18
$Ca_2Sr(C_2H_5COO)_6$	$P4_12_12$	632.8	±15(1)	$=\rho_{11}$	−6.2(1)	—	—	—	24, 25
$Gd_2(MoO_4)_3$	$Pba2$[b]	476.5	—	—	—	35(2)	—	—	27
CsH_2AsO_4	$I\bar{4}2d$	632.8	−14(1)	$=-\rho_{11}$	—	—	—	—	28
$K_2Cd_2(SO_4)_3$	$P2_12_12_1$	670	−2.7(9)	−1.8(2)	2.9(5)	—	—	—	23
K_2ZnCl_4 (300 K)	$Pna2_1$[b]	670	—	—	—	0.5(2)	—	—	31
K_2ZnCl_4 (50 K)	A1a1[b]	670	—	—	—	−12(2)	−5(1)	—	31
KH_2PO_4	$I\bar{4}2d$	500	−16(2)	$=-\rho_{11}$	—	—	—	—	19
$KLiSO_4$	$P6_3$	632.8	1.2(1)	$=\rho_{11}$	−2.5(1)	—	—	—	3
$KTiOPO_4$	$Pna2_1$[a]	632.8	—	—	—	22(2)	—	—	15
L(+)TA, $C_4H_6O_6$	$P2_1$	670	−65(2)	79(3)	85(4)	—	—	32(2)	17
$LaBGeO_5$	$P3_2$	670	−6(2)	$=\rho_{11}$	2.1(1)	—	—	—	22
$LiNH_4C_4H_4O_6 \cdot H_2O$	$P2_12_12$[b]	632.8	1.5(1)	−2.3(1)	−5.3(2)	—	—	—	26
$LiRb_4D_3(SO_4)_4$	$P4_1$	632.8	3(1)	$=\rho_{11}$	−0.29(1)	—	—	—	11
$LiRb_4H_3(SO_4)_4$	$P4_1$	632.8	2.0(5)	$=\rho_{11}$	−0.28(1)	—	—	—	11
Mannitol, $C_6H_{14}O_6$	$P2_12_12_1$[a]	600	−8(1)	−3(1)	−56(3)	—	—	—	6
$NaNH_4(C_4H_4O_6) \cdot 4H_2O$	$P2_12_12$	500	3(1)	−8(1)	2(1)	—	—	—	11
$NaNH_4SO_4 \cdot 2H_2O$	$P2_12_12_1$[a]	500	−4(1)	7(1)	−3(1)	—	—	—	14
$NH_4H_2AsO_4$	$I\bar{4}2d$	500	−40(3)	$=-\rho_{11}$	—	—	—	—	19
$NH_4H_2PO_4$	$I\bar{4}2d$	589.3	−7(1)	$=-\rho_{11}$	—	—	—	—	2
$NiSO_4 \cdot 6H_2O$	$P4_12_12$	632.8	0.0(1)	$=\rho_{11}$	−1.0(1)	—	—	—	7–9
$Pb_5Ge_3O_{11}$	$P3$[a]	632.8	14(1)	$=\rho_{11}$	−5.5(1)	—	—	—	19–21
RbH_2PO_4	$I\bar{4}2d$	632.8	−7(1)	$=-\rho_{11}$	—	—	—	—	28
$Rb_2TiOAsO_4$	$Pna2_1$[a]	670	—	—	—	17(3)	—	—	29
Rb_2TiOPO_4	$Pna2_1$[a]	600	—	—	—	18(4)	—	—	30
SiO_2	$P3_22$[a]	632.8	−10.8(5)	$=\rho_{11}$	19.10(5)	—	—	—	1, 8, 16
$Sr_2S_2O_6 \cdot 4H_2O$	$P3$[b]	632.8	−0.6	$=\rho_{11}$	2.65	—	—	—	12
TeO_2	$P4_32_12$	632.8	−169(12)	$=\rho_{11}$	−85.75(1)				4

[a] Absolute structures are given in the appendix, table A.2.
[b] Not assigned to absolute structure.

Because no attempts were made to eliminate parasitic contributions to the electrogyrative signal, it is at least doubtful whether the quadratic effects are really due to electrogyration or to parasitic effects and the observed changes of optical activity are a result of spontaneous polarization via a quadratic electrogyration. The author's own observations (unpublished) are not fully in accord with the earlier results (figure 33).

The observations of second-order electrogyration in $(N(CH_3)_4)_2ZnCl_4$ within the incommensurate phase (Saito *et al* 1987) or at room temperature in quartz (Kobayashi *et al* 1987) were derived with the same technique and leave similar doubts.

Boracites such as $Fe_3B_7O_{13}I$, $Co_3B_7O_{13}I$ and $Cu_3B_7O_{13}Cl$ were investigated with respect to optical activity. In the course of the phase transition from a paraelectric cubic phase ($\bar{4}3$) into

Table 6. The over-determined system of equations describing optical activity in TA (tartaric acid, $C_4H_6O_6$). $\rho(k)$ = optical activity in direction of the wavevector $\boldsymbol{k}$. Directions e_i° are along $n\alpha$, n_β, n_γ of the indicatrix. Direction cosines [. . .]° with respect to the indicatrix. The polarization of n_γ is 18° and the crystallographic axis $\boldsymbol{a}$ 10° anti-clockwise rotated towards $\boldsymbol{e}_1$ if looking towards [010]. The tensor components with respect to $\boldsymbol{e}_j$ are $\rho_{11} = -65.1(1.9)$, $\rho_{22} = 78.7(2.6)$, $\rho_{33} = 85.2(3.7)$, $\rho_{13} = 32.3(2.3)$ (see also table 5).

k direction cosines	$\rho(k)$ (° mm^{-1})	ρ_{11}	ρ_{22}	ρ_{33}	ρ_{23}
[100]° ($n\alpha$)	81(10)	1	0	0	0
[010]° ($n\beta$)	90(20)	0	1	0	0
[001]° ($n\gamma$)	−66(10)	0	0	1	0
[0.6230 0.783]°	−12.3(1.0)	0.388	0	0.613	0
[0 − 0.707 0.707]°	28(10)	0	0.5	0.5	−1
[00.707 0.707]°	−8(10)	0	0.5	0.5	1
Tensor in [. . .]°	ρ_{ij} (° mm^{-1})	78.7(2.6)	89.8(3.8)	−69.8(1.7)	−18.0(2.2)

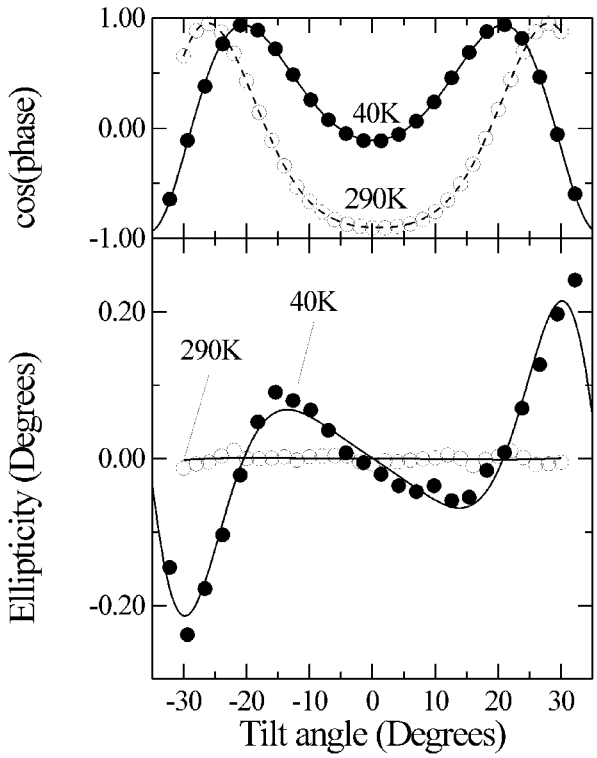

Figure 31. Typical tilt scans in K_2ZnCl_4 at room temperature and at 40 K. Shown are the cos(δ) dependence, δ = phase factor and 'ellipticity' signal y_1^{filtered} as results from the filter algorithm (figure 20).

a ferroelectric orthorhombic phase (*mm*2), in the vicinity of the critical temperatures, optical rotation revealed high peaks of the component ρ_{12} (Tomizawa *et al* 1991, Takahashi *et al* 1992). Again, quite large nonlinear electrogyrative effects for an electric field along the ferroelectric axes were observed, which were interpreted as a result of second-order electrogyration.

Asahi *et al* (1992) investigated the pyroelectric–antiferromagnetic phase transition into

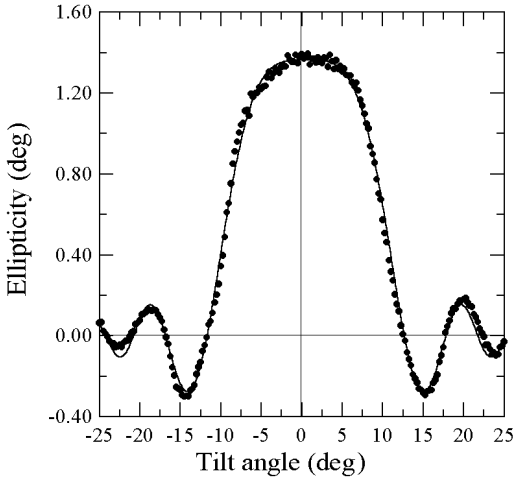

Figure 32. A tilt scan in uniaxial (SG $P3_2$) $LaBGeO_5$. The optical rotation tensor has cylindrical symmetry and the direction to which the (001) plate is tilted does not have to be specified. The figure shows Fabry–Pérot interference, which limited the accuracy of the measurement to a small extent.

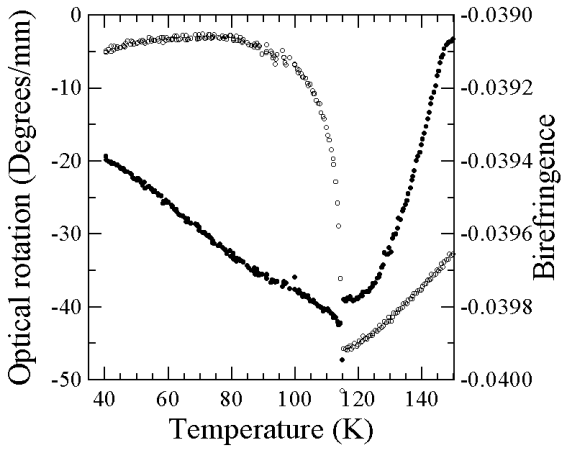

Figure 33. Optical rotation component ρ_{11} versus temperature in KH_2PO_4 (filled circles) and birefringence $n_{|c} - n_{|a}$ (open circles). The decrease of optical rotation below the Curie temperature of this artificially strained sample is less pronounced than previously reported. The strain was implemented growing KH_2PO_4 in the presence of an organic dye (see literature on the growth of dyed crystals: Rifani *et al* (1995), Kahr *et al* (1996), Subramony *et al* (1998)). The dye is grown only into (101) growth sections and causes the whole crystal to be strained. As a result, the Curie point is shifted slightly to a lower temperature, but the formation of multiple domains was suppressed.

an incommensurate phase of $BaMnF_4$. The macroscopic point groups are 2 ($T < 250$ K) and $mm2$ ($T > 250$ K), where in the low-temperature phase the incommensurate modulation is along the a-axis (= 2-fold axis in both phases). In both symmetries, the optical rotatory component ρ_{23} is allowed, which has a steep increase at 250 K. In the low-temperature phase, because of symmetry, the components ρ_{11}, ρ_{22} rise from their high-temperature zero values. However, ρ_{33} remains unobservably small.

The phase transition from orthorhombic to monoclinic $LiNH_4C_4H_4O_6 \cdot H_2O$ at 198 K causes a rotation of the optical rotation surface due to the symmetry-allowed component ρ_{13}. The other rather small components are all decreased by about 4° mm^{-1} (Saito, Cao and

Kobayashi 1992). This steep change was found to be in proportion to the shear strain in the course of the transition. A similar case will be discussed below in langbeinite crystals. Rochelle salt, to which $LiNH_4C_4H_4O_6 \cdot H_2O$ exhibits some similarities, was investigated as well in unclamped crystals (Kobayashi, Uchino and Asaki 1991a; Kobayashi, Uchino, Matasuyama and Suito 1991b). The observed effects are to be seen as a superposition of electro-optic, electrogyrative and electrostrictive effects, where the elasto-optic coefficients connect for example a secondary electro-optic effect to the spontaneous strains. Unfortunately, no discussion of these contributions was made. In addition, all effects seem to be too small to be free of parasitic contributions.

Recently, $Gd_2(MoO_4)_3$ was investigated,which exhibits a phase transition at 430 K and transforms from $Pba2$ into $P\bar{4}2_1m$ (Saito *et al* 1994). The optical rotation ρ_{12} decreases at the transition into higher temperatures, but remains non-zero. A small but non-zero ρ_{12} below 232 K was found in $(NH_4)_2SO_4$, which does not exhibit optical rotation at room temperature (Higano *et al* 1994) since the transition leads from $mm2$ into $2/mm$.

3.1.2.2. Langbeinites. In a ferroelastic–paraelastic transition, when the symmetry is broken by the spontaneous strain, the optical rotation may not be accompanied significantly by intrinsic electrogyration. If the high-temperature phase is optically isotropic, spontaneous optical birefringence occurs as a result of the elasto-optic effect, which vanishes in the paraelastic phase.

Baturina *et al* (1983, 1987) investigated the optical properties of $Tl_2Cd_2(SO_4)_3$, $Rb_2Cd_2(SO_4)_3$, $(NH_4)_2Cd_2(SO_4)_3$ and $K_2Co_2(SO_4)_3$. In the course of the phase transition in $K_2Co_2(SO_4)_3$ at 125 K the optical rotation shows no distinct variation although the birefringence drops to zero in the cubic phase at high temperature. A complete tensor determination has not been performed.

When the birefringence becomes small in the vicinity of the transition, it is difficult to obtain enough information on the optical properties from tilting the sample. In these cases additional measurements may be useful where the dispersion of δ with varying wavelength is used to avoid singularities in the measurement, which depends on $\cos\delta$ and $\sin\delta$.

As an example, the ferroelastic phase transition of the optically biaxial Cd langbeinite $K_2Cd_2(SO_4)_3$ is studied (Kaminsky 1996), (SG $P2_12_12_1 \xrightarrow{432\ K} P2_13$, Lissalde *et al* 1978), where earlier Vlokh and Lyzko (1984) found a distinct variation of optical activity along the optic axes.

A large step in the birefringence at the transition temperature was observed as well (Devarajan and Salje 1984).

The three independent tensor components in the orthorhombic phase at room temperature were measured with the 'tilter'. Because the technique is fast, it was possible to scan the samples laterally by successive repetition of the tilt procedure and shifting the sample to investigate its optical homogeneity. Measurements where the 'ellipticity' was determined as a function of the wavelength confirmed the result within the observed variations in the topography, which seem to stem from growth sections or internal strains. However, for temperatures close to the phase transition into the cubic phase the birefringence became too small and the relevant signals were observed as they varied with the temperature. The effect of the phase transition on the optical rotation is shown in figure 34, where the representation surfaces are derived for three temperatures.

Following the first of Stadnicka's rules in section 2.3 on the origin of optical rotation, i.e. the optical activity is built up from the superposition of helical arrangements in a structure where axial or tangential 'polarizability ellipsoids' determine the sign of the contributions

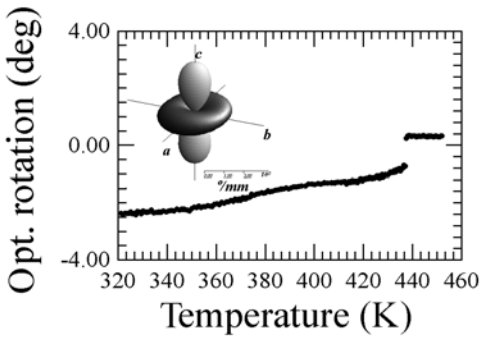

Figure 34. Measurements in Cd langbeinite (Kaminsky 1996), showing the variation of the optical activity along one of the optic axes against temperature. The inset shows the representation surface of intrinsic optical rotation at room temperature.

Table 7. The components of experimental (exp) and calculated (calc) rotatory power ($^\circ$ mm^{-1}) for different directions in Cd langbeinite. Missing values correspond to conditions where the tilting of the sample did not change the birefringence enough to allow a precise measurement. Errors are given in parentheses. The values derived with the HAUP system at room temperature (RT) for $\lambda = 680$ nm are included. The polarization directions of n_1, n_2 and n_3 are along [010], [001] and [100], respectively. [0.82 0.57 0] is the direction along an optical axis.

T (K)	[100]		[010]		[001]		[0.82 0.57 0]	
	exp.	calc.	exp.	calc.	exp.	calc.	exp.	calc.
RT^{HAUP}	−1.0(4)		−1.6(2)		3.4(2)			
298	−3.4(4)	−4.535	−2.0(2)	−0.110	2.3(2)	5.239	−2.5(3)	−3.079
351		−4.526		0.240	2.6(2)	5.175	−2.3(2)	−2.958
390		−3.894		0.305		4.512	−1.5(2)	−2.513
417	−1.5(4)	−3.093	−1.0(2)	0.349	1.4(2)	3.808	−1.3(2)	−1.961
443	0.27(5)	0.343	0.36(5)	=[100]	0.28(5)	=[100]	0.30(5)	=[100]

(Glazer and Stadnicka 1986), it was expected that the ferroelastic distortion of the unit cell only shifts the balance of the different chiral contributions, conserving the trace of the optical rotation tensor.

The expansion of the optical rotation of the cubic phase into the orthorhombic phase with respect to the elastic strains $\in_{ij}$ and the gyro-elastic tensor g_{ijkl} is

$$\Delta\rho_{ij} = g_{ijkl} \in_{kl} . \tag{3.1.2.1}$$

Because the phase transition of Cd langbeinite is a Γ-point transition, the cell volume is invariant, thus $V_0 = a_0^3 + a_0^2 \sum \in_{ii} + \mathrm{O}(\in_{ii}^2) = \text{const}$. As a result, $\sum \in_{ii} = 0$, and the trace of the optical rotation tensor is an invariant as well:

$$\mathrm{tr}(\Delta\rho_{ij}) = (g_{1111} + g_{1122} + g_{1133}) \sum \varepsilon_{ii} = 0. \tag{3.1.2.2}$$

The measurement (Kaminsky 1996) and calculations with the dipole–dipole model by Devarajan and Glazer (1986), based on the structure analysis by Abrahams, Lissalde and Bernstein (1977b), confirm the quasi-invariance of trace (ρ_{ij}) (table 7).

3.1.2.3. K_2ZnCl_4. The ferroelectric–ferroelastic phase transition of K_2ZnCl_4 at 145 K has been investigated employing the tilter method. The anisotropy of optical rotation in K_2ZnCl_4 showed a distinct discontinuity at the transition temperature.

The gyration tensor components $\rho_{\alpha\beta}$ and $\rho_{\alpha\gamma}$ of KZC (indices with respect to the refractive indices of the indicatrix) obtained with the tilter method are plotted in figure 35 as a function of temperature. Both components are almost zero within the error limits above T_3. However,

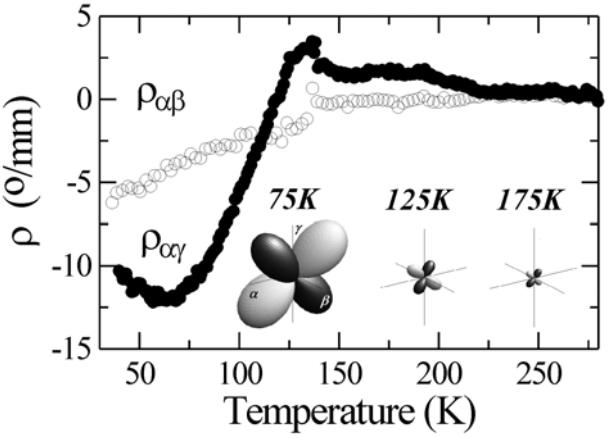

Figure 35. The temperature dependence of the gyration tensor components in K_2ZnCl_4. A first-order Landau-type discontinuity is observed at the phase transition temperature in one component.

$\rho_{\alpha\beta}$ seems to show a small discontinuity at T_3 corresponding to the C–FE phase transition. $\rho_{\alpha\beta}$ then decreases continuously. The behaviour of $\rho_{\alpha\gamma}$ is similar, with a precursor behaviour up to about 200 K, and reaches as much as -10° mm^{-1} at 70 K where it saturates.

The Landau theory, which is applicable to order–disorder phenomena, may explain the critical behaviour of the rotatory power tensor component $\rho\alpha\beta$ in the C–FE phase transition. The order parameter of this proper ferroelastic phase transition (Salje 1990) corresponds linearly to the spontaneous strain $e_{13} \propto$ constant term $+(T_3 - T)^{\frac{1}{2}}$ (with respect to $Pna2_1$) (Harada *et al* 1992). $\rho_{\alpha\beta}$ is related to the strain via the gyro-elastic coefficients g_{ijkl} of the ferroelectric C-phase, which are taken to be almost independent of the temperature. The independent components of the gyro-elastic tensor in point group $mm2$ are g_{1112}, g_{2111}, g_{1222}, g_{2221}, g_{1233}, g_{3312}, g_{1323}, g_{2313} and g_{3333}. The first and second pair of indices of this axial tensor are commutative. The only temperature dependent contribution is related to g_{2313} ($y \| n_\alpha, z \| n_\beta$) and the following expression describes well the temperature dependence of $\rho_{\alpha\beta}$:

$$\rho\alpha\beta = 2g_{\alpha\beta 13}e_{13} \propto A + B(T_3 - T)^{\frac{1}{2}}.$$

However, a strong variation in $\rho_{\alpha\gamma}$ starting at about 25 K below T_3 was detected. Thus, the assumption of a temperature independent g_{ijkl} may not be valid, and the structural changes in the course of the transition do affect the optical rotation even more than the breaking of symmetry due to the spontaneous strain.

3.1.2.4. Incommensurate crystals. The structures of incommensurate crystals are modulated such that there are periodical deviations from the average structure (figure 36). The period of these deviations is not an integer multiple of the cell parameters. The point group of such materials does not necessarily reflect the modulation. It often happens that the translational symmetry of an incommensurate crystal is compatible with an inversion symmetry of the macroscopic point group. The fundamental rule to determine the existence of tensorial properties is given by Neumann: a physical property has at least the symmetry of the crystal. This means for example that optical rotation cannot exist in centrosymmetric crystals. Because Neumann's law was manifested at a time before incommensurate crystals were discovered, its general applicability to these substances was disputed.

Thus, the optical rotation in centrosymmetric incommensurate crystals of the A_2MX_4 type is controversial. First measurements on $[N(CH_3)_4]_2ZnCl_4$ (Kobayashi *et al* 1986a, Kobayashi and Saito 1986b) and Rb_2ZnCl_4 (Kobayashi, Saito, Fukase and Matsuda 1988a), using the

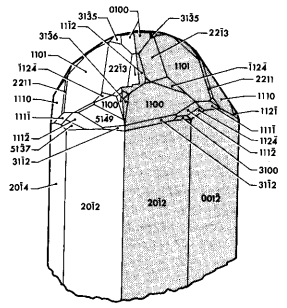

Figure 36. Incommensurate crystal $Au_{1-x}Ag_xTe_2$ (typical twin; Janner and Dam 1989, courtesy of OPA (Overseas Publishers Association) NV). The crystal faces are labelled with four integral indices. $\boldsymbol{H}_{hklm} = h\boldsymbol{a}_1^* + h\boldsymbol{a}_2^* + h\boldsymbol{a}_3^* + m\boldsymbol{q}$, where $\boldsymbol{a}_i^*$ are the reciprocal lattice vectors and $\boldsymbol{q} = \alpha\boldsymbol{a}_1^* + \beta\boldsymbol{a}_2^* + \gamma\boldsymbol{a}_3^*$ is a modulation vector. If at least one of the three α, β, γ is irrational, the structure is incommensurably modulated.

HAUP technology revealed non-zero components. However, Moxon and Renshaw (1990) showed a new way to eliminate parasitic contributions in the HAUP measurements, which was later adapted by others as well (Kremers and Meekes 1995b). With the improved technology, the optical rotation was found to be below the detection sensitivity (Folcia *et al* 1993, Ortega *et al* 1995, Kremers, Etxebarria, Folcia, Dijkstra and Meekes 1996). Still using the old method, a non-zero component g_{23} was published (Kobayashi *et al* 1993, 1994a, b), most probably as a result of the parasitic effects introduced by the crystal itself when entering the incommensurate phase. A similar discussion concerns $((CH_3)_4N)_2CuCl_4$, which shows no optical rotation according to Ortega *et al* (1992), contradicting Saito *et al* (1990). This is questioned by Kremers and Meekes (1995c), who find optical rotation and a rotation of the indicatrix, but discuss the possibility that the incommensurate phase may not be centrosymmetric. Definitely non-centrosymmetric is the mixed crystal $((CH_3)_4N)_2ZnCl_{2.8}Br_{1.2}$ (Vogels *et al* 1994, Kremers and Meekes 1996), which therefore is allowed by symmetry to possess non-zero optical rotation. In a similar light one should consider reports on optical rotation in (centrosymmetric) $(C_3H_7NH_3)_2MnCl_4$ (Saito and Kobayashi 1991, 1992).

Recently, a report on thiourea by Billesbach and Ullman (1994), using the rotating polarizer technique (Suits 1971, Wood and Glazer 1980), showed strong optical rotation in the incommensurate but still centrosymmetric phase below 200 K according to their interpretation. However, the result is much more likely to result from twinning rather than optical rotation.

3.1.3. Intrinsic Faraday effect

3.1.3.1. General remarks. The tensor relation and field dependence of the Faraday effect in an anisotropic medium is given according to equation (2.4.3) by the projection of the wavevector $\boldsymbol{k}$ on the direction of the magnetic field multiplied by the effective tensor component in the direction of the magnetic field (Kaminsky and Haussühl 1993) $\varphi = -V_{ij}u_iu_jL_k(H_k + M_k)$, where $V_{ij} = -180Z_{ij}/H_kn\lambda$ is the Verdet constant ($^\circ$ A^{-1}) (see also equation (2.6.2)), u_i are direction cosines of $\boldsymbol{H}$, L_k the thickness of the sample along $\boldsymbol{k}$, H_k the component of the magnetic field and n the refractive index.

If a material is ferromagnetic, the magnetization can be measured from the spontaneous Faraday rotation. The tricritical† behaviour of $FeCl_2$ at 23.5 K was monitored in this way (Dillon *et al* 1978).

As another example, Huang and Ho (1975) measured the magnetic properties of EuO near the Curie point using the Faraday rotation. They found a small third-order term in the relation between the Faraday rotation and magnetization. When taking into account the nonlinearity,

† Within a phase diagram, a tricritical point connects three different phases. The axes of a diagram may be temperature and pressure, temperature and a magnetic or electric field or similar.

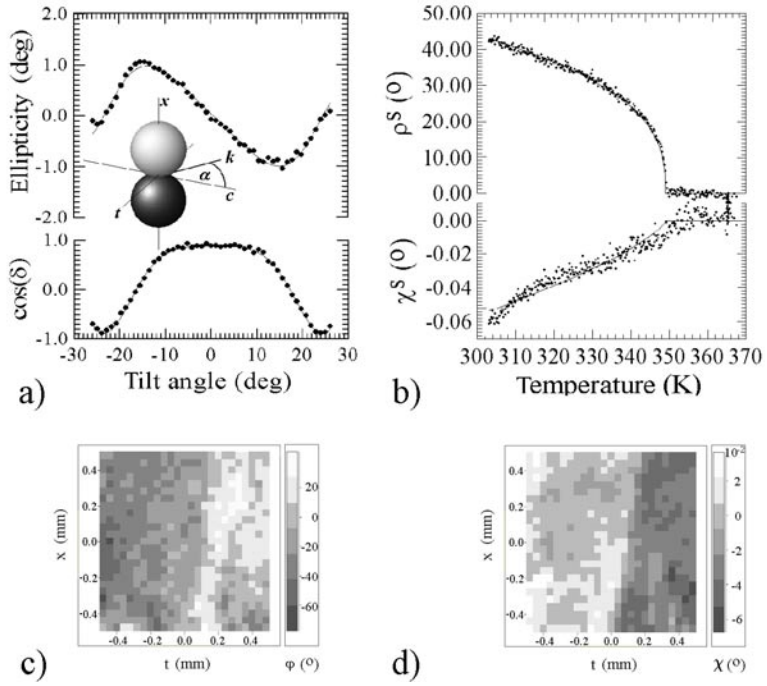

Figure 37. Measurements in $FeBO_3$. (*a*) Tilt scan of a sample cut on (001) with tilt axis perpendicular to the magnetization. (*b*) Intrinsic Faraday rotation and rotation of the indicatrix against temperature. (*c*) Topography of intrinsic Faraday rotation. (*d*) Topography of intrinsic indicatrix rotation about [100] (Kaminsky 1997).

the critical parameters obtained from magnetometric measurements are confirmed. An equal magnitude of bandwidth and bandgap is discussed as a reason for the observed nonlinearity.

3.1.3.2. $FeBO_3$. In an $FeBO_3$ sample cut on (001)—as a further example—the intrinsic Faraday rotation along $\boldsymbol{M}\|[100]$ was derived from tilt scans presented in figure 37(*a*). Figure 37(*b*) shows the effect along $\boldsymbol{M}$ as a function of the temperature and figure 37(*c*) a topography of optical rotation across the sample plate (Kaminsky 1997).

The 'tilter' method allows us to determine the complete orientation of the indicatrix. Figure 37(*d*) shows the tilting about [100] of the indicatrix which results from the Shubnikov point group transition $\bar{3}m1'$ into $2/m$ (monoclinic–ferromagnetic/ferroelastic) and which manifests itself in a magnetization dependence of χ (equation (2.2.4)) for a tilt axis parallel [100] × [001] (of the trigonal phase) and a magnetization $\boldsymbol{M}|[100]$.

The Faraday effect $V_{ij}M_iL_j = \rho_k L_k$†, with sample thickness $\boldsymbol{L}$ in the direction of the wavevector $\boldsymbol{k}$, is effectively represented by a single-rank property ρ_k (the spontaneous rotatory power, figure 37(*a*)). In a sample of thickness L cut on the $\boldsymbol{c}$-axis with $\boldsymbol{M} = [M_1, 0, 0]$ parallel to $\boldsymbol{x}|[100]$ we observe as a part of the azimuthal rotation the Faraday effect $\varphi(\boldsymbol{k}) \approx LV_{11}M_1 \sin\beta/\cos\beta$, where β is the angle between $\boldsymbol{c}$ and $\boldsymbol{k}$. $\rho^S = V_{11}M_1$ is the spontaneous Faraday effect.

The indicatrix is affected by a magnetic field according to $\Delta a_{ij} = q_{ijk}H_k + q_{ijkl}H_kH_l$

† The independent components of V_{ij} in $FeBO_3$ are $V_{11} = V_{22}$ and V_{33}. The given expression describing the Faraday effect is in accord with equation (2.4.3). However, it is not to be applied to monoclinic or triclinic crystals.

(Kharchenko 1994); here q_{ijk} is the linear and q_{ijkl} the quadratic magneto-optic tensor‡. In the Shubnikov point group $\bar{3}m1'$ of the paramagnetic high-temperature phase of $FeBO_3$, the axial tensor with $q_{ijk} = q_{jik}$ does not exist because time inversion changes the sign of $q_{ijk}H_k$, but not Δa_{ij}. The polar tensor q_{ijkl} exists and consists of the eight independent components (Haussühl 1983) q_{1111}, q_{1122}, q_{1133}, q_{1123}, q_{3311}, q_{3333}, q_{2311} and q_{1313}. Spontaneous magnetization along [100], $\{\Delta a_{ij}\} = \{q_{1111}M_1^2, 0, 0; 0, q_{1122}M_1^2, q_{2311}M_1^2; 0, q_{2311}M_1^2, q_{3311}M_1^2\}$, results in an effective monoclinic symmetry where the indicatrix is rotated about the magnetization by $\chi^S = -\Delta a_{23}/(a_{22}^o - a_{33}^o + \Delta a_{22} - \Delta a_{33}) \cong 0.5n_o^3(n_o - n_e)^{-1}q_{2311}M_1^2$ with n_o and n_e the ordinary and extra-ordinary refractive indices. Optical activity exists neither in the centrosymmetric point group $\bar{3}m1'$ nor in the effective monoclinic symmetry.

The previously determined critical exponent (Eibschütz, Pfeiffer and Nielsen 1970, Kurtzig *et al* 1969) describes well the temperature dependence of the intrinsic rotation and spontaneous tilting of the indicatrix (figure 37(*b*)).

It was found earlier (Kaminsky and Haussühl 1993, Orushinin *et al* 1986) that the Verdet constant V_{33} varies only a little in the course of the ferromagnetic transition. However, the direct experiment in the direction [100] revealed a rather large temperature dependence of V_{11}. The first experiment was carried out with an unfavourable geometry because of which depolarization effects affected the result.

The intrinsic Faraday effect was used previously to give contrast when studying domains in $FeBO_3$ with a microscope giving a higher resolution than obtained with the tilter (Scott 1974, Fedorov *et al* 1981, 1983). Apparently a quantitative determination of the indicatrix tilt (χ) has not been performed. Measurements of the spontaneous birefringence have not been published (Pisarev 1996).

3.1.4. Intrinsic electrogyration and ferroelectric TGS. It was supposed that electrogyration can occur in a ferroelectric crystal as a result of the field of spontaneous polarization. A gyrotropy which was related to this mechanism was first observed for light travelling along one of the optic axes in triglycine sulphate (TGS : $NH_2CH_2CO_2H)_3 \cdot H_2SO_4$ (Hermelbracht and Unruh 1970). The space group symmetry of the structures of TGS in the course of the second-order ferroelectric phase transition are $P2_1/m$ above and $P2_1$ below $T_c = 322.6$ K (Matthias, Miller and Remerka 1956, Landolt–Börnstein New Series 1969, 1979, 1990). The direction of spontaneous polarization is parallel to the twofold axis in TGS. Crystals cut with a plate normal vector $\boldsymbol{n}$|[010] exhibit birefringence.

The published results of gyrotropy of TGS are summarized in table 8. The results vary within a factor 10^2 (Kobayashi and Uesu 1983, 1991b, Etxebarria *et al* 1992, Kaminsky 1994), far beyond the published error limits. If these discrepancies were due to different crystal qualities, the results for the birefringence, which is sensitive to all kinds of defect would also deviate a lot, but this is not the case. Another source for deviations could be the history of the crystals with respect to heating temperature and time (annealing effects) which can affect the observed properties (Ivanov and Shuvalov 1967). Underestimating the complicated relation between the observed gyrotropy and the different optical effects including electro-optic effects could possibly explain the discrepancies.

In point symmetry 2 the gyration g, phase δ and rotation μ of the indicatrix (see equations (2.1.7), (2.2.3) and (2.2.4), where the wavevector is parallel to [010]) are assumed

‡ It is important to note that q_{ijk} and q_{ijkl} are defined here in close analogy to the electro-optic effect. One often observes the definition in the form $\Delta\varepsilon_{ij} = q'_{ijk}H_k$, where $a_{ij} = \epsilon_{ij}^{-1}$. In the form preferred by the author it is less likely to be confused with the definition of linear magnetostriction $\Delta\varepsilon_{ij} = d_{kij}H_k$.

Table 8. Results found in the literature for the difference between properties at 318 K and $T_c = 323$ K. The difference is denoted by 'd'. The symbols are dg_2 = change of spontaneous gyration along the twofold axis of TGS; dg_{oa} = same property for the wavevector along one of the optical axes; $d\Delta n_2$ = change of birefringence ($n_3 - n_1$). $d\Delta n_1$ = change of ($n_2 - n_3$); $d\mu$ = rotation of the indicatrix with rotation axis parallel to the twofold axis; λ = wavelength. Errors are given in parentheses. Only the modulus of the observed changes is given to avoid further confusion.

Reference	$dg_2(10^{-5})$	$dg_{oa}(10^{-5})$	$d\Delta n_2(10^{-4})$	$d\Delta n_1(10^{-4})$	$d\mu(10^{-3})$	λ (nm)
Ivanov and Shavalov (1966)					6.9(1)	540
Lomova *et al* (1968)			1.5(2)	4.0(2)	9(1)	529
Brezina *et al* (1969)					4.4(1)	?
Hermelbracht and Unruh (1970)		0.12(1)				589
Habryko and Koralewski (1981)		0.06(1)				633
Kobayashi and Uesu (1983)	0.7(1)		2(1)		5.9(2)	514.5
Kobayashi (1991b)	0.7(1)				6.3(3)	514.5
Etxebarria *et al* (1992)	6.5(5)		2.5(1)		5.0(2)	633
Kaminsky (1994)	0.3(1)	0.09(1)	3.2(1)	3.7(1)	4.2(1)	633

to be decomposed into

$$\begin{aligned} g &= (g^{oa}) + g^{egy}[D_2 + P_{sp}] \\ \mu &= \mu_0 + (\mu_l[D_2 + P_{sp}]) + \mu_q[D_2 + P_{sp}]^2 \\ \delta &= \delta_0 + (\delta_l[D_2 + P_{sp}]) + \delta_q[D_2 + P_{sp}]^2 \\ \chi &= \chi_0, \qquad D_2 = \varepsilon_0\varepsilon_{22}E_2 \end{aligned} \tag{3.1.4.1}$$

where D_2 is the dielectric displacement, P_{sp} the spontaneous polarization, g^{oa} and g^{egy} are the coefficients of optical rotation and electrogyration, μ_l, μ_q and δ_l, δ_q arise from the linear and quadratic electro-optic effect. The terms in round brackets and P_{sp} vanish in the paraelectric phase. The azimuthal rotation observed for incident light, closely linearly polarized 'along' $n\beta$ (the second largest refractive index), is found with the help of table 2 and equations (2.1.5) and (2.1.6) (Kaminsky 1994):

$$\begin{aligned} \varphi = {} & \theta_0 C_\delta + g^{oa} S_\delta + g^{egy} P_{sp} S_\delta + \mu_l P_{sp} C_\delta M_\beta + \mu_q P_{sp}^2 C_\delta M_\beta \\ & + g^{egy} D_2 S_\delta + \mu_l' D_2 C_\delta M_\beta + \delta_l' \theta_0 D_2 N_\delta \\ & + \mu_q D_2^2 C_\delta M_\beta + \delta_q D_2^2 \theta_0 N_\delta \\ \delta_0' = {} & \delta_0 + \delta_l P_{sp} + \delta_q P_{sp}^q, \qquad \mu_l' = \mu_l + 2\mu_q P_{sp}, \qquad \delta_l' = \delta_l + 2\delta_q P_{sp} \\ C_\delta = {} & 1 - \cos\delta_0', \qquad S_\delta = \frac{\sin\delta_0'}{\delta_0'}, \qquad N_\delta = \sin\delta_0' \\ M_\beta = {} & \frac{\cos\beta}{1 + \sin^2\beta' \frac{\Delta n_3}{\Delta n_2}}, \qquad \theta_0 \approx \frac{\mu_0 \Delta n_2 \cos\beta - \chi_0 \Delta n_1 \sin\beta}{\Delta n_3 \sin^2\beta' + \Delta n_2}. \end{aligned} \tag{3.1.4.2}$$

The birefringence $\Delta n_i = n_j - n_k$, i, j, k cyclic in 1, 2, 3, where $n_1 = n\gamma$, $n_2 = n\beta$, $n_3 = n\alpha$. θ_0, μ_0, χ_0 and δ_0 are those properties where no field is applied. For the definition of β' see equation (2.2.3). In equations (3.1.4.2), higher-order terms or products of small contributions were neglected. Inserting equations (3.1.4.1) into (2.1.7) results in an expression of similar complexity; nevertheless, a separation of the different contributions in equations (3.1.4.2) is already possible, using only the azimuthal rotation of a light wave after passing through the TGS crystal.

From a Fourier analysis with respect to the external electric field strength $D_2 = \varepsilon_{22}(E_2^{ext})$, the different contributions $\delta_0(\alpha)$ and $\beta(\alpha)$ to the azimuthal rotation φ are separated out. The first, second and third lines in equations (3.1.4.2) differ with regard to their frequency dependence with respect to a sinusoidally varying external electric field. A sinusoidally shaped

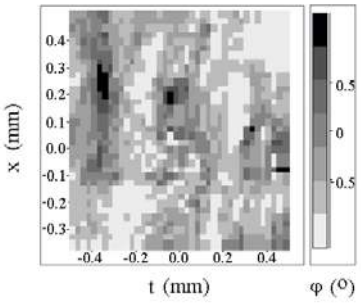

Figure 38. Electrogyration and optical rotation in TGS. Topography of gyrotropy at 300 K. The lateral dimensions are 1 × 1 mm^2 (Kaminsky and Glazer 1998).

modulation of the electric field has the advantage that the results obtained from the Fourier computation are independent of third- and higher-order contributions, although not explicitly included in the analysis. A separation of most of the different terms would be possible if the exact value of δ_0' were known, but that is not the case. The precise value of the refractive indices would be different within a collection of TGS samples on individual differences up to 10^{-5}. A refinement of starting values of the birefringence taken from the literature is established by a definite variation of δ_0'. The first, second and third lines represent the static, linear and quadratic contribution to φ with respect to the applied field. Each of the three lines depends on S_δ and C_δ. However, fortunately, the properties μ_l' and δ_l' change their sign if the sign of the applied field (and the spontaneous polarization) is switched, in contrast to g^{egy}, which does not change. Within the second line in equations (3.1.4.2), the chiral linear-to-E^{ext} ($g^{\text{egy}} D_2 S_\delta$) and electro-optic linear—but not changing sign—term ($\mu_1{}' D_2 C_\delta M_\beta$) are distinguished using the different δ-dependence of the Fourier components S_δ and C_δ. The term $\delta_l{}'\theta_0 D_2 N_\delta$ can be kept small by adjustment. A least-squares fit to the rather large $\mu_l{}' D_2 C_\delta M_\beta$ versus $\delta_0'(\alpha)$ gives ample information to refine the birefringence. The experimental result is that μ_l' is still large enough in the paraelectric phase for temperatures close to the critical temperature.

Additionally, this investigation revealed an offset signal in the electrogyrative contribution to the azimuthal rotation which was assigned to the non-homogeneity of the sample resulting from domain walls (Kaminsky 1994). The topography of optical rotation across a (010) sample plate (thickness 0.47 mm), measured with the 'tilter', is shown in figure 38, showing 'spikes' of positive optical rotation in an otherwise laevorotatory sample. The spontaneous rotation at room temperature obtained from the topography of approximately 2–3° mm^{-1} is larger than that extrapolated from the azimuthal rotation measurements. This discrepancy could be the result of extrapolation to room temperature from the experimental data points of the latter measurement collected within a rather small temperature interval at higher temperature values.

Table 9 summarizes the parameters for empirical analytic expressions which describe the thermal behaviour of the different effects. The induced effects are proportional to the relative dielectric constant ε_{22}.

3.2. Induced effects

3.2.1. Faraday effect. Below we give some examples for the determination of Faraday rotation in optically uniaxial and biaxial crystals. In order to illustrate the agreement between the theoretical description (equations (2.1.4)) and experimental results we consider tetragonal KH_2PO_4 (KDP) (see above, figure 15) to compare computed and experimental $\varphi(\alpha)$-curves. The measurements were performed employing a self-compensating fully automated double-lock-in technique, where the Faraday rotation was recorded as a function of the applied

Table 9. Empirical description of the behaviour of the different contributions to electrogyration in equations (3.1.4.2). The equations describe the properties within 5 K below and above the transition temperature. $t = \frac{1}{T_c}(T_c - T)$, $T_c = 323$ K; $k = 2$: $T < T_c$; 1: $T > T_c$. Wavelength 633 nm; maximum electric field along [010]: 5.9 kV cm^{-1}. Statistical errors in parentheses.

Term	Formula	a	b	c	d
Δn_1	$a + bt + c\sqrt{t}$	−0.0680(1)	0.35(2)	0.041(2)	
Δn_2	$a + bt + c\sqrt{t}$	−0.024 25(1)	−0.0039(2)	−0.0031(2)	
μ_0	$a\sqrt{t} + bt$	1.44(2)°	4.04(6)°		
g^{oa}	$a\sqrt{t}$	−1.8(2)° mm^{-1}			
$g^{egy}\varepsilon_{22}$	$\frac{a}{k\lvert t\rvert + b}$	6.2(3)10^{-6}° V^{-1}	0.0038(2)		
$\mu_l\varepsilon_{22}$	$\frac{1}{e^{ct}+1}\frac{a}{k\lvert t\rvert + b}$	0.17(2)10^{-6}° cm V^{-1}	0.0042(1)	220(3)	
$\mu_q\varepsilon_{22}$	$\frac{a \arctan(c(t-d))}{(k\lvert t\rvert + b)^2}$	0.083(2)10^{-12}° cm^2 V^{-2}	0.0081(2)	−346(22)	0.0039(1)

Table 10. The Verdet tensors of some non-cubic crystals for a wavelength of 633 nm at 293 K (Kaminsky and Haussühl 1993, Kaminsky and Glazer 1997). $[V] = 10^{-4}$° A^{-1}. Errors are given in parentheses. PSG: point symmetry group, n_i: indices of refraction (in orthorhombic symmetry along crystallographic axes a_i), d: density (g cm^{-3}).

Substance	PSG	d	n_1	n_2	n_3	V_{11}	V_{22}	V_{33}
KH_2PO_4	$\bar{4}2$	2.338	1.5074	$=n_1$	1.4669	5.7(1)	$=V_{11}$	2.72(1)
$NH_4H_2PO_4$	$\bar{4}2$	1.798	1.525	$=n_1$	1.479	6.6(2)	$=V_{11}$	3.15(3)
$(NH_4)_2PF_7$	$4mm$	2.015	1.3692	$=n_1$	1.3669	1.22(4)	$=V_{11}$	1.51(3)
TeO_2	42	6.01	2.2597	$=n_1$	2.3935	21(1)	$=V_{11}$	22.5(3)
$LiNaSO_4$	$3m$	2.530	1.4901	$=n_1$	1.4959	2.49(3)	$=V_{11}$	2.30(1)
$Cs_2S_2O_6$	$6m$	3.49	1.523	$=n_1$	1.544	3.5(1)	$=V_{11}$	2.91(2)
$K_2CuCl_4 \cdot 2H_2O$	$4mm$	2.40	1.6460	$=n_1$	1.6105	11.7(2)	$=V_{11}$	5.9(1)
$Rb_2CuCl_4 \cdot 2H_2O$	$4mm$	2.93	1.6368	$=n_1$	1.6130	8.6(2)	$=V_{11}$	5.0(1)
$(NH_4)_2CuCl_4 \cdot 2H_2O$	$4mm$	1.99	1.6722	$=n_1$	1.6440	17.1(3)	$=V_{11}$	5.6(1)
$(NH_4)_2MnCl_4 \cdot 2H_2O$	$4mm$	1.893	1.6472	$=n_1$	1.6084	7.3(2)	$=V_{11}$	3.73(2)
$Na_2[Fe(CN)_5NO] \cdot 2H_2O$	mmm	1.725	1.6074	1.6515	1.5560	3.4(1)	7.8(4)	8.7(1)
$Li_2Ge_7O_{15}$	mmm	4.226	1.7194	1.7163	1.7242	7.6(1)	7.4(1)	8.3(1)
K_2SO_4	mmm	2.662	1.4935	1.4947	1.4973	2.22(3)	2.26(3)	2.28(2)
$C_6H_{14}O_6$ (mannitol)	222	1.4856	1.5505	1.5169	1.5569	4.1(1)	2.1(1)	3.4(2)

Table 11. The symmetric part of the Faraday tensor of $KH_3(COO)_4 \cdot 2H_2O$. The indices refer to the Cartesian reference system $\boldsymbol{e}_2 \| \boldsymbol{a}_2^*$, $\boldsymbol{e}_3 \| \boldsymbol{a}_3$, $\boldsymbol{e}_1 = \boldsymbol{e}_2 \times \boldsymbol{e}_3$; $\boldsymbol{a}_i$ are the crystallographic axes in the setting given by Groth (1921).

V_{11}	V_{12}	V_{13}	V_{22}	V_{23}	V_{33}
6.3(5)	0.1(3)	−3.6(2)	5.5(6)	−0.5(3)	5.1(5)

magnetic field (Kaminsky and Haussühl 1993). Table 10 gives some further examples for the anisotropy of the Faraday effect. The tensorial character was controlled from additional cut crystal plates different to those necessary to determine completely the tensor coefficients. Tables 11 and 12 present the details of the anisotropy of the Faraday effect in a triclinic point group $\bar{1}$, $KH_3(C_2O_4)_2 \cdot 2H_2O$ (Kaminsky and Haussühl 1993).

In measuring the Faraday effect along birefringent sections note that the observed effect is independent of the sign of the retardation δ (see equations (2.1.4)). This feature enables one to measure the change of the retardation in birefringent samples in the course of structural

Table 12. The direction cosines u_{ij} of the principal refractive indices n_i and principal Verdet constants V_{ii}° in $KH_3(COO)_4 \cdot 2H_2O$.

n_i	u_{ij}			V_{ii}°	u_{ij}		
1.412	0.823	0.200	0.531	9.4	0.76	0.10	−0.65
1.535	−0.518	−0.199	0.847	2.0	−0.64	−0.10	−0.76
1.558	0.233	−0.972	0.006	5.5	0.14	−0.99	0.00

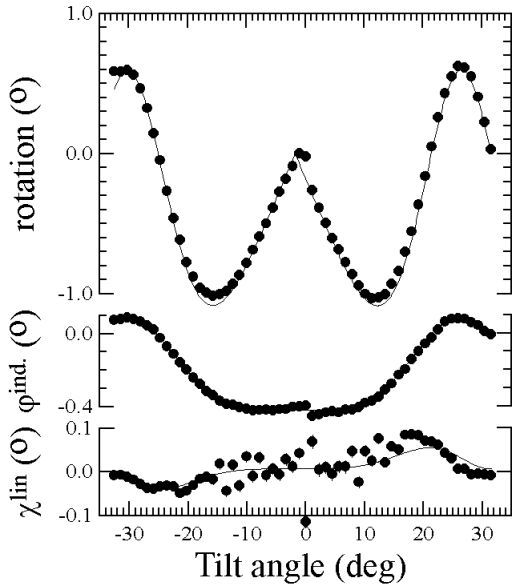

Figure 39. Tilt scans in $FeBO_3$ at a wavelength of 632.8 nm, thickness 0.15 mm. Top: the ellipticity signal due to spontaneous Faraday rotation. The magnetization is parallel to the external magnetic field and points to the left in the above figure for positive tilt angles and to the right for negative angles (sgn(β')-dependence). Middle: the induced Faraday effect φ^{ind}. Bottom: the pseudo-linear (bilinear) magneto-optic rotation of the indicatrix $\chi^{\mathrm{lin}} = (1 - \cos\delta)\chi(HM_1)$. The continuous lines are calculated from theory. Larger errors arise where the induced and spontaneous Faraday rotation is large (from Kaminsky 1997).

phase transitions independent of 90° domain formation (Kaminsky and Haussühl 1993, 1990, Kaminsky *et al* 1994).

The case of ferromagnetic $FeBO_3$ serves as another example of the complex relations similar to those of the induced electrogyration and indicatrix rotation of TGS which connect the azimuthal rotation of the light after passing through the crystal to the optical features.

The $FeBO_3$ sample was tilted about an axis perpendicular to the wavevector with an additional magnetic field parallel to the wavevector (for tilt angle $\alpha = 0$). The induced changes of azimuthal rotation φ, where the component M_1 of the magnetization is easily switched by the component of the magnetic field along [100] which results in $H|M_1$ when a (001) cut sample is tilted ($\beta_o \approx 0$) is given by

$$\varphi \approx \frac{\sin\delta}{\delta}\left[V_{11}\cos^2\beta\frac{LH}{\cos\beta} + V_{11}|M_1|\mathrm{sgn}(H)\frac{\sin\beta}{\cos\beta}\right] + (\cos\delta - 1)$$

$$\times\left[\frac{\chi_0}{\sin\beta}+\frac{n_o^3}{2(n_o-n_e)}q_{2311}(|M_1H|\mathrm{sgn}(\beta)+H^2\sin\beta+M_1^2)\right]. \qquad (3.2.1.1)$$

A Fourier analysis with respect to a sinusoidally varying magnetic field ($H_{max} = \pm 1000$ kA m^{-1}) is performed to separate out the different contributions of the above equation shown in figure 39. Because the value of M_1^2 is not modulated by the external field, this contribution to the azimuthal rotation is not distinguished from the static offset $\chi_0/\sin\beta$. The term $H^2\sin\beta$ was not resolved from the background noise. The value found for $\frac{n_o^3}{2(n_o-n_e)}|HM_1|q_{2311}\mathrm{sgn}(\beta) = -2.4(5)\times 10^{-2\circ}$. From this follows $HM_1q_{2311} = -0.5(1)\times 10^{-5}$. Because the experimental H_{max} is $M_1/5$ at room temperature (Le Craw *et al* 1969), the estimated value of $M_1^2q_{2311}$ is $-2.5(5)\times 10^{-5}$. This is to be compared with $-2.3(5)\times 10^{-5}$ obtained above from the intrinsic rotation with the 'tilter' (section 3.1.3.2).

3.2.2. Electrogyration. With the exception of TGS described above (intrinsic electrogyration), where induced (linear in field) electrogyration was part of the measured azimuthal rotation observed for an electric field along the twofold axis, reliable measurements are performed almost only in cubic crystals because a Fourier analysis is required to separate electrogyration from electric field induced rotation of the indicatrix (Vlokh and Eksp 1971, Miller 1973). Even then, as demonstrated in mannitol, $C_6H_{14}O_6$ (Kaminsky 1997), it is likely that the resulting coefficients, when measured in a strongly birefringent crystal section, are influenced by electro-optic contributions. Only a weakly birefringent Cr-doped (<10%) K alum has been previously studied to good effect (Weber and Haussühl 1974). This study takes account of the effect of a small birefringence using a numerical calculation of the superposition of small optical effects including optical rotation and circular dichroism. Table 13 reviews results published so far. Some results are compared with calculations employing the DES model (see section 2.5).

The electrogyrative signal is derived in almost all cases from the azimuthal rotation φ as a function of the applied electric field. Using equation (2.1.5) and table 2, this results in

$$\frac{\partial\varphi}{\partial E}=\frac{\partial\varphi_0}{\partial E}\frac{\sin\delta}{\delta}+\frac{\partial\theta}{\partial E}(1-\cos\delta)$$
$$+\frac{\partial\delta}{\partial E}\left[(\theta_0+Y_0)\sin\delta-\varepsilon_P\cos\delta-\frac{\varphi_0}{\delta}\left(\frac{\sin\delta}{\delta}+\cos\delta\right)\right]. \qquad (3.2.2.1)$$

Additional contributions to the pure electrogyration thus result from different sources in a non-centrosymmetric crystal when electro-optic effects are possible. This is the case in measurements of electrogyration in quartz, where the ΔY-error ($Y_0 \neq 0$ due to the parasitic ellipticities of the polarizer and analyser) and a misalignment of the sample contribute to the electrogyrative signal even in the case where a Fourier analysis or similar steps (Vlokh and Eksp 1971) are performed to separate $\sin\delta$ and $(1-\cos\delta)$ terms. The measurement in mannitol is made with transparent electrodes along $[111]^P$ where no rotation of the indicatrix was expected. However, $\partial\delta/\partial E$ appeared not to be zero. The measurement suffers from the same problem as that of quartz†. Thus, measurements in quartz (Vlokh and Eksp 1971, Kobayashi *et al* 1987)

† A detailed inspection of the correction terms is necessary to elucidate the origin of the observed quasi-electrogyrative signal. The retardation varies with the applied electric field along $[111]^P$ according to $\frac{1}{L}\frac{\partial\delta}{\partial E} = k\frac{\partial\Delta n_1}{\partial E}+k\frac{\Delta n_1}{L}\frac{\partial L}{\partial E}$; $\frac{\partial\Delta n_i}{\partial E} = -\frac{n^3}{2}\frac{\partial\Delta a_{jk}}{\partial E}$, where $\Delta a_{jk} = a_{jj}-a_{kk}$ denotes the difference of the polarization tensor components $a_{ii} = n_i^{-2}$. When defining a new set of coordinates which relate the indicatrix to the direction of the wavevector along $[111]^P$: $e_1' = \frac{1}{\sqrt{3}}[111]^P$, $e_2' = \frac{1}{\sqrt{2}}[01\bar{1}]^P$, $e_3' = \frac{1}{\sqrt{6}}[\bar{2}11]^P$, it follows (in mannitol: $a_{22}\approx a_{33}$, $n_{1/2/3} = 1.5505/1.5171/1.5568$) that $\Delta n_{1'} \approx -n\frac{3}{6}(a_{22}+a_{33}-2a_{11}) = 0.009\,05$. An electric field along e_1' causes $\frac{\partial\Delta a_{23}}{\partial E} = r'_{331}-r'_{221}$, where $r'_{ijk} = u_{il}u_{jm}u_{kn}r_{lmn}$. The r_{lmn} are the electro-optic coeffcients. The result is $r'_{331}-r'_{221} = \frac{2}{3\sqrt{3}}(r_{231}-r_{123}-r_{312})$,

Table 13. Coefficients of electrogyration. The induced rotation ρ_{ijk} is given in $10^{-7\circ}$ V^{-1}. In older publications the unit 1 rad statVolt $\equiv 0.19^\circ$ V^{-1}. Further, for electric field parallel to the wave vector, a positive component ρ_{111} describes a clockwise rotation if looking *against* the wavevector. ρ_{ijk}^{calc} is obtained with the DES model. Polarizability $[\alpha] = \text{Å}^3$, $\alpha(H^+) = 0$, $\alpha(C^{4+}) = 0.10$, $\alpha(S^{6+}) = 0.05$, $\alpha(N^{5+}) = 0.05$. The polarizabilities given in the table were found from a fit of the calculated refractive indices to the experimental values with the exception of $Bi_{12}GeO_{20}$, where the experimental optical rotation served as a reference. Al $\rightarrow$ Fe := 10.4 means the value given for $\rho_{123}(KAl(SO_4)_2 \cdot 12H_2O)$ when Al is substituted by Fe has to be increased by $10.4 \times 10^{-7\circ}$ V^{-1}, which results in $12.3 \times 10^{-7\circ}$ V^{-1}.

Substance	ρ_{ijk}	ρ_{ijk}^{calc}	Polarizability	Structure	λ (nm)	Reference
$Bi_{12}GeO_{20}$	$\rho_{123} = 11\,970$[a]		O : 2.0	Svensson *et al* (1979)	510	Lenzo *et al* (1966, 1967)
			Bi : 1.40			Moore *et al* (1969)
	=65	175	Ge : 0.7		600	Miller (1973)
α-SiO_2 ($P3_22$)	$\rho_{111} = 29\,000$[a]	0.12	Si^{4+} : 0.23	Le Page and Donnay (1976)	461	Vlokh and Eksp (1971)
	=2600[a]		O^{2-} : 1.19		633	Kobayashi *et al* (1987)
$KAl(SO_4)_2 \cdot 12H_2O$	$\rho_{123} = 1.84$	$\rho_{123} = 0.101$	K^+ : 0.8		550	Weber and Haussühl (1974)
	Al $\rightarrow$ Fe : +10.4			Weber and Haussühl (1976)		
	Al $\rightarrow$ Ga : −1.7					
	S $\rightarrow$ Se : +0.5					
	K $\rightarrow$ Rb : −1.1	K $\rightarrow$ Rb : −0.13	Rb^+ : 1.7			
	K $\rightarrow$ Cs : +0.9		(O^{2-} : 1.6)			
	K $\rightarrow$ NH_4 : −1.6		($\varepsilon_r = 10$)			
$PbMO_4$	$\rho_{333} = \pm 1400$				590	Stasyuk and Kotsur (1985a,b)
$NaClO_3$ (dextrorotative)	$\rho_{321} = 1.25$	1.7	O^{2-} : 1.4, Na^+ : 1	Abrahams and	633	Weber (1979)
			Cl^{5+} : 0.06	Bernstein (1977)		
$NH_3CH_3AL(SO_4)_2 \cdot$	$\rho_{123} = -15.2$				550	Weber and Haussühl (1976)
$12H_2O$	Al $\rightarrow$ Ga : +1.7					
$NH_3CH_3AL(SeO_4)_2 \cdot$	$\rho_{123} = -33.2$				550	Weber and Haussühl (1976)
$12H_2O$						
$Pb(NO_3)_2$	$\rho_{123} = -28$	−34	Pb^{2+} : 3.8	Hamilton (1957)	633	Weber and Haussühl (1977)
	Pb $\rightarrow$ Ba : +18		O^{2-} : 1.2			Kaminsky *et al* (1992)
	Pb $\rightarrow$ Sr : +20					
TGS	$\rho_{222}/\varepsilon = -0.8$–−8	−0.64	O^{2-} : 1.8	Itoh and Mitsui (1973)	633	Kaminsky (1994)
Mannitol, $C_6H_{14}O_6$	$\Sigma\rho_{ijk} = 17\,000$[a]	32.2	C^{4+} : 0.2	Kaminsky and	633	Kaminsky and Glazer (1997)
			O^{2-} : 1.9	Glazer (1997)		

[a] Electro-optic contributions were not eliminated. Electrogyration has also been measured in Cr_2O_3 (Odell and White 1970) in α-HiO_3 (Vlokh *et al* 1973) and $BaMO_4$ as well as $SrMO_4$ (Belogurov *et al* 1979). The signs given in publications by Weber (1974, 1976, 1977, 1979) are reversed because we use a different definition of sign here, i.e. that of optical rotation.

are by no means free of parasitic effects and one therefore has to conclude that the rather large effect (table 13) is not at all related to electrogyration.

In a cubic crystal with a very small parasitic $\delta = \delta_0$ we find

$$\frac{\partial\varphi}{\partial E} \simeq \frac{\partial\varphi}{\partial E} + \frac{\partial\theta}{\partial E}\frac{1}{2}\delta_0^2 + \frac{\partial\delta}{\partial E}(\varepsilon_P + \delta_0[\theta_0 + Y_0 - \varphi_0]). \tag{3.2.2.2}$$

The alums and $Pb(NO_3)_2$ are of point symmetry $m3$ where no linear electro-optic and linear electrostrictive effect pollute the electrogyrative measurement, which consist only of pure electrogyration in contrast to the case of $Bi_{12}GeO_{20}$, where the electro-optic contributions most probably dominate the observation. It is therefore more or less correct to say that electrogyration has not been discovered by Lenzo *et al* (1966), as pointed out earlier (Miller 1973).

The measurements in TGS are slightly affected in a similar way as outlined above; however, the pure electrogyrative signal is much larger than that part related to the $\partial\delta/\partial E$ term, which in addition is separated easily from pure electrogyration as it does not change its sign when the applied electric field is reversed.

When we release the restraint of extinction angle θ to be small, but still assume that optical gyration φ_0 is reasonably small, (3.2.2.2) can be rewritten as (Weber 1979, neglecting Y_0)

$$\frac{\partial\varphi}{\partial E} \approx \frac{\partial\varphi_0}{\partial E} + \frac{\partial\delta}{\partial E}\left(\varepsilon_P - \frac{\delta}{4\varphi_0}\sin 4\theta_0\right) \tag{3.2.2.3}$$

and a similar equation is found for the ellipticity of the wave after the sample:

$$2\varepsilon\frac{\partial\varepsilon}{\partial E} \approx \frac{\partial\delta}{\partial E}\frac{\delta_0}{4}(1 - \cos 4\theta_0). \tag{3.2.2.4}$$

The latter equation depends only on the electro-optic effect. $\partial\varphi/\partial E$ and $2\varepsilon\partial\varepsilon/\partial E$ are found from the equation that relates the variation of the light intensity ratio I/I_0 to the ellipticity and azimuthal rotation of the light wave emerging from the sample (compare with (2.1.5)). The exact formula is given by Ramachandran and Ramaseshan (1961):

$$\begin{aligned}\frac{1}{I_0}\frac{\partial I}{\partial E}(\varepsilon, \varphi, \Omega) &= \frac{1}{2}\frac{\partial}{\partial E}(1 - \cos 2\varepsilon\cos 2\varphi) \\ &\approx \frac{\partial\varphi}{\partial E}\sin 2\Omega + 2\varepsilon\frac{\partial\varepsilon}{\partial E}\cos 2\Omega \qquad \varepsilon \ll 1.\end{aligned} \tag{3.2.2.5}$$

This equation can be used to derive the coefficient $\partial\varphi/\partial E$ in (3.2.2.3) and $2\varepsilon\partial\varepsilon/\partial E$ in (3.2.2.4). The coefficients are then modulated in addition to the rotation by analyser angle Ω in rotating the sample to different extinctions θ_0. The parasitic effects of the optical train are found by comparing different geometrical arrangements of light wave and electric field. This technique was used to find the electrogyration, piezogyration and electro-optic effect in $NaClO_3$ (Weber 1979). The coefficients for piezogyration in the dimensions of an induced optical rotatory power in dextrorotative $NaClO_3$ at 633 nm are $\Gamma'_{1111} = 30.8 \times 10^{-7\circ}$ m N^{-1}, $\Gamma'_{1122} = 5.7 \times 10^{-7\circ}$ m N^{-1}, $\Gamma'_{1122} = -32.8 \times 10^{-7\circ}$ m N^{-1}, $\Gamma'_{2323} = 3.8 \times 10^{-7\circ}$ m N^{-1}. Further details concerning piezogyration in GaAs, InP, ZnSe and CdTe are found in the review by Koopmans *et al* (1998).

whereas $\partial L/\partial E = \frac{2}{3\sqrt{3}}(d_{123} + d_{231} + d_{312})$. Assuming that the linear electrostriction d_{ijk} is similar to or larger in magnitude than the electro-optic effect ($r_{ijk} \approx 0.2$ pm V in mannitol) we obtain $k\delta\Delta n/\partial E = 1.4 \times 10^{-6}$ V^{-1}, $k\Delta n/L * \partial L/\partial E \geqslant 30 \times 10^{-6}$ V^{-1}. $\partial\theta/\partial E = 0$ in mannitol for this direction. With E along $[111]^P$, 0.1°–$3^\circ = \theta_0 \gg Y_0$, $L = 0.635$ mm, and $\rho(111) = -22^\circ$ mm^{-1}, the largest contribution by far with $\sin\delta/\delta$-dependence is due to $\delta\theta_0\frac{\Delta n}{L}\frac{\partial L}{\partial E} \approx 10^{-2\circ}$ V^{-1} or larger. This is about as large as the observed parasitic effect of 0.3° V^{-1} (Kaminsky and Glazer 1997). We therefore conclude that the electrogyration in mannitol is probably 100 times or more smaller than the observed effect.

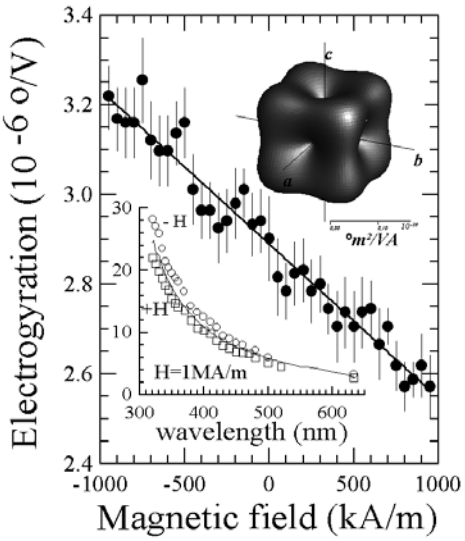

Figure 40. Magneto-electrogyration in $Pb(NO_3)_2$ along [111] at 632.8 nm. Top inset: the representation surface of longitudinal magneto-electrogyration. Bottom inset: dispersion of the magneto-electrogyration along [111] (Kaminsky *et al* 1992).

3.2.3. Effects induced with combined fields. Observations of the magnetic and electric field induced gyration are rare. Reports are given on $Bi_{12}SiO_{20}$ (Odell and White 1970), where the magnetic field created by the magneto-electric effect causes Faraday rotation. This effect, however, is not strictly a combined field effect. The electro-Faraday effect was found in $Cd_{0.49}Mn_{0.51}Te$ (Koyanagi *et al* 1989). An observation of magneto-electrogyration was claimed by Kaminsky *et al* (1992) in $Pb(NO_3)_2$, where linearity in the magnetic field of the observed excess rotation to the electrogyration has been demonstrated (figure 40).

Such an effect can result from the temperature change caused by conduction losses in the sample which change the Faraday rotation. This effect could cause an excess rotation linear with the magnetic field. However, the 'thermal' contribution is quadratic in the electric field.

Formally, we need to assume that the tensor for mangneto-electrogyration reverses sign with reversal of time. This is the case in antiferromagnetic materials for example.

$$\frac{D_i}{\varepsilon_0} = \ldots g^{\mathrm{meg}}_{ijklm}\mathrm{sgn}(t)\frac{\partial E_j}{\partial x_k}E_l H_m = \ldots \mathrm{i}k_k g^{\mathrm{meg}}_{ijklm}E_j\mathrm{sgn}(t)(E_l H_m) \qquad (3.2.3.1)$$

then describes an electric and magnetic field induced gyrotropy. Lead dinitrate is not an antiferromagnetic material; however, considering the small size of the observed effects and taking into account that Pb^{2+} containing substances interact quite strongly with external magnetic fields, and considering also the cubic symmetry of this material, we might come close to the antiferromagnetic case. Further studies are definitely required here.

Table 14 summarizes the complete tensor determination of the magneto-electrogyration in $Pb(NO_3)_2$, $Ba(NO_3)_2$ and $Sr(NO_3)_2$ on the basis of a linear response of magneto-electrogyration to each of the applied fields (Kaminsky *et al* 1992).

In ferroelectric substances, the magneto-electrogyration is caused by an interaction of the spontaneous polarization and an external magnetic field (Vlokh 1981, Vlokh *et al* 1984, 1986a,b). These experimental results caused a controversy concerning the invariance to time inversion and it was assumed that only second-order effects are possible in ferroelectrics (Pisarev 1994). Magneto-electric effects were discussed by Chupis (1997), who gives a quantum mechanical interpretation. The effect should be observed for parallel electric and magnetic fields and should basically vanish for perpendicular external fields. This observation would be supported by the experiments in lead nitrate (Kaminsky *et al* 1992).

4. Discussion

4.1. General remarks

4.1.1. Technical aspects. Modern polarimeters (based on HAUP etc) allow the determination of an intrinsic gyrotropy with such an accuracy in transparent crystals that in the worst case (high values of birefringence) it is possible to obtain the sign and, at least, the dimension of the magnitude of the gyrotropy. In general, the resolution of non-induced gyrotropy separated from double refraction is between 0.05° and 5° in a birefringent direction†.

Many very reliable results were obtained using the Wavelength scanning HAUP method developed by Moxon and Renshaw (1990), which, however, still is slightly affected by the so-called 'ΔY'-error as a result of a small misalignment of polarizer and analyser before the measurement is started. The most recent achievement ('tilter') tries to take account of all unwanted effects which contribute to the observed signals, including the 'ΔY'-error, and the future will show whether this method becomes a standard approach to measure intrinsic optical rotation.

One basic achievement of the 'tilter' method compared with other methods is its high speed, because of which it is possible to derive topographies of, for example, the optical rotation and the intrinsic Faraday effect within a reasonable time. As a special feature, the 'tilter' method can distinguish in some cases between Faraday effect and optical rotation, even if both are mutually present. However, the 'tilter' is a method rather than a device and unites most of the previous technical ideas. For example, the modulation of the intensity used in the 'tilter' version of the present author with the sequence quarter-wave-plate Pockels modulator could be replaced by a combination of a Faraday rotator and a polarizer or simply by a single mechanically driven polarizer.

Another sensitive technique which in principle could be combined with the 'tilter' idea is for example the Sagnac interferometer (Dodge *et al* 1994). A great disadvantage of the Sagnac interferometer in the case described here is its sensitivity only to non-reciprocal (changing sign with time inversion) phase shifts, because it is not possible to obtain the $2Y\Omega\cos\delta$-contribution in the signal, which is needed to derive the (reciprocal) phase shift.

With the technical state so far achieved it becomes possible to characterize spontaneous changes of the polarization tensor $\{a_{ij}\}$ and spontaneous gyrations such as the Faraday rotation or optical rotation of (weakly) ferromagnetic or ferrimagnetic magnetoelectrics and ferroelectrics at zero magnetic and electric fields‡.

The demonstration with ferroelectric TGS and ferromagnetic $FeBO_3$ as test samples shows how, in principle, modern, computerized polarimeters can be applied to other transparent materials and optical effects similar to those described above. The complexity of the interference of induced chiral and linear optical properties has sometimes been underestimated. The separation of different Fourier components by complete use of the analytic information available when the sample is tilted and the effects are at the same time induced by an electric or magnetic field was shown to be successfully applied to these difficult cases.

The measurements in TGS (Kaminsky 1994) revealed a special optical anomaly of crystals which undergo a phase transition: the inhomogeneity due to the formation of domains. The mixture of domains and domain walls even in the para-phases, where no macroscopic order is observed, lead to an additional contribution to a gyrotropy which is different from intrinsic optical rotation or electrogyration. Measurements in which no modulation of the retardation is performed are insensitive to this difference in origin of a gyrotropy. It is very likely that non-homogeneity, whatever the origin, is basically responsible for any anomalous gyrotropy in

† As a rule of thumb, one can expect a reliability of $\pm 50^\circ\ \mathrm{mm}^{-1}\Delta n$, where Δn is the double refraction of the sample.
‡ This allows the study of spin-glass systems without applying a magnetic field.

incommensurate crystals or mysterious peaks of quasi-optical rotation at critical temperatures.

When inducing the Faraday effect via a magnetic field, the birefringence of any sample in the course of a phase transition is measured independently of the formation of 90° domains, because within the term $\sin(\delta)/\delta$ any change of sign in δ cancels. The change in birefringence due to the magnetic field can be neglected (Dvoran 1993).

Other polarimetric techniques, such as the rotating analyser technique (see, e.g., Glazer *et al* 1996), although of great value to study the birefringence, will probably not reach the sensitivity of those techniques described above where small deviations from a crossed polarizers settings, with the ellipsoidal cross-section closely aligned to the polarizer, modulate the intensity off its minimum value. It actually can be shown that the overall resolution is a maximum for a modulation equivalent to a rotation of the polarizer and analyser of a few degrees only.

4.1.2. Overview of experimental results. Although chiro-optical properties have been investigated for almost 190 years, reliable data on the anisotropy of the different effects are quite rare. Assignments of the optical rotation to the absolute structures of crystals have recently been attempted in some cases and further work on the large number of optically active materials (in the sense of optical rotation) has to follow†.

To find the absolute structure assignment, it is necessary to specify the so called 'Flack enantiopole parameter' x: $|F(\boldsymbol{h}, x)|^2 = (1 - x)|F(\boldsymbol{h})|^2 + x|F(-\boldsymbol{h})|^2$ (Flack 1983). This number is 0 if the structure of the crystal and that of the model used for the refinement are identical, and it takes the value 1 if the model structure is the point inverse of the real crystal. Without reasonable anomalous scattering of a substance, the Flack enantiopole parameter cannot be derived. Recently, the high-resolution chi-scan method and the RenningerÑUmweg interference (three-beam case) promises to be much more efficient in deriving the absolute structural configuration (Weckert 1997).

Some confusion still remains with respect to the optical rotation of non-enantiomorphous but still non-centrosymmetric crystals (point groups $\bar{4}2m$, $\bar{4}$, $mm2$, m). Although predicted as early as 1882 by Gibbs and Pockels (1906), many believe that optical rotation requires enantiomorphism. Experiments by Hobden (1967, 1968a,b, 1969) in $AgGaS_2$ (PG $\bar{4}2\ m$), Futama and Pepinsky (1962) in $LiH_3(SeO_3)_2$ (PG $mm2$) and $NaNO_2$ (PG m), confirmed by Chern and Phillips (1970a,b, 1972) in the latter case, showed optical rotation. It exists in certain directions governed by the tensorial symmetry of optical rotation (figure 41). A first complete tensor determination for PG m has just recently been accomplished in K_2ZnCl_4, which enters this symmetry below 145 K (Kim *et al* 2000). The job of measuring such a tensor thus has been completed 94 years after the prediction by Pockels of this symmetry. We can say now that optical rotation requires at least the absence of an inversion centre where the dipole–dipole interactions add up to a non-vanishing optical rotation in certain directions, and does not necessary require a structural chirality.

Earlier on in their theoretical treatment of optical rotation, Pine and Dresselhaus (1971) suggested a relation between the optical rotation components of uniaxial crystals of the form $\rho_c/\rho_a \approx -2c/a$, where ρ_c and ρ_a are the rotatory power along the crystallographic c- and a-axis, respectively. There is a majority of crystals which show at least a difference in sign between the components. However, if crystals of a lower symmetry are included, we find in L(+)-tartaric acid an interesting case, because the rotatory power along the acute bisectrix is opposite in sign to those along the other principal directions, which in addition are of a similar

† A difficulty arises when the optical rotation is published in form of the so called g-tensor. To find the observable rotation the average refractive index n has to be known, since $\rho(^\circ\,\mathrm{mm}^{-1}) = \frac{0.18}{n\lambda(m)}g$. Usually, n is not given and sometimes it is not clear at which wavelength λ the measurements have been performed. Because it is the rotatory power ρ which is measured, the given results are incomplete if only g is published.

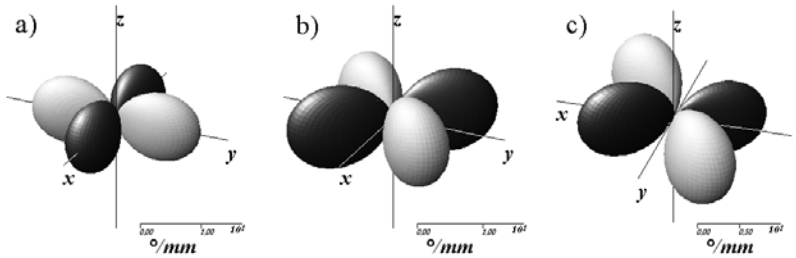

Figure 41. Representation surfaces of optical rotation in non-enantiomorphous crystals. (*a*) KH_2PO_4 ($\bar{4}2m$), (*b*) $RbTiOAsO_3$ ($mm2$), (*c*) K_2ZnCl_4 (m, 70 K). No measurement is known in symmetry $\bar{4}$.

magnitude (table 6). This result is in contrast to orthorhombic mannitol, where all components are of the same sign. A further exception to 'Pine's rule' is TeO_2.

Second-order optical rotation has been discussed but attempts to validate it by experiment have not succeeded so far (Haussühl 1990).

Induced chiral effects of third and higher tensorial rank have been measured. Only in those cases where the samples are centro-symmetric, the electrogyration and magneto-electrogyration could have been observed with conventional techniques because these symmetries do not exhibit an induced indicatrix rotation or induced changes of the retardation as the linear electro-optic effect is forbidden by symmetry. In other cases the contribution due to the electro-optic induced rotation of the indicatrix or change of the retardation value are responsible for the large magnitude of the observed quasi-chiral signals. When looking at published quadratic electrogyration data, at least a doubt is left to what extent the observed signals are connected to electrogyration, because the linear effects are already difficult to observe.

4.2. Model calculations and structure

4.2.1. Empirical models. Estimations of the Faraday rotation with the 'periodic table' of specific Faraday rotations of ions (figure 2) are most reliable in cubic and other optically isotropic materials. A similar additive rule was established earlier to describe the refractive indices (see Tessman *et al* 1953). For main-group ions with closed shells the specific Faraday rotation is in proportion almost to the square of the electronic polarizability of the ions (figure 42). The Faraday rotation of other ions seems to be not correlated to the polarizability.

4.2.2. The dipole–dipole model. The models used in this presentation to calculate optical rotation and electrogyration are based on the electronic polarizability of the atoms and the atomic structure. These calculations show good accord with the experimental results with respect to the optical rotation when the bonds are not semiconducting or metallic. Even in the case of organic molecular crystals the model seems to estimate the anisotropy of the optical rotation; however, the absolute values derived in organic crystals deviate quite strongly from the experimental results. Most of the signs are obtained correctly.

When the highest symmetry in a structure is a 2_1-screw axis, the sign of the optical rotation depends on the atomic coordinates and it is not possible to specify the enantiomorph as easily as in the case of three-, four- or sixfold screw axes. The optical activity of mannitol ($P2_12_12_1$) serves as an example. The structure when looking towards the c-axis is shown in figure 43, where the ellipsoids represent the effective anisotropic electronic polarizabilities. An improper

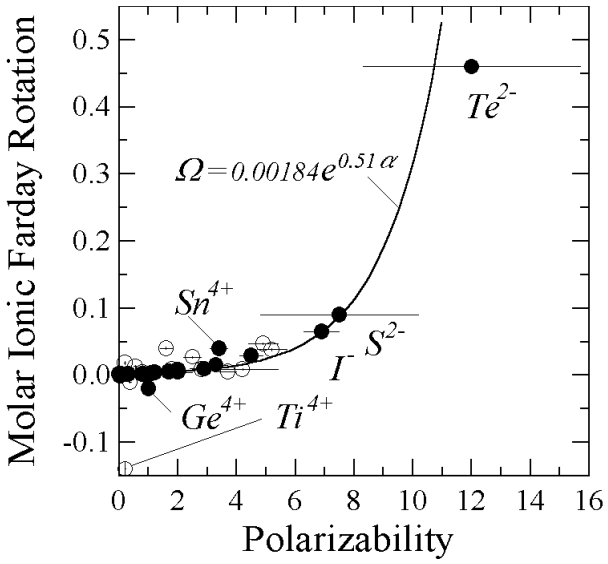

Figure 42. The molar ionic Faraday rotations Ω (see figure 15) plotted against the electronic polarizability α[Å^3] of the ions (Tessman *et al* 1953). The error bars result from averaging the different values given for the polarizability. Exceptional ions are labelled. Ions of the main group elements are plotted with filled circles, others in open circles.

threefold screw axis (this means that along a specific directions an infinite sequence of atoms is approximately arranged in the form of a screw axis) is denoted by the numbers 1/2/3 etc, following the atoms from back to front. The polarizabilities of the oxygens are largest in the direction of the improper screw axis (radial orientation). According to the rules 2 and 3 outlined in section 2.3 for discussing a structure with respect to optical rotation, we can expect the polarization to be rotated anti-clockwise when looking towards the light source, i.e. when the beam comes from back to front. The improper fourfold axis denoted by *a*/*b*/*c*/*d* consists of polarizability ellipsoids whose directions of largest polarizability are oriented radially as well as tangentially to the screw axis. The axis is rather close to being a twofold screw and does not contribute much to optical activity. According to the definition of the sign of optical activity, this results in a negative coefficient ρ_{33}, which agrees well with the observation.

Figure 44 shows the structure of $LaBGeO_5$ ($P3_1$) viewed towards the *c*-axis. The bonds of this inorganic substance are mainly ionic and should be described well by the dipole–dipole model. The ellipsoids illustrate the anisotropy of the electronic polarizability as calculated with the dipole–dipole model. Distinguished are the anti-clockwise helix of radial BO_3 oxygen polarizabilities and a clockwise helix of tangential oriented polarizability ellipsoids of La and Ge. Both distinct helices give a positive, i.e. clockwise, optical rotation. However, the contribution of the other oxygens seems to be more or less opposite to these helixes. The experimental result for space group symmetry $P3_1$ are $\rho_{33} = -2.1(1)^\circ$ mm^{-1}, $\rho_{11} = 6(2)^\circ$ mm^{-1}. The structure shows a specific behaviour, i.e. there is no unique set of parameters which permits the correct calculation of the refractive indices: in fact there are many equivalent sets for the polarizability volumes (table 13). However, one particular set matches the experiment very well: $\alpha_B = 0.00$ Å^3, $\alpha_{Ge} = 0.427$ Å^3, $\alpha_O = 1.561$ Å^3, $\alpha_{La} = 1.45$ Å^3. These polarizability volumes are not far from those published earlier (Tessman *et al* 1953). In this case we find $\rho_{33} = -2.768^\circ$ mm^{-1}, $\rho_{11} = 6.466^\circ$ mm^{-1}.

Table 14. The system of equations, geometrical arrangement and effective magneto-electrogyration Γ' ($10^{-22\circ}$ m^{-2} V^{-1} A^{-1}) for a wavelength of 633 nm and room temperature. $\boldsymbol{G}$: wavevector, $\boldsymbol{E}^{\mathrm{o}}$: direction of electric field, $\boldsymbol{H}^{\mathrm{o}}$: direction of magnetic field. The last four columns indicate the contribution of the components to the observed value Γ'. For example the fourth row should be read $\Gamma' = \frac{1}{3}\cdot\Gamma_{1111} + \frac{1}{3}\cdot\Gamma_{1122} + \frac{1}{3}\cdot\Gamma_{1133} + \frac{2}{3}\cdot\Gamma_{1221} + \frac{2}{3}\cdot\Gamma_{1331}$. Errors are given in parentheses.

g	E^{o}	H^{o}	Γ'(Pb)	Γ'(Ba)	Γ'(Sr)	Γ_{1111}	Γ_{1122}	Γ_{1133}	Γ_{1221}	Γ_{1331}
[100]	[100]	[100]	−6.1(2)	−4.2(3)	−3.9(4)	1	0	0	0	0
[100]	[010]	[010]	−2.0(4)	−0.3(3)	−0.2(3)	0	1	0	0	0
[100]	[001]	[001]	−2.7(3)	−0.2(3)	−0.2(3)	0	0	1	0	0
[111]	[111]	[111]	−19.0(8)	−5.4(4)	−2.4(1)	$\frac{1}{3}$	$\frac{1}{3}$	$\frac{1}{3}$	$\frac{2}{3}$	$\frac{2}{3}$
[110]	[110]	[110]	−14.9(3)	−4.2(3)	−3.0(3)	$\frac{1}{2}$	$\frac{1}{4}$	$\frac{1}{4}$	$\frac{1}{2}$	$\frac{1}{2}$
[110]	[1$\bar{1}$0]	[110]	−4.7(4)	−0.5(2)	−0.4(1)	0	0	0	$-\frac{1}{2}$	$\frac{1}{2}$
[210]	[210]	[210]	−10.9(5)	−4.1(3)	−3.4(5)	$\frac{17}{25}$	$\frac{4}{25}$	$\frac{4}{25}$	$\frac{8}{25}$	$\frac{8}{25}$
[210]	[001]	[001]	−2.6(9)	−0.4(3)	0.1(2)	0	$\frac{1}{5}$	$\frac{4}{5}$	0	0
				$Sr(NO_3)_2$		−4.0(3)	−0.2(2)	0.0(1)	−0.4(1)	−1.1(1)
Components of Γ_{ijkl}				$Ba(NO_3)_2$		−4.0(4)	−0.3(4)	−0.3(3)	−1.9(4)	−2.9(4)
				$Pb(NO_3)_2$		−6.0(3)	−2.0(5)	−2.7(4)	−6.0(6)	−14(1)

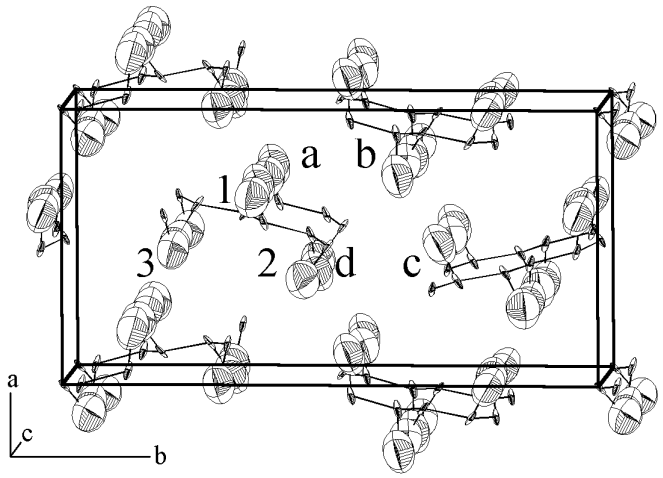

Figure 43. The structure of mannitol ($P2_12_12_1$) when looking towards the *c*-axis. The ellipsoids represent the effective anisotropic electronic polarizabilities. An improper threefold screw axis is denoted by the numbers 1/2/3 etc, following from back to front. An improper fourfold axis is denoted by *a*/*b*/*c*/*d*. The axis is rather close to being a twofold screw and does not contribute much to optical rotation.

Table 15. The calculation of refractive indices (Kaminskii *et al* 1991) and optical rotation in space group $P3_1$. Polarizability volumes α in Å^3. Wavelength 680 nm.

α-La	α-O	α-Ge	ρ_{11} ($^\circ$ mm^{-1})	ρ_{33} ($^\circ$ mm^{-1})
0.85	1.7673	0.0682	2.211	−9.647
1.00	1.7128	0.1809	4.279	−8.179
1.15	1.6603	0.2748	5.525	−6.404
1.30	1.6101	0.3544	6.162	−4.556
1.45	1.5605	0.4271	6.466	−2.768
1.60	1.5117	0.4937	6.515	−1.121

The criticism may be made that both examples used the calculated polarizabilities instead of the thermal ellipsoids as a basis for the visual interpretation. Firstly, it is comforting to note that the general rule, which sees a large electronic polarizability in a direction where the thermal parameter is small, is fully confirmed. Secondly, using the polarizabilities gives a slightly easier access to the interpretation because it helps to distinguish between important and insignificant atoms inside a structure. Hydrogen, for example, showed a rather large thermal motion in mannitol, whereas its polarizability was entirely negligible (see Kaminsky and Glazer 1997).

4.2.3. Optical rotation in iso-structural crystals. If the optical rotation is so closely correlated to the electronic polarizability as outlined above, it should be possible to specify a function from which optical rotation can be derived for iso-structural crystals. The KDP family should serve as an example. An investigation of optical rotation versus the polarizability of the cations (phosphorus and potassium) at constant oxygen polarizability $\alpha_O = 1.6$ Å^3 and constant cell parameters (average over the KDP family) is compared with the experimental results. The general behaviour is that the modulus of the optical rotation increases strongly with the polarizability on the phosphorus position but decreases in proportion to the polarizability on the potassium location. The electronic polarizabilities of the cations in increasing order are

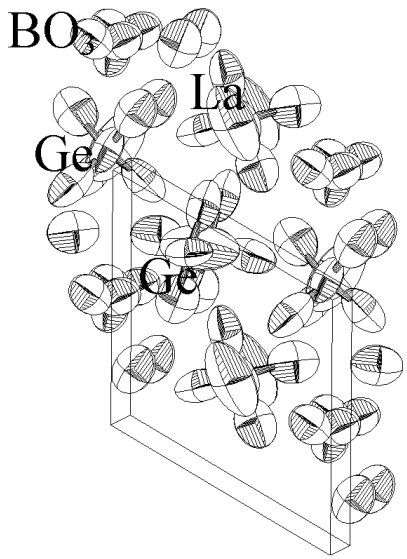

Figure 44. The structure of $LaBGeO_5$ ($P3_1$) when seen towards approximately the *c*-axis. The dextrorotative contribution to optical rotation is dominated by the screw-axis-like sequence La–Ge–La–Ge etc. The other oxygen seem to counterbalance the dextrorotative helices.

P < As < K < Rb < NH_4 < Cs. According to the observations made above, this would result in the series (increasing modulus of optical rotation) $NH_4H_2PO_4 < RbH_2PO_4 < KH_2PO_4 < CsH_2AsO_4 < NH_4H_2AsO_4$. At 633 nm, one experimentally obtains the optical rotations ρ_{22} of 6/7/10/14/25° mm^{-1} (table 5) when assuming a simplified λ^{-2} dispersion of optical rotation.

Another example is $NaBrO_3$ and $NaClO_3$. It has been known for more than a century that these isostructural compounds, when having the same handedness in their structures, still possess opposite sign in the optical rotation. Calculations with the dipole–dipole model do just result in different signs. It is also observed that the calculations depend critically on the structures used. However, when the polarizability of Br^{5+} is varied for fixed values for Na^+ and O^{2-} there is a distinct reduction of optical rotation for a realistic polarizability of the ions.

4.2.4. The DES model. On the basis of the dipole–dipole model introduced by Devarajan and Glazer (1986), the idea of virtually shifting the atoms in proportion to their polarizability volumes (Kaminsky and Glazer (1997), DES model) led to a successful calculation of electrogyration in several crystals. This idea is not restricted to the calculation of electrogyration. Calculated electro-optic effects and second-harmonic coefficients were surprisingly close to the experimental values.

As an example, the experimental results in the course of the phase transition of TGS were recalculated (Kaminsky and Glazer 1997) using the structures published for different temperatures by Itoh and Mitsui (1973). The calculations needed the experimental dielectric constants. In a first step, polarizability volumes were modelled to find those values with which the refractive indices were calculated as close to the experimental values as possible. On the basis of these parameters the linear and quadratic electro-optical properties were confirmed. A distinct difference between the structural displacements caused by an external electric field and those caused by the forces arising from the ferroelectricity became quite obvious: the induced electrogyration has opposite sign to the spontaneous optical rotation. This result confirms the experimental observation (Kaminsky 1994). The electro-optical properties seem to be less sensitive to these differences in the atomic displacements.

A further example for the calculation of optical properties is $NaClO_3$. After modelling the

polarizability volumes (Å^3) for O: 1.4, Na^+: 1, Cl^{5+}: 0.06 to approximate the refractive index and optical rotation, one finds an electrogyration of $\rho_{321} = 1.7 \times 10^{-7\circ}$ V^{-1} (experiment $1.25 \times 10^{-7\circ}$ V^{-1}) and the electro-optic effect is $r_{321} = -0.33$ pm V^{-1} (experiment -0.38 pm V^{-1}), where the relative dielectric constant was set to three for the dextroroative structure.

The DES model still needs experimental dielectric constants. An attempt was made to connect the dielectric features to the thermal ellipsoids describing the motion of the atoms in a structure, which itself is correlated with the ionic polarizability $\alpha_{ij}(k)$ of the atoms (Kittel 1976, Kaminsky and Glazer 1997): $\alpha_{ij}(k) = \beta_k^2 Q U_{ij} (T = 300$ K), $q_k = \beta_k e$; e: electron charge of atom k. $[\alpha_{ij}] =$ Å^3, $[U_{ij}] =$ Å^2, $Q = 288$ Å. The anisotropy of the dielectric constants is derived by adjusting β_k to the average dielectric constant and then using the Clausius–Mosotti equation:

$$\frac{\varepsilon_{ij} - 1}{\varepsilon_{ij} + 2} = \frac{4\pi}{3} \sum_k N \alpha_{ij}(k)$$

to find the anisotropy of the dielectric constants, where $N = dN_A/M$, $d =$ density, $M =$ molecular weight and N_A is Avogadro's number. This approach needs to be tested on a larger number of crystals and may need some modifications. However, in the case of mannitol, where the oxygens have by far the largest polarizability, it described the anisotropy of the dielectric constants with reasonable accuracy.

Principally the DES model predicts the electro-optical effects at constant strains. However, quasi-static measurements are performed usually at constant pressure, not strain (unclamped case). Thus, one would expect large differences between calculation and experiment when there is a large contribution to the observed effects via the elasto-optic constants or other secondary mechanisms, which are a result of the deformation of the crystal due to electrostriction. Rochelle salt is such a case whereas TGS is only weakly affected by electrostriction.

5. Conclusions

Here we have shown how to measure gyrotropy by modulating the retardation while accounting for parasitic effects as well as sample inhomogeneity.

Circular birefringence is described by different theories which account for special cases. Natural optical rotation and related effects are strongly connected to the dipole–dipole interaction phenomenon, where electrogyration arises from the symmetry breaking effect of an applied electric field which shifts the nuclei relative to the electronic shells in proportion to the polarizability of each atom.

Calculations performed on that basis automatically obey Neumann's rule. This rule is conserved in centrosymmetric incommensurate phases where previously reported effects are of a parasitic nature.

Acknowledgments

I wish to express my great gratitude to Professor Bart Kahr, Professor Anthony Michael Glazer, Professor Siegfried Haussühl and the referees for careful revision of the manuscript at different stages of its composition.

Appendix A. Tables

Table A.1. Verdet constants in optical isotropic directions which have not been published by Haussühl and Effgen (1988) but were used for the periodic system of molar Verdet constants in figure 13 (Kaminsky 1989). ρ, density (g cm^{-3}); $\alpha(10^{-6}\mathrm{K}^{-1})$, linear cubic expansion coefficient; $V(10^{-4\circ}\mathrm{A}^{-1})$, Verdet constant in the isotropic direction of the wavevector; $\mathrm{d}\log\varphi/\mathrm{d}T\,(10^{-4}\mathrm{K}^{-1})$, linear temperature coefficient; Q (K A^{-1}), paramagnetic temperature coefficient. Wavelength: 633 nm. $T_\circ = 293$ K. $V(T) = V\{1 + (\mathrm{d}\log\varphi/\mathrm{d}T - \alpha)\ (T - T_\circ)\}$ (linear); $V(T) = V + Q/T$ (paramagnetic).

Substance	ρ	α	V	$\mathrm{d}\log\varphi/\mathrm{d}T$	Q
$Cd_{1.5}PMo_{12}O_{40} \cdot 30H_2O$	2.637	82	1.17(3)	−10(1)	
$Co(H_2PO_2)_2 \cdot 6H_2O$			4.0(1)		−0.0457(3)
$Co_{1.5}PMo_{12}O_{40} \cdot 30H_2O$	2.547	81	1.38(1)		−0.013(1)
$Cu_{1.5}PMo_{12}O_{40} \cdot 30H_2O$	2.562	80	1.29(2)	−22(2)	
$EuPMo_{12}O_{40} \cdot 30H_2O$	2.642		0.93(1)		
$(Na_3PO_4)_2 \cdot NaF \cdot 19H_2O$	2.217		3.28(6)	1.07(6)	
$NdPMo_{12}O_{40} \cdot 30H_2O$	2.639		0.347(4)		−0.017(1)
$NH_3OHCr(SO_4)_2 \cdot 12H_2O$			3.56(2)		−0.0160(6)
$(NH_4)_4Fe(CN)_6 \cdot 2NH_4Cl \cdot 3H_2O$	1.490		5.1(1)	0.3(6)	
$Ni(BrO_3)_2 \cdot 6H_2O$			7.0(1)	−3.2(2)	
$Ni_{1.5}PMo_{12}O_{40} \cdot 30H_2O$	2.549	86	1.62(2)	−8(4)	
$MnCl_2 \cdot$ betain			3.73(1)		−0.0358(4)
$Sr(BF_4)_2$			1.62(3)	−1.7(4)	
SrF_2	4.33		2.10(6)	0.96(4)	
TlBr	7.557		30(1)	4(1)	
$Zn_{1.5}PMo_{12}O_{40} \cdot 30H_2O$	2.560	73	1.24(2)		

Table A.2. Absolute structure of laevorotatory SiO_2 (low quartz) $P3_12$ (Le Page and Donnay 1976). $a = 4.913$ Å, $c = 5.405$ Å.

Si	0.530 13	0.530 13	$\frac{2}{3}$
O	0.414 1	0.268 1	0.8812

Table A.3. Absolute structure of laevorotatory α-$AlPO_4$, $P3_22$ (Ngo Thong and Schwarzenbach 1979). $a = 4.9423$ Å, $c = 10.9446$ Å.

Al	0.466 43	0	$\frac{2}{3}$
P	0.466 85	0	$\frac{1}{6}$
O(1)	0.416 3	0.2922	0.6023
O(2)	0.415 6	0.2576	0.1164

Table A.4. Absolute structure of laevorotatory α-HgS, $P3_22$ (Auvrey and Genet 1973, Auvrey 1976). $a = 4.145$ Å, $c = 9.496$ Å.

Hg	0.7198	0	$\frac{2}{3}$
S	0.4889	0	$\frac{1}{6}$

Table A.5. Absolute structure of laevorotatory $Bi_{12}SiO_{20}$, $a = 10.104\,33$ Å and $Bi_{12}GeO_{20}$, 10.145 40 Å; SG $I23$ (Abrahams, Bernstein and Svensson 1979, Svensson *et al* 1979).

Bi	0.175 5	0.317 4	0.015 9
Si	0	0	0
O(1)	0.134 8	0.252 3	0.485 8
O(2)	0.195 0	0.195 0	0.195 0
O(3)	0.905 9	0.905 9	0.905 9
Bi	0.175 87	0.318 32	0.016 00
Ge	0	0	0
O(1)	0.134 9	0.251 4	0.480 6
O(2)	0.195 3	0.195 3	0.195 3
O(3)	0.899 8	0.899 8	0.899 8

Table A.6. Absolute structure of dextrorotative $NaClO_3$, $P2_13$ (Abrahams and Bernstein 1977). $a = 6.578$ Å.

Na	0.0687	0.0687	0.0687
Cl	0.4182	0.4182	0.4182
O	0.3035	0.5924	0.5047

Table A.7. Absolute structure of laevorotatory $NaBrO_3$, $P2_13$ (Abrahams, Glass and Nassau 1977). $a = 6.7072$ Å.

Na	0.0775	0.0775	0.0775
Br	0.4067	0.4067	0.4067
O	0.2882	0.5964	0.5085

Table A.8. Absolute structure of laevorotatory α-$LiIO_3$, $P6_3$ (Svensson *et al* 1983). $a = 5.4818$ Å, $c = 5.1725$ Å.

Li	0	0	−0.0822
I	$\frac{1}{3}$	$\frac{2}{3}$	0
O	0.2479	0.3426	0.1618

Table A.9. Absolute structure of $NaNH_4SO_4 \cdot 2H_2O$, $P2_12_12_1$, $\rho_{33} < 0$ (without hydrogens) (Arzt 1995). $a = 6.253$ Å, $b = 8.228$ Å, $c = 12.856$ Å.

S	0.3729	0.0841	0.1283
Na	0.9112	0.2652	0.4848
O(1)	0.1884	0.0674	0.1990
O(2)	0.5732	0.0652	0.1882
O(3)	0.3674	0.2453	0.0805
O(4)	0.1399	0.0402	0.5468
O(5)	0.6896	0.2118	0.6352
O(6)	0.6590	0.0791	0.4040
N	0.3696	0.1729	0.8553

Table A.10. Absolute structure of mannitol, $C_6H_{14}O_6$, $P2_12_12_1$ $\rho_{33} < 0$ (without hydrogens) (Kaminsky and Glazer 1997). $a = 8.694$ Å, $b = 16.902$ Å, $c = 5.549$ Å.

C(1)	−0.0009	−0.4940	0.4263
C(2)	0.0240	−0.4561	0.1819
C(3)	0.0702	−0.3686	0.2061
C(4)	0.0867	−0.3278	−0.0377
C(5)	0.1185	−0.2385	−0.0138
C(6)	0.1310	−0.1982	−0.2583
O(1)	−0.1115	−0.4520	0.5677
O(2)	−0.1163	−0.4631	0.0509
O(3)	0.2151	−0.3632	0.3268
O(4)	0.2048	−0.3653	−0.1776
O(5)	−0.0053	−0.2016	0.1120
O(6)	−0.0031	−0.2106	−0.4014

Table A.11. Absolute structure of laevorotatory $NiSO_4 \cdot 6H_2O$, $P4_12_12$ (without hydrogens) (Stadnicka *et al* 1987). $a = 9.783$ Å, $c = 18.288$ Å.

Ni	0.210 60	0.210 60	0
S	0.709 43	0.709 43	0
O(1)	0.172 7	−0.047 0	0.0528
O(2)	0.470 5	0.244 9	0.0561
O(3)	0.065 8	0.359 9	0.0850
O(4)	0.620 9	0.620 3	0.0658
O(5)	0.923 7	0.673 1	0.0003

Table A.12. Absolute structure of laevorotatory $K_2S_2O_6$ $P32_1$ (Gomes, Ortega, Etxebarria, Zuniga and Breczewski 1996). $a = 9.782$ Å, $c = 6.298$ Å.

K(1)	0.619 48	0	0
K(2)	0.293 63	0	$\frac{1}{2}$
S(1)	0	0	0.829 10
S(2)	$\frac{1}{3}$	$\frac{2}{3}$	0.737 90
S(3)	$\frac{1}{3}$	$\frac{2}{3}$	0.398 59
O(1)	0.155 7	0.1241	0.768 2
O(2)	0.204 6	0.5117	0.798 5
O(3)	0.175 0	0.6235	0.344 1

Table A.13. Absolute structure of laevorotatory $KLiSO_4$, $P6_3$, $a = 5.147$ Å, $c = 8.8633$ Å (Ortega *et al* 1993).

K	0	0	0
S	$\frac{1}{3}$	$\frac{2}{3}$	0.2051
O(1)	$\frac{2}{3}$	$\frac{1}{3}$	0.4609
O(2)	0.4020	0.3437	0.2401
Li	$\frac{1}{3}$	$\frac{2}{3}$	0.1797

Table A.14. Absolute structure of $Rb_4LiH_3(SO_4)_4$, $P4_1$, $a = 7.615$ Å, $c = 29.458$ Å (Zuniga *et al* 1990) (not complete).

Pb(1)	0.0645	0.8853	0.718 0
Pb(2)	0.3652	0.3840	0.704 91
Pb(3)	0.5291	0.9751	0.083 43
Pb(4)	0.2271	0.4808	0.073 56
S(1)	0.4620	0.1245	0.204 59
etc			

Table A.15. Absolute structure of $RbTiOAsO_4$ as a representative of the KTP family. $Pna2_1$, $a = 13.2640$ Å, $b = 6.6820$ Å, $c = 10.7700$ Å.

Ti(1)	0.3738	0.5046	0.0015
Ti(2)	0.2488	0.2693	0.7514
As(1)	0.4996	0.3282	0.7444
As(2)	0.1800	0.5049	0.4903
Rb(1)	0.3830	0.7825	0.6729
Rb(2)	0.1090	0.6938	0.9261
O(1)	0.4875	0.4889	0.8614
O(2)	0.9892	0.9620	0.1107
O(3)	0.3940	0.1878	0.7228
O(4)	0.9000	0.6775	0.2469
O(5)	0.2169	0.0544	0.6103
O(6)	0.7188	0.5489	0.3620
O(7)	0.1093	0.3032	0.4527
O(8)	0.6073	0.7961	0.5222
O(9)	0.2576	0.5445	0.3675
O(10)	0.7576	0.0408	0.6098

References

Abrahams S C and Bernstein J L 1977 *Acta Crystallogr.* B **33** 3601–4

Abrahams S C, Bernstein J L and Svensson C 1979 *J. Chem. Phys.* **71** 788–92

Abrahams S C, Glass A M and Nassau K 1977a *Solid State Commun.* **29** 515–6

Abrahams S C, Lissalde F and Bernstein J L 1977b *J. Chem. Phys.* **68** 1926–35

Amos R D 1982 *Chem. Phys. Lett.* **87** 23

Anderson W J and Phil Won Yu Park YS 1974 *Opt. Commun.* **11** 392–5

Applequist J 1987 *Am. Sci.* **75** 59–68

Arago F 1811 *Memoires de la Classe des Sciences Mathematiques et Physiques de l'Institut Imperial de France* **1** 93–134

Arzt S D 1995 *Phil Thesis* (Oxford: Oxford University Press)

Arzt S and Glazer A M 1994 *Acta Crystallogr.* B **50** 425–31

Asahi T, Tomizawa M, Kobayashi J and Kleemann W 1992 *Phys. Rev.* B **45** 1971–87

Atkins P W and Miller M H 1968 *Mol. Phys.* **15** 491

Auvrey P 1976 *Bull. Soc. Fr. Minéral. Cristallogr.* **99** 373–8

Auvrey P and Genet F 1973 *Bull. Soc. Fr. Minéral. Cristallogr.* **96** 218–9

Azzam R M A and Bashara N M 1977 *Ellipsometry and Polarized Light* (Amsterdam: North-Holland)

Barron L D 1982 *Molecular Light Scattering and Optical Activity* (Cambridge: Cambridge University Press)

Bartholin R 1669 *Experiments with the Double Refracting Iceland Crystal* (Copenhagen)

Bartus J and Vogel O 1994 *Polym. Int.* **33** 25–36

Bartus J, Weng D X and Vogel O 1993 *Monatshefte Chem.* **124** 217–27

——1994a *Polym. Int.* **34** 433–42

——1994b *Monatshefte Chemie* **125** 671–80

Baturina O A, Brzezina B, Bogachek P, Perekalina Z B and Konstantinova A F 1987 *Kristallographia* **32** 1440–4 (Engl. Transl. 1987 *Sov. Phys.–Crystallogr.* **32** 843–9)

Baturina O A, Perekalina Z B, Konstantinova A F and Brzezina B 1983 *Kristallographia* **28** 731–5 (Engl. Transl. 1983 *Sov. Phys.–Crystallogr.* **28** 433–5)
Becker H, Brach D, Otto A and Weber H J 1990 *Rev. Sci. Instrum.* **62** 1196–205
Belogurov D A, Okroashvili T G, Syvokon T A and Shaldin Yu V 1979 *Fiz. Tverd. Tela* **21** 2524
Bequerel J and de Haas W J 1928 *Z. Phys.* **52** 678
Bergmann L and Schäfer C 1978 *Optik* (Berlin: de Gruyter)
Berlin I A, Gladkov S O and Goldankiiii V I Kuzmin 1989 *Dokl. Akad. Nauk* **306** 844–7
Beurskens-Kerssen G, Kroon J, Endeman H J, van Laar J and Bijvoet J M 1963 *Crystallography and Crystal Perfection* ed G Ramachandran (London: Academic) pp 225–36
Billesbach D P and Ullman F G 1994 *Ferroelectrics* **155** 221–6
Biot J B 1812 *Memoires de la Classe des Sciences Mathematiques et Physiques de l'Institut Imperial de France* **1** 1–372
Bohaty L 1984 *Z. Kristallogr.* **166** 97– 119
Born M 1915 *Z. Phys.* **16** 251
Born M 1933 *Optic* (Berlin: Springer)
Born M and Goeppert-Mayer M 1933 *Handbuch Phys.* **24** 623–794
Boswarva S M, Howard R E and Lidiard A B 1962 *Proc. R. Soc.* A **269** 125–41
Brezina B, Gulanov E K, Ivanov N R, Kislovskii L D and Shuvalov I A 1969 *Sov. Phys.–Crystallogr.* **13** 710–2
Brown P J and Forsyth J B 1996 *Acta Crystallogr.* A **52** 408–12
Bruhat G and Grivet P 1935 *J. Physique Radium* **6** 12–26
Caldwell D J and Eyring H 1971 *The Theory of Optical Activity* (New York: Wiley)
Chandrasekhar S 1961 *Proc. R. Soc.* A **105** 531–53
Charney E 1979 *The Molecular Basis of Optical Activity* (New York: Wiley)
Chern M-J and Phillips R A 1970a *J. Opt. Soc. Am.* **60** 1230–2
——1970b *J. Opt. Soc. Am.* **60** 1542A
Chern M-J and Phillips R A 1972 *J. Appl. Phys.* **43** 496–9
Chupis I E 1997 *Ferroelectrics* **204** 173–80
Condon E U 1937 *Rev. Mod. Phys.* **9** 432–57
Condon E U, Altar W and Eyring H 1937 *J. Chem. Phys.* 5753–75
Craxton R S 1981 *IEEE J. Quantum Electron.* **17** 1771–82
Devarajan V and Glazer A M 1986 *Acta Crystallogr.* A **42** 560–9
Devarajan Y and Salje E 1984 *J. Phys. C: Solid State Phys.* **17** 5525–37
Dijkstra E 1991 Incommensurate crystal optics *DPhil Thesis* Nijmegen
Dillon J F, Chen E Yi and Guggenheim H 1978 *J. Phys. Rev.* B **18** 377–87
Dodge J S, Kapitulnik A and Fejer M M 1994 *Ferroelectrics* **162** 387–95
Dvoran P 1993 Cotton–mouton effect in alkalihalogeniden *Diplomarbeit Köln*
Eibschütz M, Pfeiffer L and Nielsen J W 1970 *J. Appl. Phys.* **41** 1276–80
Endeman H J 1965 Berekening van de optische activiteit van natriumcloraat en bromaaatkristalllen en van α-kwarts *Dissertation* Utrecht
Etxebarria J, Ortega J and Breczewski T 1992 *J. Condens Matter* **4** 6851–8
Evdishenko E A, Konstantinova A F and Greshushnikov B N 1991 *Kristallographia* **36** 842–6
Ewald P P 1921 *Ann. Phys.* **64** 253–87
Eyring H, Walter J and Kimball G E 1944 *Quantum Chemistry* (New York: Wiley)
Faraday M 1839 1844 1855 *Experimental Researches in Electricity* (London: Taylor and Francis)
Faraday M 1846 *Phil. Trans.* **136** 1
Fedorov Y U M, Leksikov A A and Aksenov A E 1983 *JETP Lett.* **37** 161
Fedorov Y U M, Leksikov A A, Aksenov A E and Edelmann L S 1981 *Phys. Status Solidi* b **106** K127–30
Fillipov V V, Tronin A Y and Konstantinova A F 1994 *Kristallographia* **39** 360–82
Flack H 1983 *Acta Crystallogr.* A **39** 876–81
Folcia C L, Ortega J, Etxebarria J and Breczewski T 1993 *Phys. Rev.* B **48** 695–700
Fredericq E and Houssier C 1973 *Electric Dichroism and Electric Birefringence* (Oxford: Clarendon)
Fresnel A 1824 *Bull. Soc. Philomath. Paris* 147–58
Futama H and Pepinsky R 1962 *J. Phys. Soc. Japan* **17** 725
Gibbs J W 1882 *Am. J. Sci.* **23** 460–76
Glazer A M, Lewis J G and Kaminsky W 1996 *Proc. R. Soc.* A **452** 2751–65
Glazer A M and Stadnicka K 1986 *J. Appl. Crystallogr.* **19** 108–22
Glazer A M, Stadnicka K and Singh S 1981 *J. Phys. C: Solid State Phys.* **14** 5011–29
Gomes E D, Ortega J, Etxebarria J, Zuniga F J and Breczewski T 1996 *J. Phys.: Condens. Matter* **8** 2063–71

Gomes E D, Zuniga F J, Ortega J and Extebarria J 1994 *J. Appl. Crystallogr.* **27** 563–6
Graham E B and Raab R E 1991 *Phil. Mag.* B **64** 267–74
——1992 *Phil. Mag.* B **66** 269–84
Groth P 1921 *Chemische Kristallographie* (Munich: Oldenburg)
Gulbransson D B 1979 *Das Olaf Gulbransson Buch* (Munich: Müller)
Habryko S and Koralewski H 1981 *Acta Phys. Pol.* A **60** 147–50
Hameka H F 1970 *Chem. Phys. Lett.* **7** 157–60
Hamilton C H 1957 *Acta Crystallogr.* **10** 103–7
Handbook of Chemistry and Physics 1973 53rd edn (Cleveland, OH: Chemical Rubber Company) p E46
Harada S, Iwata M and Ishibashi Y 1992 *J. Phys. Soc. Japan* **61** 3436
Haussühl S 1983 *Kristallphysik* (Weinheim: Physik–Chemie)
——1990 *Z. Kristallogr.* **192** 245–8
Haussühl S and Effgen W 1988 *Z. Kristallogr.* **183** 153–74
Helgaker T, Ruud K, Bak K L, Jørgensen and Olsen J 1994 *Faraday Discuss.* **99** 165
Hermelbracht K and Unruh H G 1970 *Z. Angew. Phys.* **28** 285–8
Herschel J W F 1822 *Phil. Soc. Proc.* **1** 46–50
Higano M, Asahi T, Sato Y, Okubo K and Kobayashi J 1994 *Ferroelectrics* **152** 285–7
Hobden M V 1967 *Nature* **216** 678
——1968a *Acta Crystallogr.* A **24** 676– 80
——1968b *Nature* **220** 78
——1969 *Acta Crystallogr.* A **25** 633–8
Horinaka H, Sonomura H and Moyauchi T 1980 *Japan. J. Appl. Phys.* (Suppl.) **3** 111–5
Huang S H and Ito J T 1975 *Phys. Rev.* B **12** 5255
Itoh K, Mishima N and Nakamura E 1981 *J. Phys. Soc. Japan* **50** 2029–36
Itoh K and Mitsui T 1973 *Ferroelectrics* **5** 235–51
Ivanov N R and Koniak C 1975 *Sov. Phys.–Crystallogr.* **19** 755–6
Ivanov N R and Shuvalov L A 1966 *Sov. Phys.–Crystallogr.* **11** 534–8
——1967 *Sov. Phys.–Crystallogr.* **11** 648–51
Iwasaki H, Miazawa S, Koizumi H, Sugii K and Niizeki N 1972 *J. Appl. Phys.* **43** 4907–15
Janner A and Dam B 1989 *Acta Crystallogr.* A **45** 115
Jeggo C R 1972 *J. Phys. C: Solid State Phys.* **5** 330–7
Jonsson L, Levine Z H and Wilkins J W 1996 *Phys. Rev. Lett.* **76** 1372–5
Jørgensen P, Jensen H J and Olsen J 1988 *J. Chem. Phys.* **89** 3654
Kahr B, Jang S-H, Subramony J A, Kelley M P and Bastin L 1996 *Adv. Mater.* **8** 941–3
Kaminskii A A, Butashin A V, Maslyanizin I A, Mill B V, Mironov V S, Rozov S P, Sarkisov S E and Shigorin V D 1991 *Phys. Status Solidi* a **125** 671–96
Kaminsky W 1989 *Dissertation* Cologne
——1994 *Phase Transitions* **52** 235–59
——1996 *Phase Transitions* **59** 121–33
——1997 *Ferroelectrics* **204** 233–46
——2000 *J. Appl. Crystallogr.* at press
Kaminsky W and Bismayer U 1993 *Phase Transitions* **46** 41–6
Kaminsky W, Corker D and Glazer A M 2000 at press
Kaminsky W, Fahnenstich A and Haussühl S 1992 *Ann. Phys., Lpz.* **1** 92–7
Kaminsky W, Fitzmaurice A J and Glazer A M 1998 *J. Phys. D: Appl. Phys.* **31** 767–75
Kaminsky W and Glazer A M 1996 *Ferroelectrics* **183** 133–41
——1997 *Z. Kristallogr.* **212** 283–96
——1998 *Phase Transitions* **66** 1–21
Kaminsky W and Hartmann E 1993 *Z. Phys.* B **90** 47–50
Kaminsky W and Haussühl S 1990 *Ferroelectr. Lett.* **11** 63–7
——1993 *Z. Kristallogr.* **203** 79–91
Kaminsky W, Haussühl S, Brandstädter A and Balarew C 1994 *Z. Kristallogr.* **209** 395–9
Kaminsky W, Thomas P A and Glazer A M 2000b *Z. Kristallogr.* at press
Kharchenko N F 1994 *Ferroelectrics* **162** 173–89
Kielich S 1976 *Molecular Electro-optics* ed C T O Konski (New York: Dekker) chapter 13
Kim D-Y, Kaminsky W and Glazer A M 2000 *Phase Transitions* submitted
Kittel C 1976 *Introduction to Solid State Physics* 5th edn (New York: Wiley)
Kobayashi J, Asahi T, Ichiki M and Oikawa A 1995a *Ferroelectrics* **171** 69–94

Kobayashi J, Asahi T, Ichiki M, Saito K, Shimasaki T, Yoshii H, Itagaki Y and Ikawa H 1995b *Phys. Rev.* B **51** 763–78
Kobayashi J, Asahi T and Takahashi S 1987 *Ferroelectrics* **75** 139–52
Kobayashi J, Kumoni H and Saito K 1986a *J. Appl. Crystallogr.* **19** 377
Kobayashi J and Saito K 1986b *Proc. Japan. Acad.* B **62** 177–80
Kobayashi J, Saito K, Fukase H and Matsuda K 1988a *Phase Transitions* **12** 225–33
Kobayashi J, Saito K, Takahashi N and Kamiya I 1993 *Phys. Rev.* B **48** 10 038–46
——1994a *Phys. Rev.* B **49** 6539–47
Kobayashi J, Saito K, Takahashi N, Kamiya I and Utsumi H 1994b *Phys. Rev.* B **50** 2766–74
Kobayashi J, Takada M, Hosogaya N and Someya T 1988b *Ferroelectr. Lett.* **8** 145–52
Kobayashi J, Uchino K and Asahi T 1991a *Phys. Rev.* B **43** 5706–12
Kobayashi J, Uchino K, Matasuyama H and Suito U 1991b *J. Appl. Phys.* **69** 409–13
Kobayashi J and Uesu Y 1983 *J. Appl. Crystallogr.* **16** 204–11
——1985 *Ferroelectrics* **64** 115–22
Kobayashi J, Uesu Y and Takahashi H 1983 *J. Appl. Crystallogr.* **16** 212–9
Kondru R K, Wipf P and Beratan D N 1998 *Science* **282** 2247
——1999 *J. Phys. Chem.* A **103** 6603–11
Konstantinova A F, Evdishenko E A and Ulukhanov I T 1994 *Kristallografia* **39** 790–7
Konstantinova A F, Ivanov N R and Greshushnikov B N 1969 *Kristallografija* **14** 283–392
Konstantinova A F and Nabatov B V 1995 *Kristallographia* **40** 713–5
Koopmans B, Etchegoin P, Santos P and Cardona M 1996 *Solid State Commun.* **97** 261–6
Koopmans B, Santos P N and Cardona M 1998 *Phys. Status Solidi* b **205** 419–63
Koyanagi K, Yamano K, Sota T, Nakamura K and Matsubara K 1989 *Japan. J. Appl. Phys.* **28** L669–71
Kremers M, Dijkstra E and Meekes H 1996 *Phys. Rev.* B **54** 3125–35
Kremers M and Meekes H 1995a *J. Phys. D: Appl. Phys.* **28** 1212–24
——1995b *J. Phys. D: Appl. Phys.* **28** 1195–211
——1995c *J. Phys.: Condens. Matter* **7** 8119–38
——1996 *Phys. Rev.* B **54** 3136–41
Kurtzig A J, Wolfe R, Le Craw R C and Nielsen J W 1969 *Appl. Phys. Lett.* **14** 350–2
Landolt–Börnstein New Series 1969 Group III, vol 3 (Berlin: Springer) pp 185ff
——1979 Group III, vol 11 (Berlin: Springer)
——1990 Group III, vol 28 (Berlin: Springer) pp 206ff
Le Craw R C, Wulfe R and Nielson J W 1969 *Appl. Phys. Lett.* **14** 352–4
Lenzo P V, Spencer E G and Ballman A A 1966 *Appl. Opt.* **5** 1688
——1967 *Phys. Rev. Lett.* **19** 641–4
Le Page Y and Donnay G 1976 *Acta Crystallogr.* B **32** 2456–9
Levine Z H 1994 *Int. J. Quantum Chem.* **S28** 411–9
Lingard R J 1994 *DPhil Thesis* University of Oxford
Lissalde F, Abrahams S C, Bernstein J L and Nassau K 1978 *J. Appl. Phys.* **50** 845–51
Lomova L G, Sonin A S and Reguls'skaja T A 1968 *Sov. Phys.–Crystallogr.* **13** 68–70
Mason S F 1982 *Molecular Optical Activity and the Chiral Discriminations* (Cambridge: Cambridge University Press)
Matsuda K, Sugiya H and Kobayashi J 1990 *Ferroelectrics* **107** 39–44
Matthias B T, Miller C E and Remeika J P 1956 *Phys. Rev.* **104** 849
Meyers M B and Vedam K 1965a *J. Opt. Soc. Am.* **55** 1180–1
——1967 *J. Opt. Soc. Am.* **57** 1146–8
Michl J and Thulstrup E W 1986 *Spectroscopy with Polarized Light* (New York: VCH)
Miller A 1973 *Phys. Rev.* B **8** 5902–8
Miller R C 1964 *Appl. Phys. Lett.* **1** 17–9
Moore G F, Lenzo V P, Spencer E G and Ballman A A 1969 *J. Appl. Phys.* **40** 2361–3
Moxon J R L and Renshaw A R 1990 *J. Phys.: Condens. Matter* **2** 6807–36
Moxon J R L, Renshaw A R and Tebutt I J 1991 *J. Phys. D: Appl. Phys.* **24** 1187–92
Mucha D, Stadnicka K, Kaminsky W and Glazer A M 1997 *J. Phys.: Condens. Matter* **9** 10 829–42
Ngo Thong and Schwarzenbach D 1979 *Acta Crystallogr.* A **35** 658–66
Nye J F 1957 *Physical Properties of Crystals* (Oxford: Clarendon)
Odell T H and White E A D 1970 *Phil. Mag.* **22** 649–53
O'Loane J K 1980 *Chem. Rev.* **80** 41–61
Ortega J, Etxebarria J and Breczewski T 1993 *J. Appl. Crystallogr.* **26** 549–54
Ortega J, Etxebarria J, Folcia C L and Breczewski T 1995 *J. Phys.: Condens. Matter* **7** 421–31
Ortega J, Etxebarria J, Zubillaga J, Breczewski T and Tello M J 1992 *Phys. Rev.* B **10** 5155–62

Orushinin V V, Pavlovskii A L, Pisarev R V, Tatsenko O M and Platonov V V 1986 *JETP Lett.* **43** 362–5
Pasteur L 1897 *Researches on the Molecular Asymmetry of Natural Organic Products* (Edinburg: Alembic)
Perekalina Z B, Kaldybaev K A, Konstantinova A F and Belyaev L M 1977 *Sov. Phys.–Crystallogr.* **22** 318–21
Piepho S B and Schatz P N 1983 *Group Theory in Spectroscopy* (New York: Wiley)
Pine A S and Dresselhaus G 1971 *Proc. Int. Enrico Fermi School of Physics Course LII* ed E Burnstein (New York: Academic)
Pisarev P V 1994 *Ferroelectrics* **162** 191–209
——1996 private communication
Pockels F 1906 *Lehrbuch der Kristalloptik* part 2 (Leipzig: Teubner) pp 313–8
Ramachandran G N 1963 *Crystallography and Crystal Perfection* (London: Academic) pp 225–36
Ramachandran G N and Ramaseshan S 1961 Crystal optics *Handbuch der Physik* ed S Flügge (Berlin: Springer)
Reijnhart R 1970 *Dissertation* Delft
Rifani M, Yin Y Y, Elliott D S, Jay M J, Jang S-H, Kelley M P, Bastin L and Kahr B 1995 *J. Am. Chem. Soc.* **117** 7572–3
Rosenfeld L 1928 *Z. Phys.* **52** 161–74
Saito K, Asahi T, Takahashi N, Higano M, Kamiya I, Sato Y, Okubo K and Kobayashi J 1994 *Ferroelectrics* **152** 231–6
Saito K, Cao F T and Kobayashi J 1992 *Japan. J. Appl. Phys.* **1, 31** 3225–8
Saito K, Kawabe T and Kobayashi J 1987 *Ferroelectrics* **75** 153–66
Saito K and Kobayashi J 1991 *Japan. J. Appl. Phys.* **1, 30** 2416–8
——1992 *Phys. Rev.* B **45** 10 264–70
Saito K, Sugiya H and Kobayashi J 1990 *J. Appl. Phys.* **68** 732–5
Salje E K H 1990 *Phase Transitions in Ferroelastic and Co-Elastic Crystals* (Cambridge: Cambridge University Press)
Schütz W 1936 Magnetooptik *Handbuch der Experimentalphysik* vol 16
Schwarzenbach D 1966 *Z. Kristallogr.* **123** 161–85
Scott G B 1974 *J. Phys. D: Appl. Phys.* **7** 1574–87
Singh S 1984 *J. Phys. C: Solid State Phys.* **17** 5421–35
Smith S D 1976 Magneto-optics *Handbuch der Physik* vol 234
Stadnick K and Brozek Z 1991 *Acta Crystallogr.* B **47** 484–92
Stadnicka K, Glazer A M and Koralewski M 1987 *Acta Crystallogr.* B **43** 319–25
Stadnicka K, Glazer A M and Moxon J 1985 *J. Appl. Crystallogr.* **18** 237–40
Stadnicka K, Madej A, Tebbutt I J and Glazer A M 1992 *Acta Crystallogr.* B **48** 16–21
Stasyuk I V and Kotsur S S 1985a *Phys. Status Solidi* b **129** 577–86
——1985b *Phys. Status Solidi* b **130** 103–13
Stedmann G E 1985 *Adv. Phys.* **34** 513
Stephens P J 1965 *Inorg. Chem.* **4** 1690–2
——1974 *Annu. Rev. Phys. Chem.* **25** 201–32
Subramony J A, Lovell S and Kahr B 1998 *Chem. Mater.* **10** 2053–7
Suits J C 1971 *Rev. Sci. Instrum.* **42** 19–22
Svensson C, Abrahams S C and Bernstein J L 1979 *Acta Crystallogr.* B **35** 2687–90
Svensson C, Albertsson J, Liminga R, Kvick A and Abrahams S C 1983 *J. Chem. Phys.* **78** 7343–52
Swindells D C N and Gonzales J L 1988 *Acta Crystallogr.* B **44** 12–5
Szivessy G and Münster C 1934 *Ann. Phys.* **20** 703–36
Takahashi N, Tomizawa M and Kobayashi J 1992 *Japan. J. Appl. Phys.* **31** 3209–11
Tebutt I J 1991 Optical activity and crystal structure *DPhil Thesis* Oxford
Tessman J R, Kahn A H and Shockley W 1953 *Phys. Rev.* **92** 891–5
Thomas P A, Tebbutt I J and Glazer A M 1991 *J. Appl. Crystallogr.* **24** 963–7
Tomizawa M, Sugiya H and Kobayashi J 1991 *Japan. J. Appl. Phys.* **30** 2419–22
Van Laar J, Endeman H J and Bijvoet J M 1968 *Acta Crystallogr.* A **24** 52–6
Vlokh O G 1981 *Ukr. Fiz. Zh.* **26** 1623
Vlokh O G and Eksp Z H 1971 *JETP Lett.* **13** 81–3
Vlokh O G, Klepatch N I and Shopa Y I 1986a *Ferroelectrics* **69** 267–74
——1986b *Kristallographiya* **31** 195–7
Vlokh O G, Kushnir O S and Shopa Y I 1992 *Acta Phys. Pol.* A **81** 571–8
Vlokh O G and Lyzko L A 1984 *Ferroelectrics* **56** 103–6
Vlokh O G, Lyzko L A and Nesterenko V Ya 1973 *Sov. Phys.–Crystallogr.* **17** 1091–2
Vlokh O G and Sergatyuk V A 1986 *Sov. Phys.–Dokl. Acad. Sci.* **291** 832

Vlokh O G, Zheludev I S and Sergatyuk V A 1984 *Sov. Phys. Izv. Acad. Sci.* **48** 1771
Vogels L J P, Meekes H and Deboer J L 1994 *J. Phys.: Condens. Matter* **6** 8205–18
Weber H J 1979 *Acta Crystallogr.* A **35** 225–32
Weber H J and Haussühl S 1974 *Phys. Status Solidi* b **65** 633–9
——1976 *Acta Crystallogr.* A **32** 892–5
——1977 *Z. Kristallogr.* **146** 303
Weckert E 1997 *Z. Kristallogr.* (Suppl.) **12** 5
Wedding W 1888 *Ann. Phys., Lpz.* **35** 25
Wiener O 1888 *Ann. Phys., Lpz.* **35** 1–24
Wood I G and Glazer A M 1980 *J. Appl. Crystallogr.* **13** 217–23
Xi F, Bartus J and Vogel O 1993 *Polym. Int.* **31** 183–96
Yabana K and Bertsch G F 1999 *Phys. Rev.* A **60** 1271
Yamaoka K and Charney E 1972 *J. Am. Chem. Soc.* **94** 8963
Yoshii H, Shimasaki T, Ichiki M, Itagaki Y, Asahi T, Saito K, Kobayashi J and Ikawa H 1994 *Japan. J. Appl. Phys.* **1** 5435–9
Zuniga F J, Etxebarria J, Madariaga G and Breczewski T 1990 *Acta Crystallogr.* C **46** 1199–202